AEDC-TR-75-15
AFATL-TR-75-21

cy. 1

AN INVESTIGATION OF THE FLOW FIELD OF THE A-7D AIRCRAFT WITH SEVERAL EXTERNAL STORE LOADINGS AT MACH NUMBERS 0.70 AND 0.95

J. B. Carman, Jr.
ARO, Inc.

PROPULSION WIND TUNNEL FACILITY
ARNOLD ENGINEERING DEVELOPMENT CENTER
AIR FORCE SYSTEMS COMMAND
ARNOLD AIR FORCE STATION, TENNESSEE 37389

April 1975

Final Report for Period October 9 – 15, 1974

Approved for public release; distribution unlimited.

Prepared for

AIR FORCE ARMAMENT LABORATORY (AFATL/DLJC)
EGLIN AIR FORCE BASE, FLORIDA 32542

NOTICES

When U. S. Government drawings specifications, or other data are used for any purpose other than a definitely related Government procurement operation, the Government thereby incurs no responsibility nor any obligation whatsoever, and the fact that the Government may have formulated, furnished, or in any way supplied the said drawings, specifications, or other data, is not to be regarded by implication or otherwise, or in any manner licensing the holder or any other person or corporation, or conveying any rights or permission to manufacture, use, or sell any patented invention that may in any way be related thereto.

Qualified users may obtain copies of this report from the Defense Documentation Center.

References to named commercial products in this report are not to be considered in any sense as an endorsement of the product by the United States Air Force or the Government.

This report has been reviewed by the Information Office (OI) and is releasable to the National Technical Information Service (NTIS). At NTIS, it will be available to the general public, including foreign nations.

APPROVAL STATEMENT

This technical report has been reviewed and is approved for publication.

FOR THE COMMANDER

LAMAR R. KISSLING
Lt Colonel, USAF
Chief Air Force Test Director, PWT
Directorate of Test

FRANK J. PASSARELLO
Colonel, USAF
Director of Test

REPORT DOCUMENTATION PAGE		READ INSTRUCTIONS BEFORE COMPLETING FORM
1 REPORT NUMBER AEDC-TR-75-15 AFATL-TR-75-21	2 GOVT ACCESSION NO	3 RECIPIENT'S CATALOG NUMBER
4 TITLE (and Subtitle) AN INVESTIGATION OF THE FLOW FIELD OF THE A-7D AIRCRAFT WITH SEVERAL EXTERNAL STORE LOADINGS AT MACH NUMBERS 0.70 AND 0.95		5 TYPE OF REPORT & PERIOD COVERED Final Report for Period October 9-15, 1974 6 PERFORMING ORG REPORT NUMBER
7 AUTHOR(s) J. B. Carman, Jr., ARO, Inc.		8 CONTRACT OR GRANT NUMBER(s)
9 PERFORMING ORGANIZATION NAME AND ADDRESS Arnold Engineering Development Center (XO) Air Force Systems Command Arnold Air Force Station, Tennessee 37389		10 PROGRAM ELEMENT, PROJECT, TASK AREA & WORK UNIT NUMBERS Program Element 27121F Project 5221
11 CONTROLLING OFFICE NAME AND ADDRESS Air Force Armament Laboratory (AFATL/DLJC) Eglin AFB, Florida 32542		12 REPORT DATE April 1975 13 NUMBER OF PAGES 78
14 MONITORING AGENCY NAME & ADDRESS(if different from Controlling Office)		15 SECURITY CLASS (of this report) UNCLASSIFIED 15a DECLASSIFICATION DOWNGRADING SCHEDULE N/A

16 DISTRIBUTION STATEMENT (of this Report)

Approved for public release; distribution unlimited.

1. Stores -- Effects
2 " -- Flow fields

17 DISTRIBUTION STATEMENT (of the abstract entered in Block 20, if different from Report)

3 Airplanes -- " "
4 " " -- Store effects

18 SUPPLEMENTARY NOTES

Available in DDC

19 KEY WORDS (Continue on reverse side if necessary and identify by block number)

A-7D aircraft	pylons	transonic flow
flow fields	fuel tanks	wind tunnel tests
external-store effects	bombs	captive tests
pods	rockets	trajectories

20 ABSTRACT (Continue on reverse side if necessary and identify by block number)

Wind tunnel tests were conducted using 0.05-scale models to study the flow field of the A-7D aircraft with several different external store load configurations. The flow-angularity data were obtained at selected axial, lateral, and vertical positions under the inboard, center, and outboard pylons of both wings of the aircraft. Parent aircraft angles of attack were 2, 6, and 10 deg at zero sideslip for free-stream Mach numbers of 0.70 and 0.95.

DD FORM 1 JAN 73 1473 EDITION OF 1 NOV 65 IS OBSOLETE

PREFACE

The work reported herein was done by the Arnold Engineering Development Center (AEDC) and was sponsored by the Air Force Armament Laboratory (AFATL/DLJC), Air Force Systems Command (AFSC), under Program Element 27121F, Project 5221.

The test results presented were obtained by ARO, Inc. (a subsidiary of Sverdrup & Parcel and Associates, Inc.), contract operator of the AEDC, AFSC, Arnold Air Force Station, Tennessee. The tests were conducted from October 9 through 15, 1974, under ARO Project No. P41C-58A. The manuscript (ARO Control No. ARO-PWT-TR-74-127) was submitted for publication on December 19, 1974.

CONTENTS

ILLUSTRATIONS

Figure

Figure | Page

TABLES

1.0 INTRODUCTION

Flow-angularity measurements were obtained in the flow field of the A-7D aircraft using a 40-deg conical probe attached to a six-degree-of-freedom captive trajectory store separation system (CTS). Local flow angle velocities were measured beneath the inboard, center, and outboard pylons of both wings of the parent aircraft to determine the effects of external store configuration on flow-field characteristics. The data were recorded at Mach numbers 0.7 and 0.95 in the Aerodynamic Wind Tunnel (4T) of the Propulsion Wind Tunnel Facility (PWT) using 0.05-scale models. The probe was positioned at selected axial, lateral, and vertical positions in the aircraft flow field for parent-aircraft angles of attack of 2, 6, and 10 deg at zero sideslip.

2.0 APPARATUS

2.1 TEST FACILITY

The Aerodynamic Wind Tunnel (4T) is a closed-loop, continuous flow, variable-density tunnel in which the Mach number can be varied from 0.1 to 1.3. At all Mach numbers, the stagnation pressure can be varied from 300 to 3700 psfa. The test section is 4 ft square and 12.5 ft long with perforated, variable porosity (0.5- to 10-percent open) walls. It is completely enclosed in a plenum chamber from which the air can be evacuated, allowing part of the tunnel airflow to be removed through the perforated walls of the test section.

Two separate and independent support systems were used to support the models. The parent aircraft model was inverted in the test section and supported by an offset sting attached to the main pitch sector. The flow-field survey probe was supported by the CTS which extends down from the tunnel top wall and provides probe movement (six degreees of freedom) independent of the parent-aircraft model. An isometric drawing of a typical installation is shown in Fig. 1.

Also shown in Fig. 1 is a block diagram of the computer control loop used during testing. The analog system and the digital computer work as an integrated unit and, utilizing required input information, control the probe movement. Positioning is accomplished by use of six individual d-c electric motors. Maximum translational travel of the CTS is ±15 in. from the tunnel centerline in the lateral and vertical directions and 36 in. in the axial direction. Maximum angular displacements are ±45 deg in pitch and yaw and ±360 deg in roll. A schematic showing the test section details and the location of the models in the tunnel is shown in Fig. 2.

2.2 TEST ARTICLE

The probe used to obtain flow-field measurements was attached directly to the CTS and consisted of a single cone-cylinder with a 40-deg included tip angle (Fig. 3). There were four equally spaced static pressure orifices on the cone surface and a total pressure orifice at the cone apex.

The basic details of the 0.05-scale A-7D parent model are presented in Fig. 4. The parent model is geometrically similar to the full-scale airplane except for the faired nose/inlet geometry. The horizontal tail surfaces were removed to minimize interference with the CTS support movement. Details of the A-7 pylons, multiple ejection rack (MER), and triple ejection rack (TER) are shown in Figs. 5, 6, and 7, respectively. Details of the external store models are given as follows: 300-gal fuel tank (Fig. 8), MK-82GP (Fig. 9), MK-82SE (Fig. 10), SUU-30H/B (Fig. 11), MK-20 "Rockeye" (Fig. 12), MK-84EOGB (Fig. 13), and QRC-335A ECM Pod (Fig. 14). The orientation of the suspension lugs on the MER and TER are shown in Fig. 15. A typical tunnel installation photograph showing parent aircraft, probe, and CTS is presented in Fig. 16.

2.3 INSTRUMENTATION

Static and total pressures on the cone probe were measured with 5-psid transducers. Translational and angular positions of the probe were obtained from digital computer commands during flow-field testing. The parent-model angle of attack was determined using an internal, gravimetric angular position indicator. The pylons contained a touch wire system which enabled the probe to be accurately positioned initially with respect to the parent aircraft. The system was also wired to automatically stop the CTS motion and give visual indication should the probe or sting support make contact with any surface other than the touch wire.

3.0 TEST DESCRIPTION

3.1 TEST CONDITIONS

The nominal wind tunnel test conditions are given below:

M_∞	p_t	T_t	q_∞	p_∞	V_∞	$Re_\infty \times 10^{-6}$
0.70	1200	560	300	870	770	2.1
0.95	1200	560	420	670	1010	2.4

A complete test summary is given in Tables 1 and 2.

3.2 DATA ACQUISITION

All flow-field measurements were obtained in the pylon-axis system. Definitions of the positive directions of the flow-field velocity vectors and probe displacements are given in Fig. 17. During testing, tunnel conditions were established and the probe tip was positioned at a known coordinate point relative to the parent aircraft. At this position, initial-point data were obtained which oriented the computer program controlling CTS movement (see block diagram, Fig. 1). After the initital data were recorded, the computer automatically positioned the probe at preselected locations (see Tables 1 and 2) where tunnel conditions and probe tip pressures were recorded. Using predetermined probe calibration data, the probe pressure measurements were reduced to flow-angularity data, and these were tabulated point-by-point with the same digital computer which controlled the CTS movement.

3.3 CORRECTIONS

Probe free-stream calibration data were used to obtain corrections to account for any minor misalignment in the probe pitch or yaw orientation. However, no attempt was made to correct the measured flow angles for deflections resulting from aerodynamic loading on the probe.

3.4 PRECISION OF DATA

Uncertainties in the basic tunnel parameters, p_t, T_t, and M_∞, were estimated from repeat calibrations of the instrumentation and from repeatability and uniformity of the test section flow during tunnel calibration. These uncertainties were then used to estimate the uncertainties in other free-stream properties, using the Taylor Series method of error propagation (Ref. 1).

	Uncertainty, percent						
Free-Stream Mach Number	ΔM_∞	Δp_t	ΔT_t	Δq_∞	Δp_∞	ΔV_∞	ΔRe_∞
0.70	±0.3	±0.1	±0.4	±0.4	±0.2	±0.3	±0.6
0.95	±0.3	±0.1	±0.4	±0.3	±0.4	±0.4	±0.5

The estimated uncertainties in probe positioning from the ability of the CTS to set on a specified value were ±0.08 ft (full-scale equivalent) in X_P, Y_P, and Z_P, ±0.15 deg in pitch and yaw, and ±1.0 deg in roll. The estimated uncertainty in parent-aircraft angle of attack is ±0.1 deg and the estimated uncertainty in $V_{YZ,P}$ is ±5 ft/sec.

4.0 RESULTS AND DISCUSSION

Data obtained during the test consisted of basic flow angularity measurements in the flow field of the A-7D aircraft with several different external store loadings. A test summary and a definition of the survey regions are listed in Tables 1 and 2, and aircraft loading configurations are given in Table 3. Because of the large volume of data obtained, only representative data are presented herein.

The data (Figs. 18 through 25) are presented as the projection of the velocity vector ($V_{YZ,P}$) in the pylon axis Y_P-Z_P plane, with the tails of the vectors plotted at the Y_P,Z_P position of the measurement for the X_P location indicated. The magnitudes of the velocities are given by the length of the vectors, and flow directions are as shown. Note that when data at the same X_P location are presented for adjacent pylons, a truly planar flow field is not represented since the fuselage stations and the waterlines of the origins are different. However, since the spanwise vector distribution is in true perspective, a reasonably good quantitative representation of the flow field is still obtained.

Flow-field measurements under the left wing of the A-7D aircraft with no external stores are shown in Fig. 18. An examination of these data showed that the transverse velocities varied with vertical distance from the pylons, spanwise distance from and axial distance along the aircraft centerline, parent aircraft angle of attack, and free-stream Mach number. For the test conditions shown, the flow-field patterns generally changed in an orderly fashion and the flow field essentially returned to free-stream conditions at 20 ft below the pylons.

Shown in Figs. 19 to 25 are flow-field data for configurations 2 through 8. The regions surveyed around the outboard pylons (with the exception of configuration 8, right wing) mapped the flow field at the nose and tail of the installed MK-82 store that would next separate from the armament station of the MER or TER in the normal ejection sequence. Note that the data presented cover all the normal release possibilities from either wing. Except for the right wing of configuration 8, external store loadings on both center pylons for these configurations consisted of an MER with a full complement of MK-82 stores, whereas the inboard pylons were empty.

The portion of the basic A-7D flow field within 10 ft of the pylons was substantially perturbed by the presence of external stores. The degree of disturbance was a function of parent-aircraft attitude, free-stream Mach number, and, of course, external store load configuation. For the present test conditions, the flow-field data for the aft MER release positions 1, 3, and 5 (Figs. 19, 20, and 23) were quite similar as were the data for the forward MER release positions 2, 4, and 6 (Figs. 19, 21, and 22) and TER release positions 1, 2, and 3 (Figs. 23 and 24). Also, the flow on the left and right wings for the

nonsymmetric MER release positions 4, 5, and 6 (Figs. 19, 20, 21, and 23) and TER release position 3 (Figs. 24 and 25) were similar. Therefore, for the present test conditions, it can be concluded that different store loadings on the MER or TER did not appreciably alter the flow field at the points where the data were obtained. However, these consistencies should not be assumed true at another flight condition or for an MER or TER in another aircraft load configuration.

The effect of large pylon-mounted stores on the flow field can be seen by comparing the right wing data of configuration 8 (Fig. 25) with the empty-aircraft data (Fig. 18). The X_P survey positions for these data correspond to the nose and tail positions of the MK-84 EOGB stores mounted on the pylons.

Initial separation tendencies of the respective stores would be difficult to predict from the present flow-field data because the near flow field around the stores in the carriage position is unknown, and ejector force effects would have to be accounted for. However, these data would certainly help to explain a store motion once it reached the position in the flow field where the data were obtained. A comparison of MK-82 separation trajectories of Refs. 2 and 3 for comparative configurations with the present flow-field measurements showed reasonably good correlation once the store had moved a foot or so away from the MER or TER carriage position.

REFERENCES

1. Beers, Yardley. Introduction to the Theory of Error. Addision-Wesley Publishing Company, Inc., Reading, Massachusetts, 1957, pp. 26-36.

2. Kukainis, Janis and Roberts, Robert H. "Separation Characteristics of Six Stores from the A-7D Aircraft at Mach Numbers from 0.42 to 0.95." AEDC-TR-70-19 (AD864651), January 1970.

3. Roberts, Robert H. "Separation Characteristics of Eight Stores from the A-7D Aircraft at Mach Numbers from 0.42 to 0.95." AEDC-TR-70-127 (AD869970), June 1970.

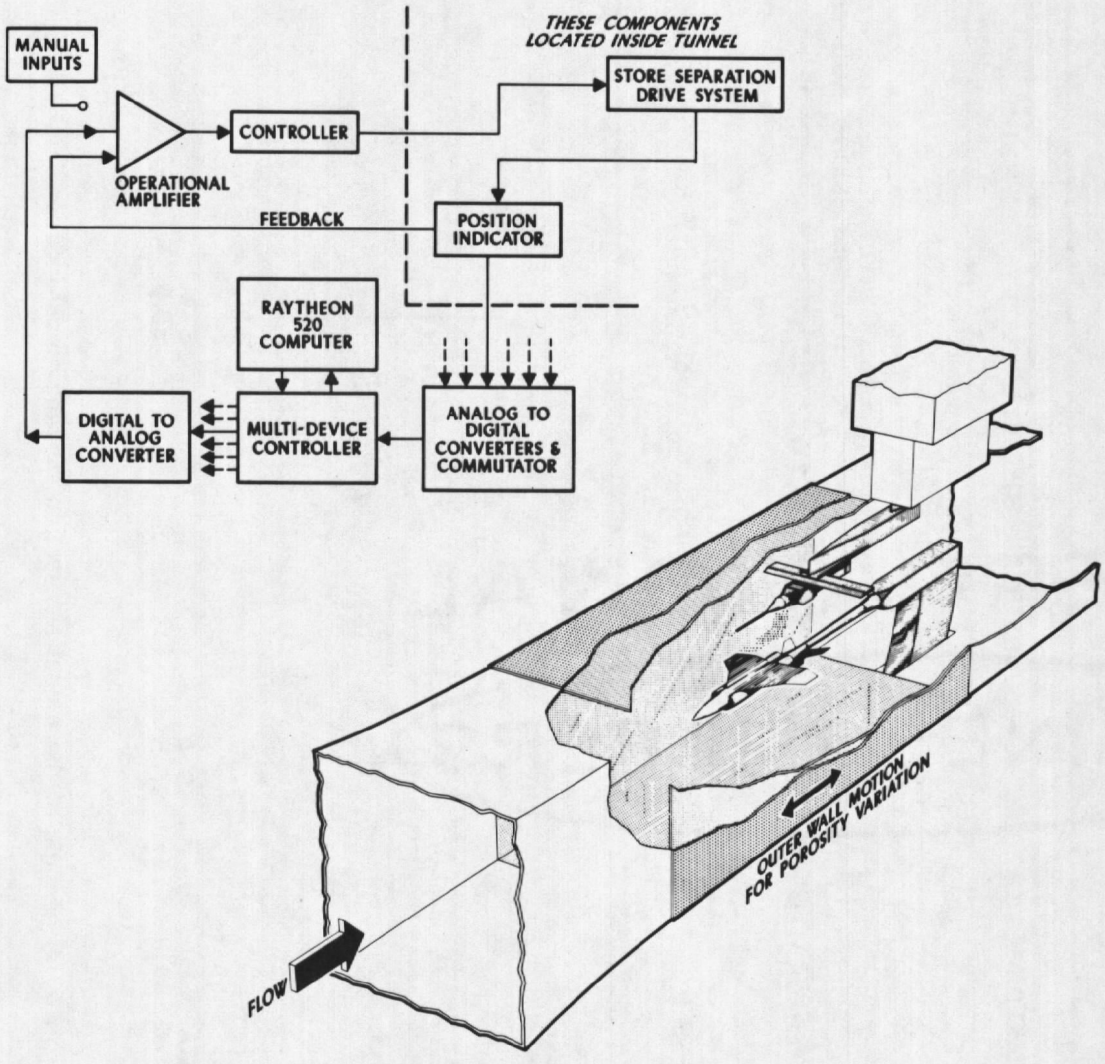

Figure 1. Isometric drawing of a typical flow-field probe installation and a block diagram of the computer control loop.

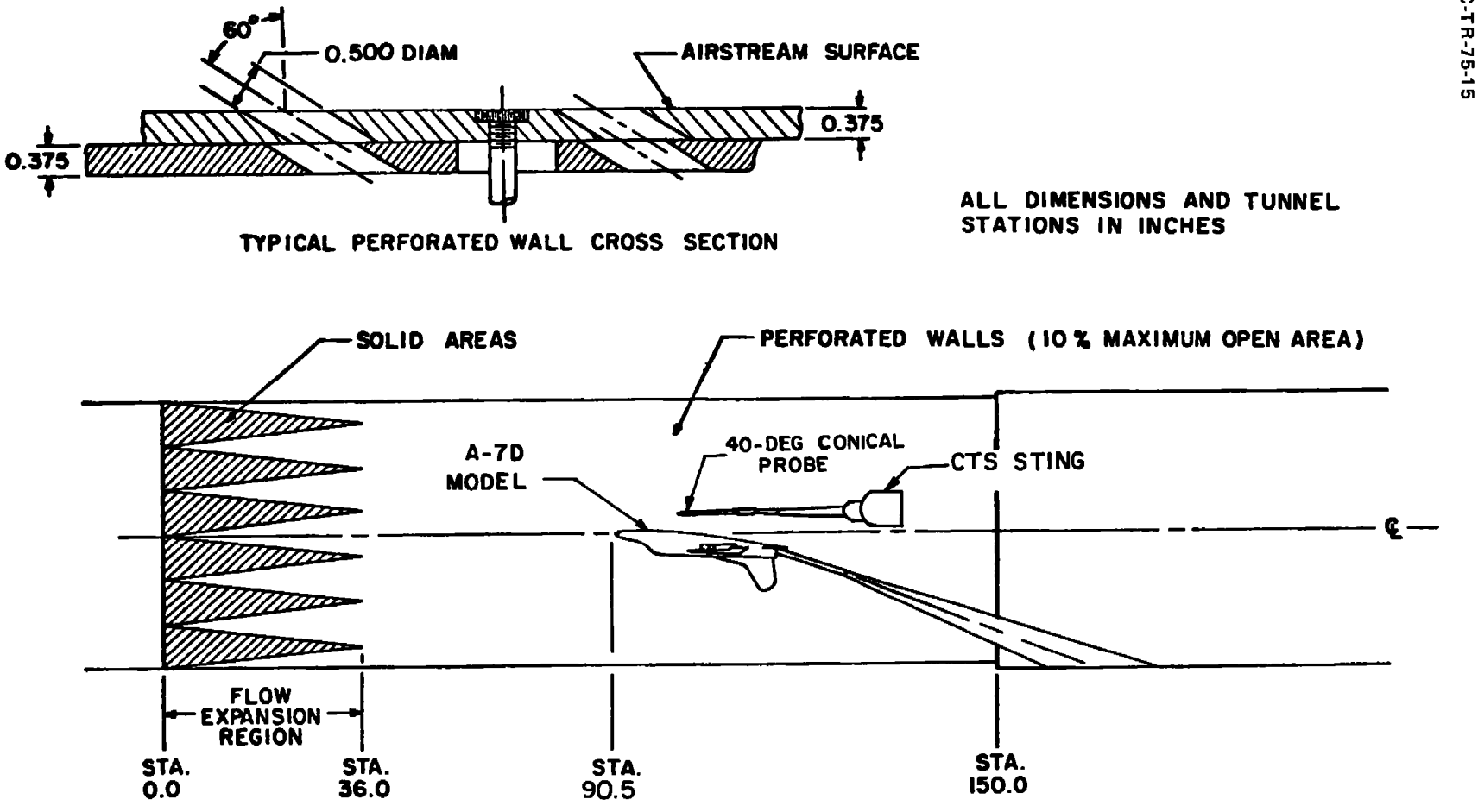

Figure 2. Schematic of the tunnel test section showing model location.

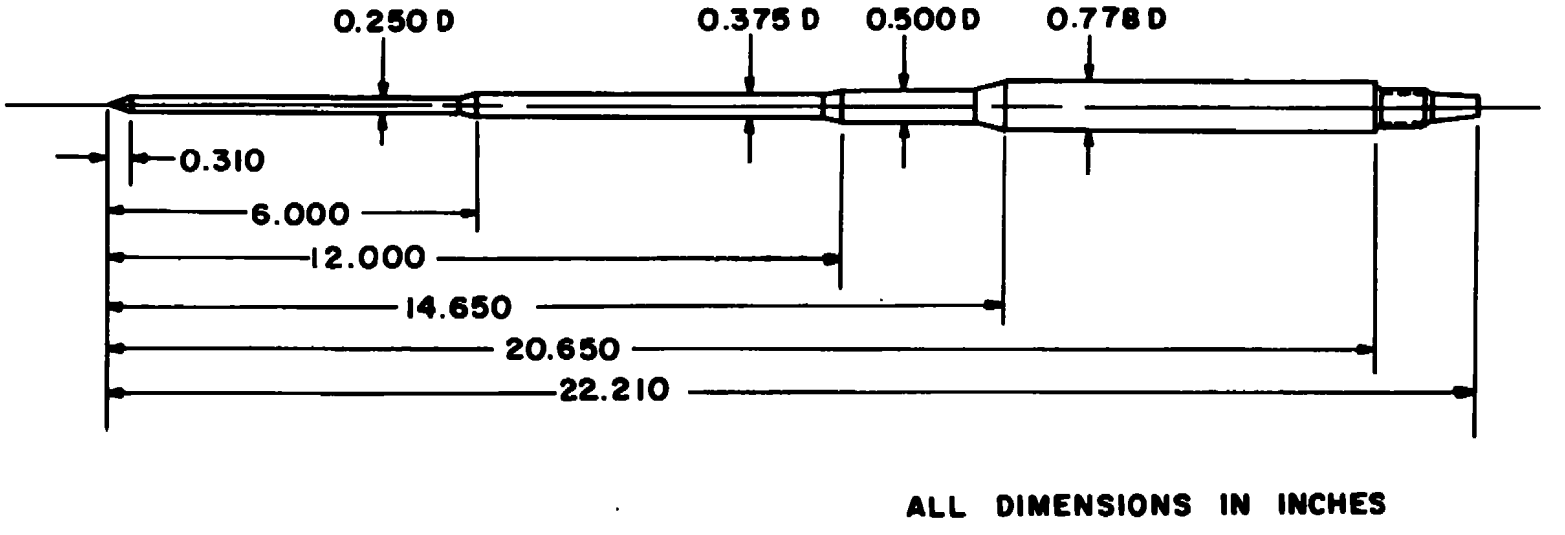

a. Basic configuration

Figure 3. Details of the 40-deg conical probe.

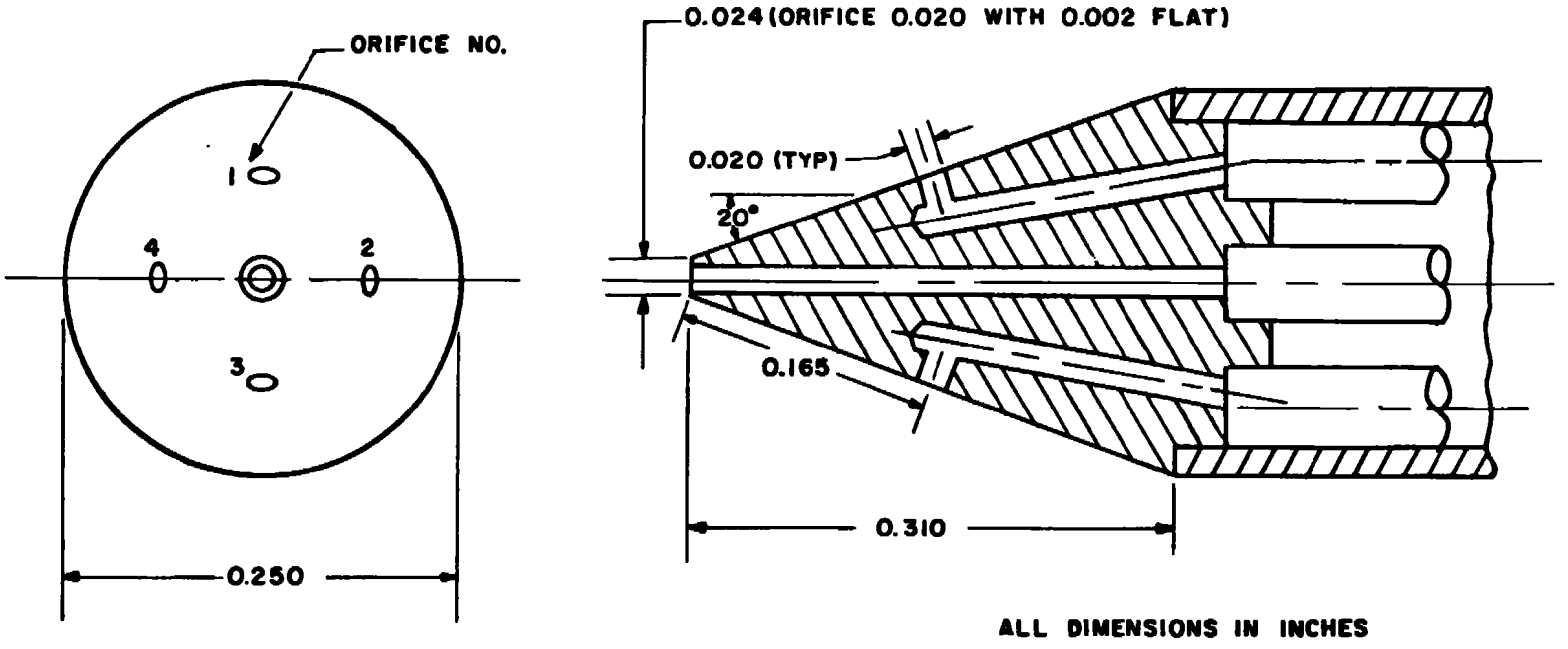

b. Probe tip
Figure 3. Concluded.

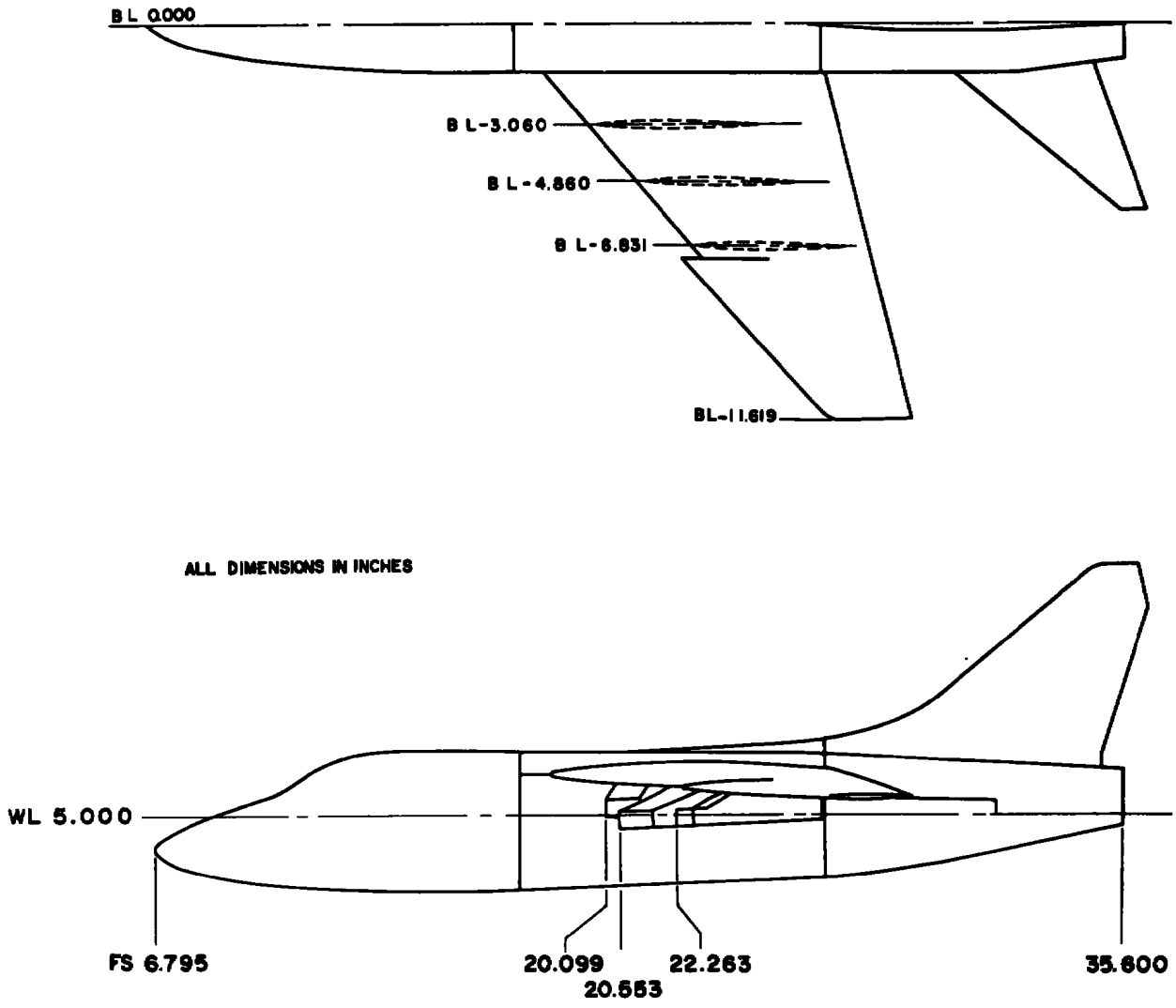

Figure 4. Sketch of the A-7D parent-aircraft model.

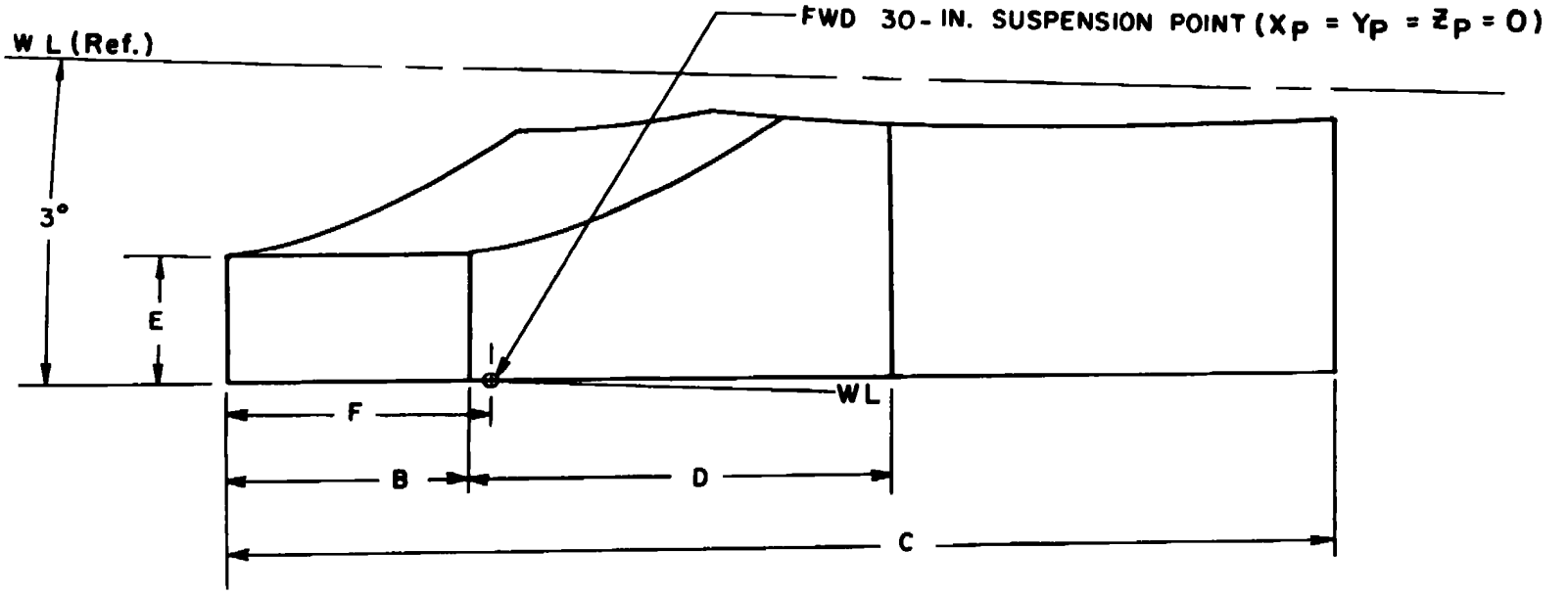

	INBOARD	CENTER	OUTBOARD
B	1.030	1.030	0.515
C	4.580	4.850	4.437
D	1.630	1.905	2.008
E	0.575	0.575	0.513
F	0.950	0.950	0.750
WL	4.968	4.695	4.717

ALL DIMENSIONS IN INCHES

Figure 5. Details of the A-7 pylon models.

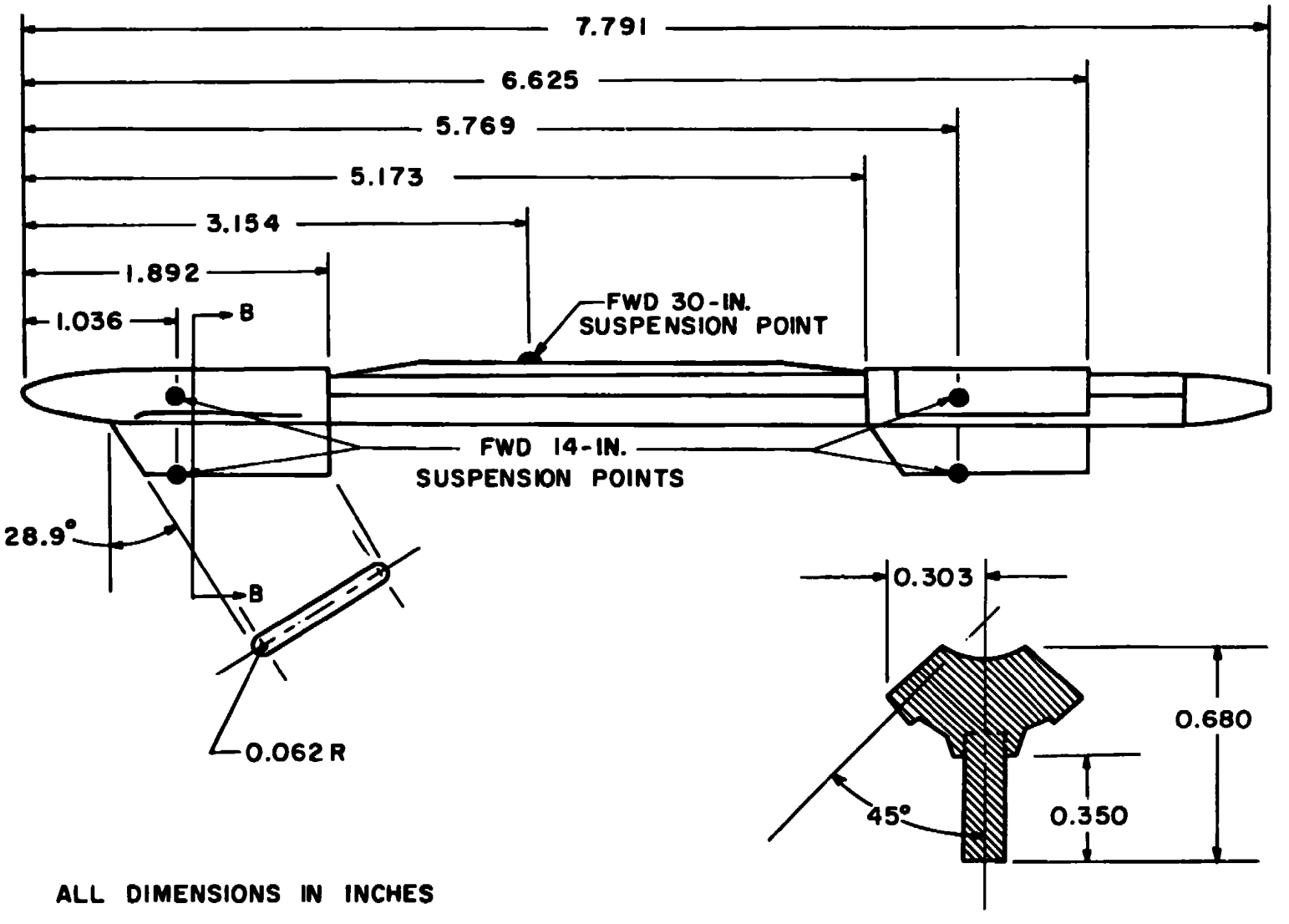

Figure 6. Details of the A-7 MER model.

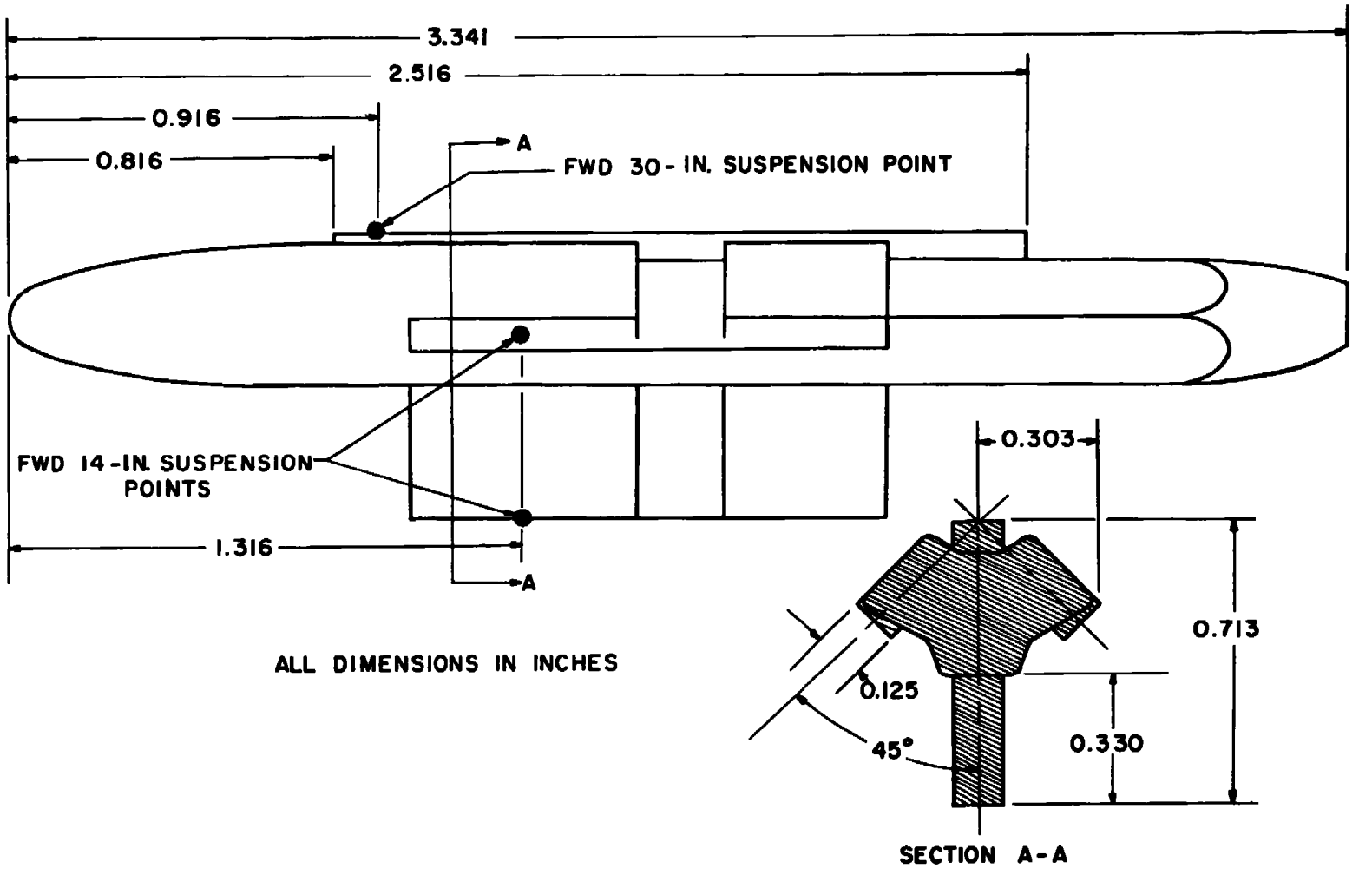

Figure 7. Details of the A-7 TER model.

ORDINATES

MODEL STA "X"	RADIUS "R"	MODEL STA "X"	RADIUS "R"
0 000	0 0000	2 250	0 5531
0 060	0 0000	2 500	0 5777
0 100	0 0511	2 750	0 5989
0 150	0 0751		CONSTANT SLOPE
0 200	0 0981	3 450	0.6625
0 250	0 1203		CONSTANT DIAM
0 300	0 1415	6 638	0 6625
0 350	0 1619		CONSTANT SLOPE
0 400	0 1815	7.713	0 5680
0 450	0 2003	7 763	0 5637
0 500	0 2183	8.013	0 5409
0 550	0 2355	8 263	0 5162
0 600	0.2521	8 513	0 4899
0 650	0.2680	8 763	0 4620
0 700	0 2833	9 013	0 4327
0 750	0 2979	9 113	0 4206
0 800	0 3119		CONSTANT SLOPE
0 850	0 3253	10 900	0 1815
0 900	0.3383	10 950	0 1733
1 000	0 3625	11 000	0 1646
1 250	0 4153	11 100	0.1441
1 500	0 4587	11 200	0 1170
1 750	0 4950	11 300	0 0725
2 000	0 5260	11 350	0.0000

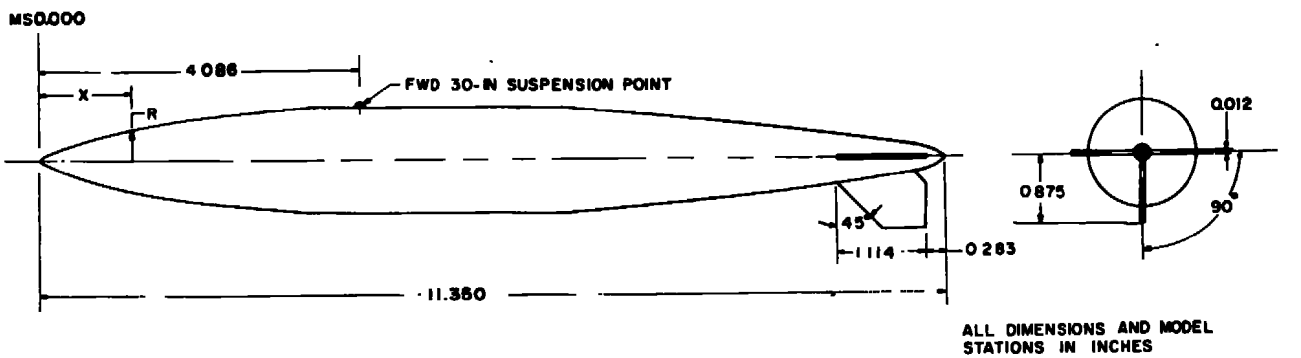

Figure 8. Details of the A-7 300-gal fuel tank model.

STA.	DIAM
0.000	0.150
0.210	0.150
0.212	0.231
0.312	0.282
0.412	0.322
0.512	0.361
0.612	0.391
0.712	0.421
0.812	0.445
0.912	0.465
1.012	0.483
1.112	0.497
1.212	0.510
1.312	0.520
1.412	0.525
1.512	0.530
1.612	0.532
1.712	0.533
1.812	0.535
1.912	0.537
2.312	0.537
2.412	0.535
2.512	0.525
2.612	0.520
2.712	0.510
2.812	0.497
2.912	0.483
3.012	0.465
3.173	0.438

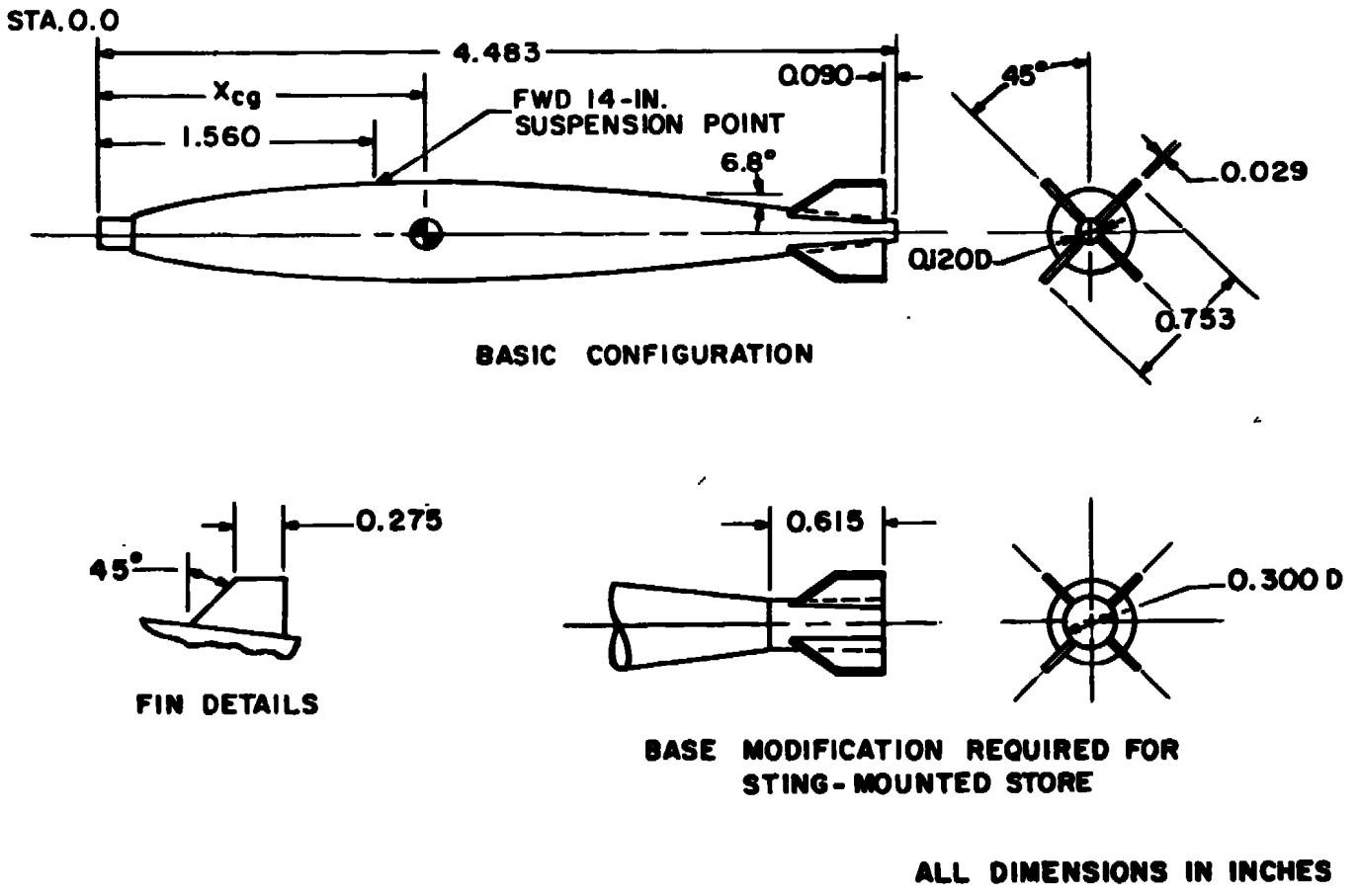

Figure 9. Details of the MK-82GP model.

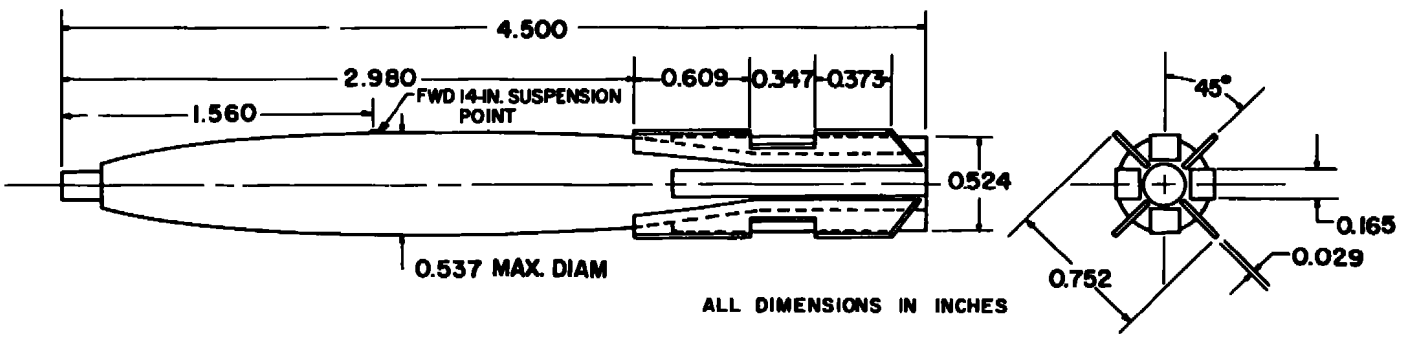

Figure 10. Details of the MK-82SE model.

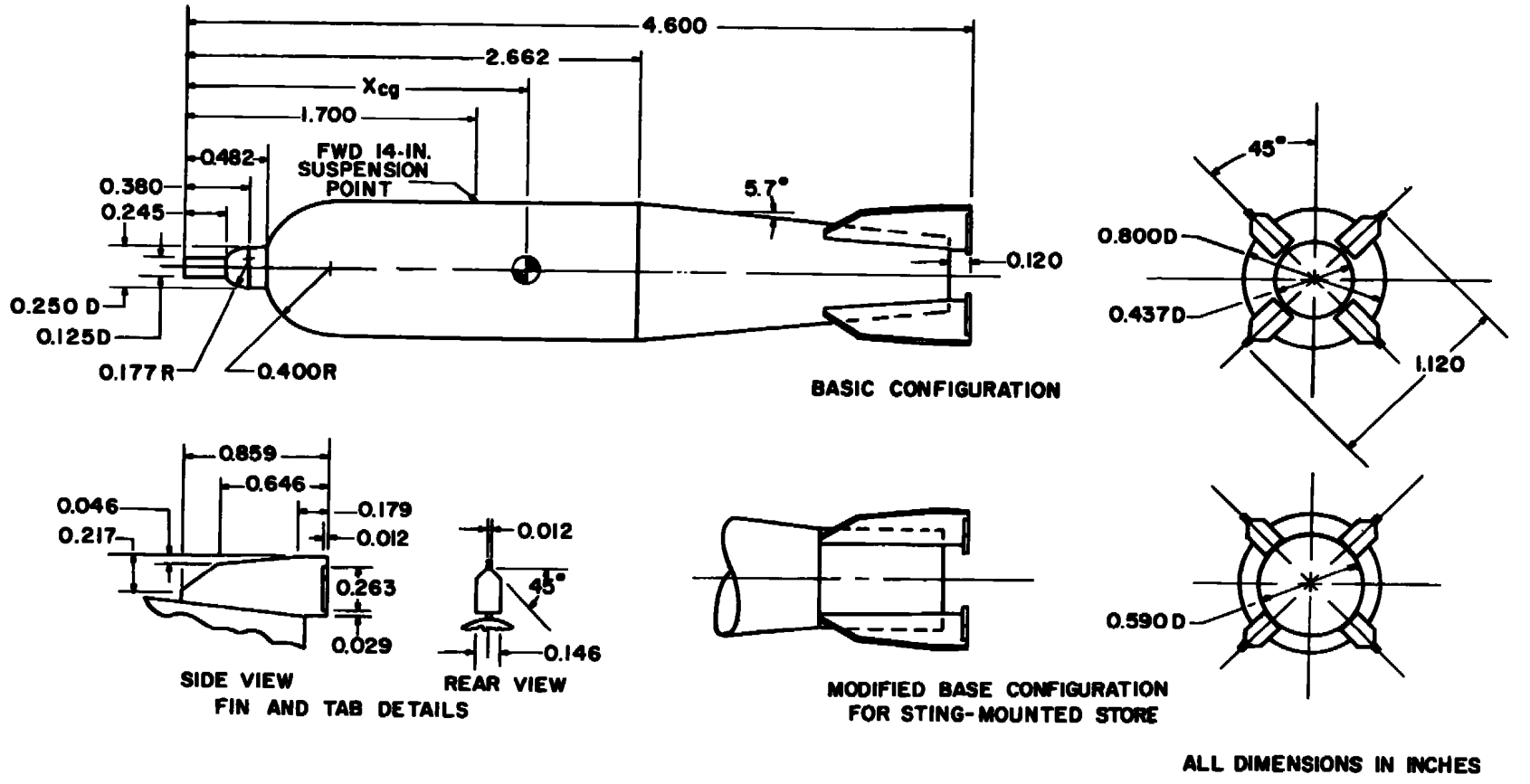

Figure 11. Details of the SUU-30H/B model.

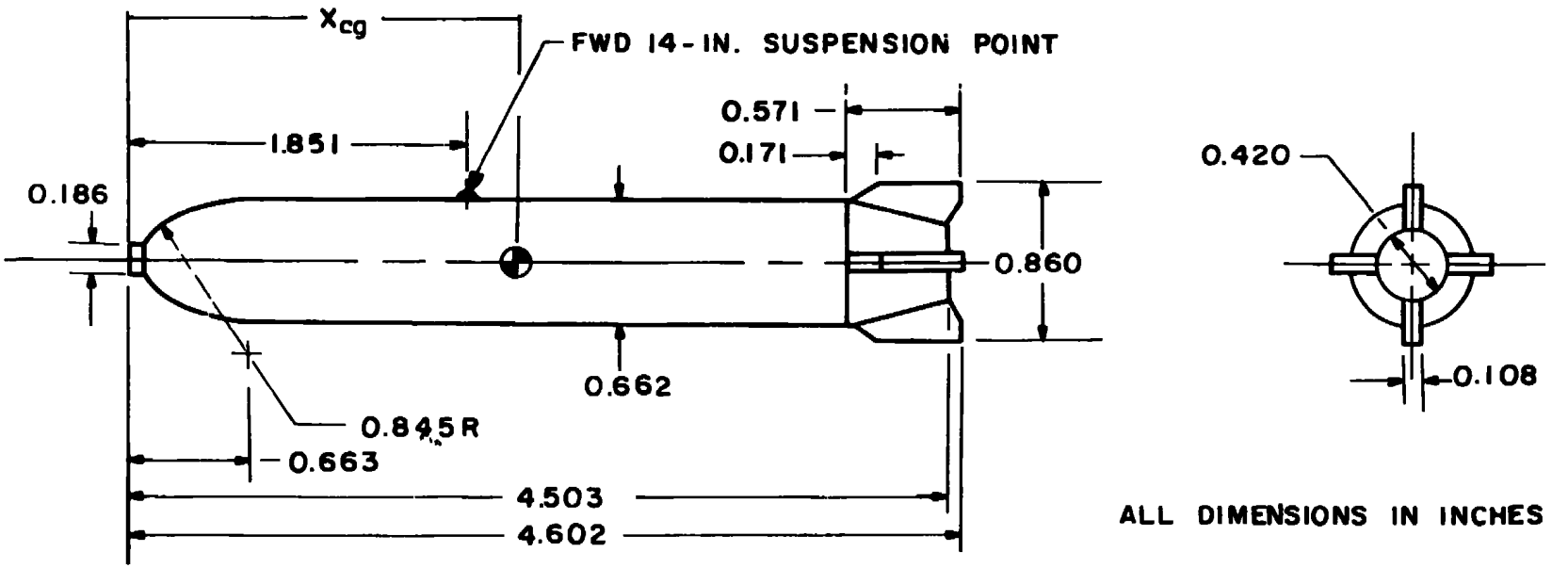

Figure 12. Details of the MK-20 "Rockeye" model.

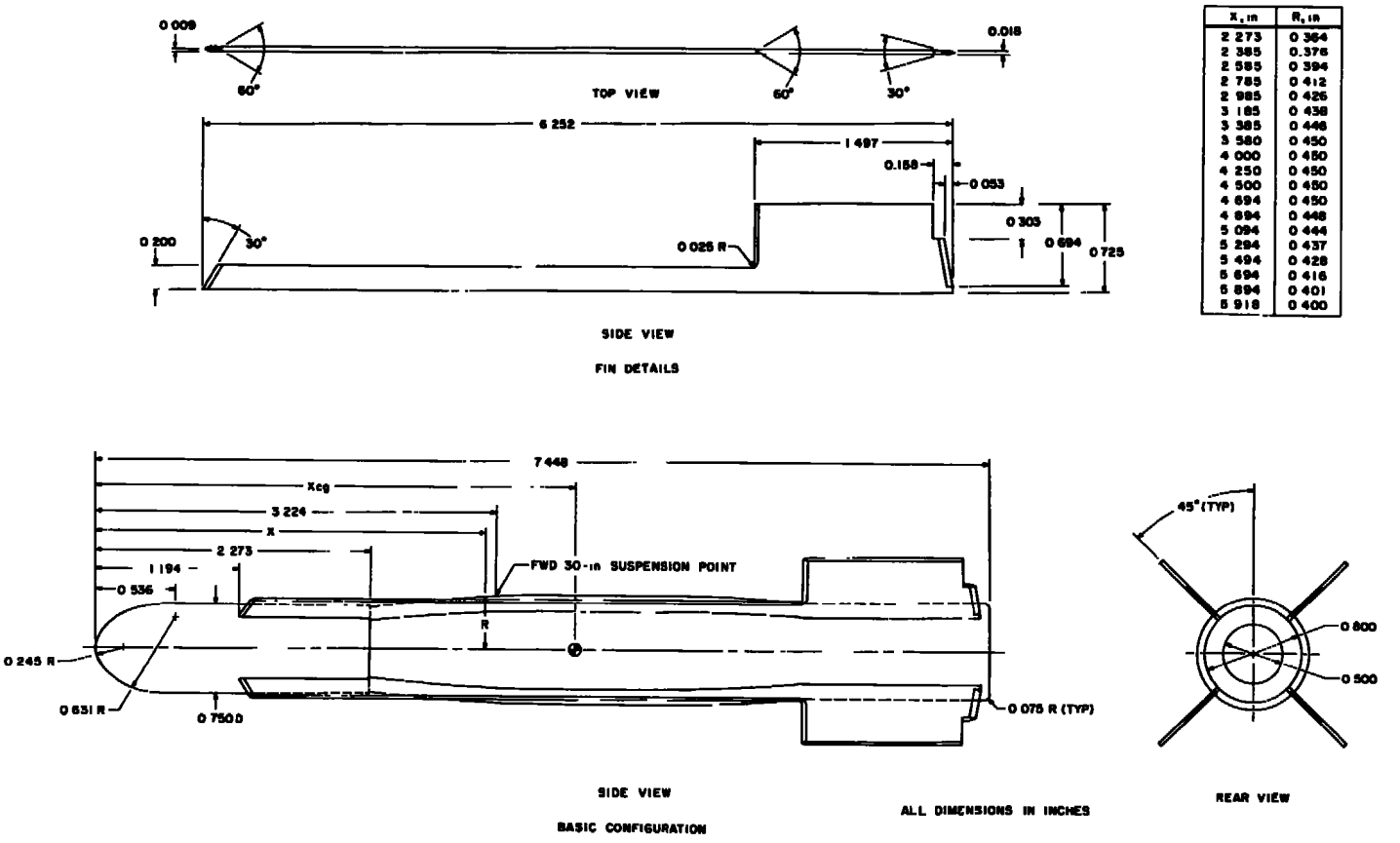

X, in	R, in
2 273	0 364
2 385	0.376
2 585	0 394
2 785	0 412
2 985	0 426
3 185	0 438
3 385	0 446
3 580	0 450
4 000	0 450
4 250	0 450
4 500	0 450
4 694	0 450
4 894	0 448
5 094	0 444
5 294	0 437
5 494	0 428
5 694	0 416
5 894	0 401
5 918	0 400

Figure 13. Details of the MK-84EOGB model.

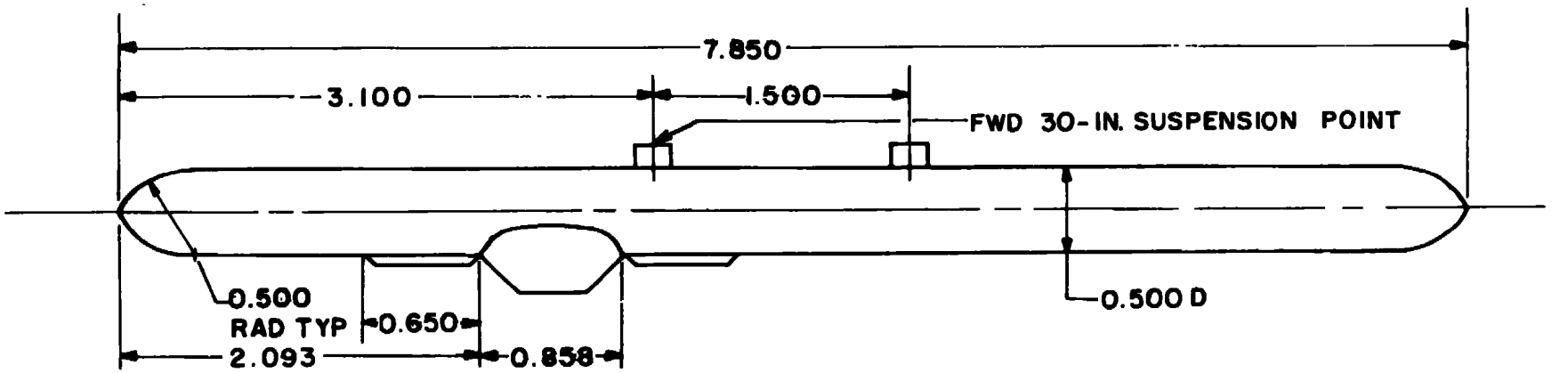

ALL DIMENSIONS IN INCHES

Figure 14. Details of the QRC-335A ECM pod model.

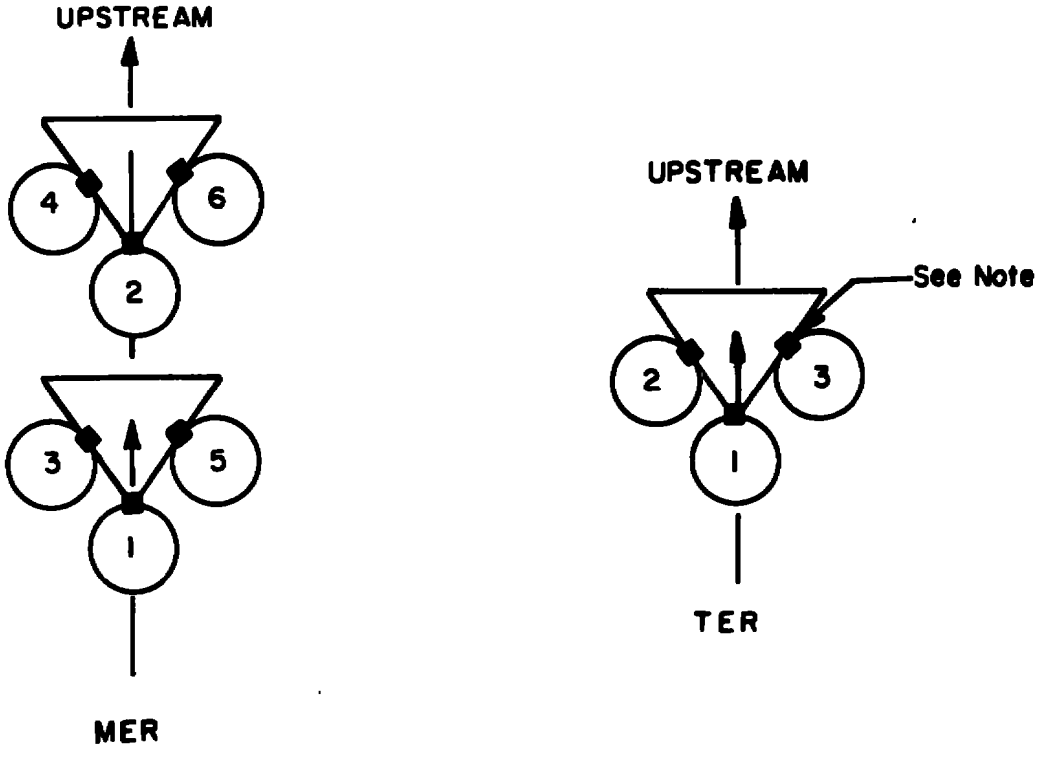

NOTE: The square indicates the orientation of the suspension lugs

TYPE RACK	STATION	ROLL ORIENTATION, deg
MER	1	0
	2	0
	3	45
	4	45
	5	-45
	6	-45
TER	1	0
	2	45
	3	-45

Figure 15. Schematic of the MER and TER store stations and orientations.

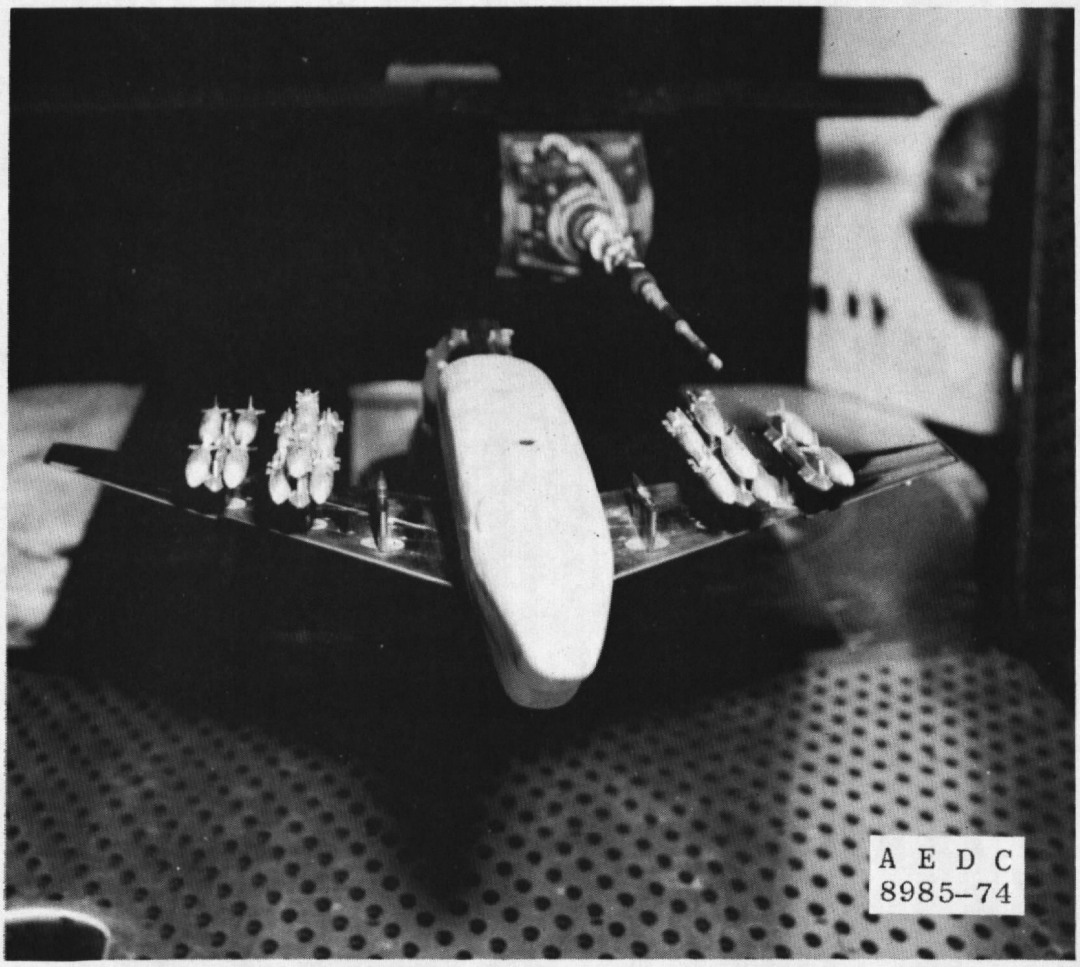

Figure 16. Tunnel installation photograph showing parent aircraft, probe, and CTS.

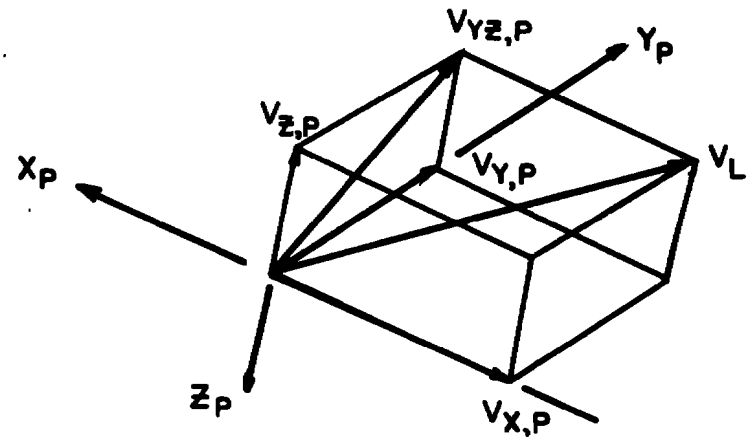

Note: Pylon axis system origin ($X_P = Y_P = Z_P = 0$) at forward 30-in. suspension point of each pylon (see Fig. 5).

Figure 17. Axis system defining directions and velocity vectors for flow-field measurements.

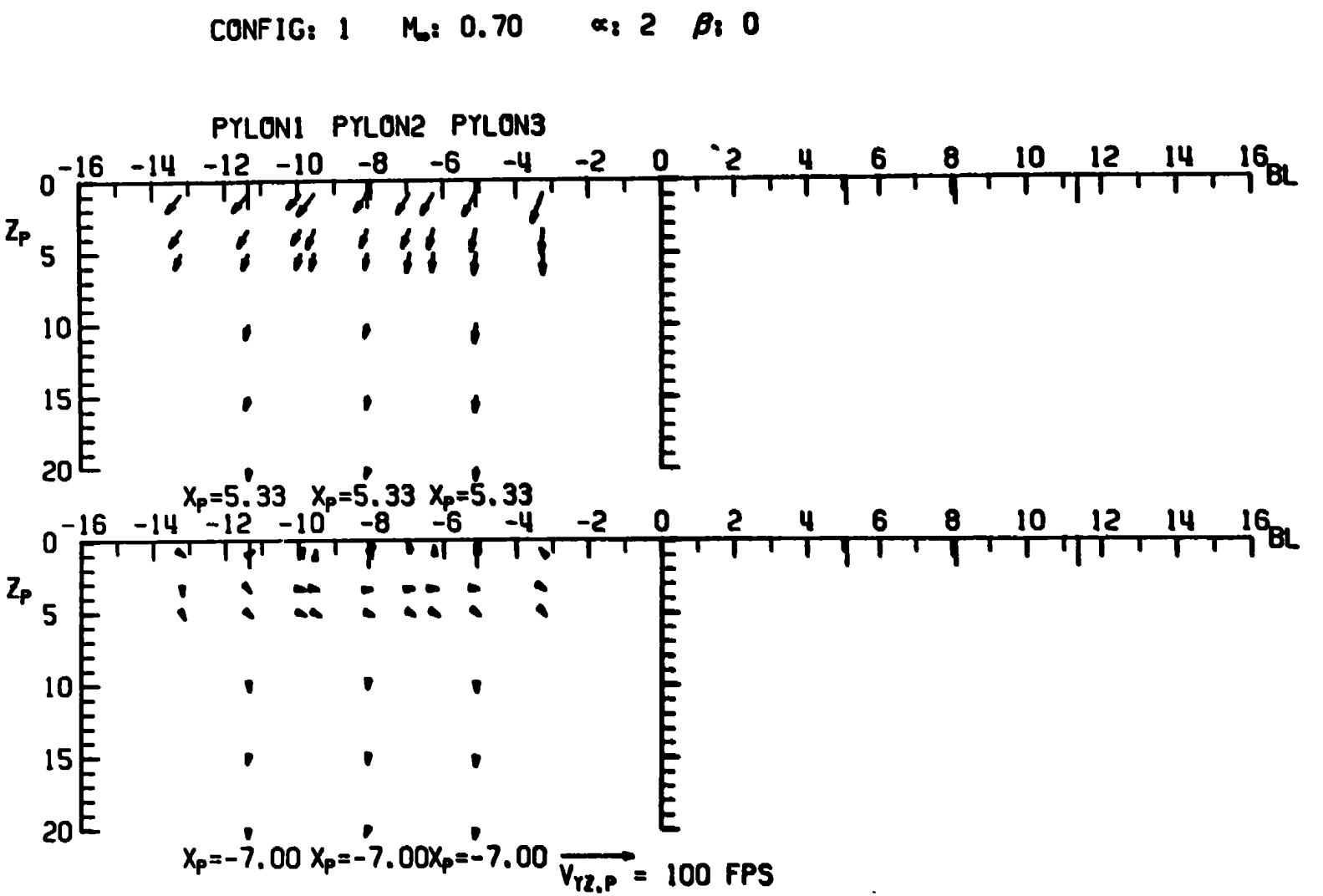

a. $M_\infty = 0.70$, $\alpha = 2$ deg

Figure 18. Flow-field measurements under the left wing of the A-7D with no external stores, configuration 1.

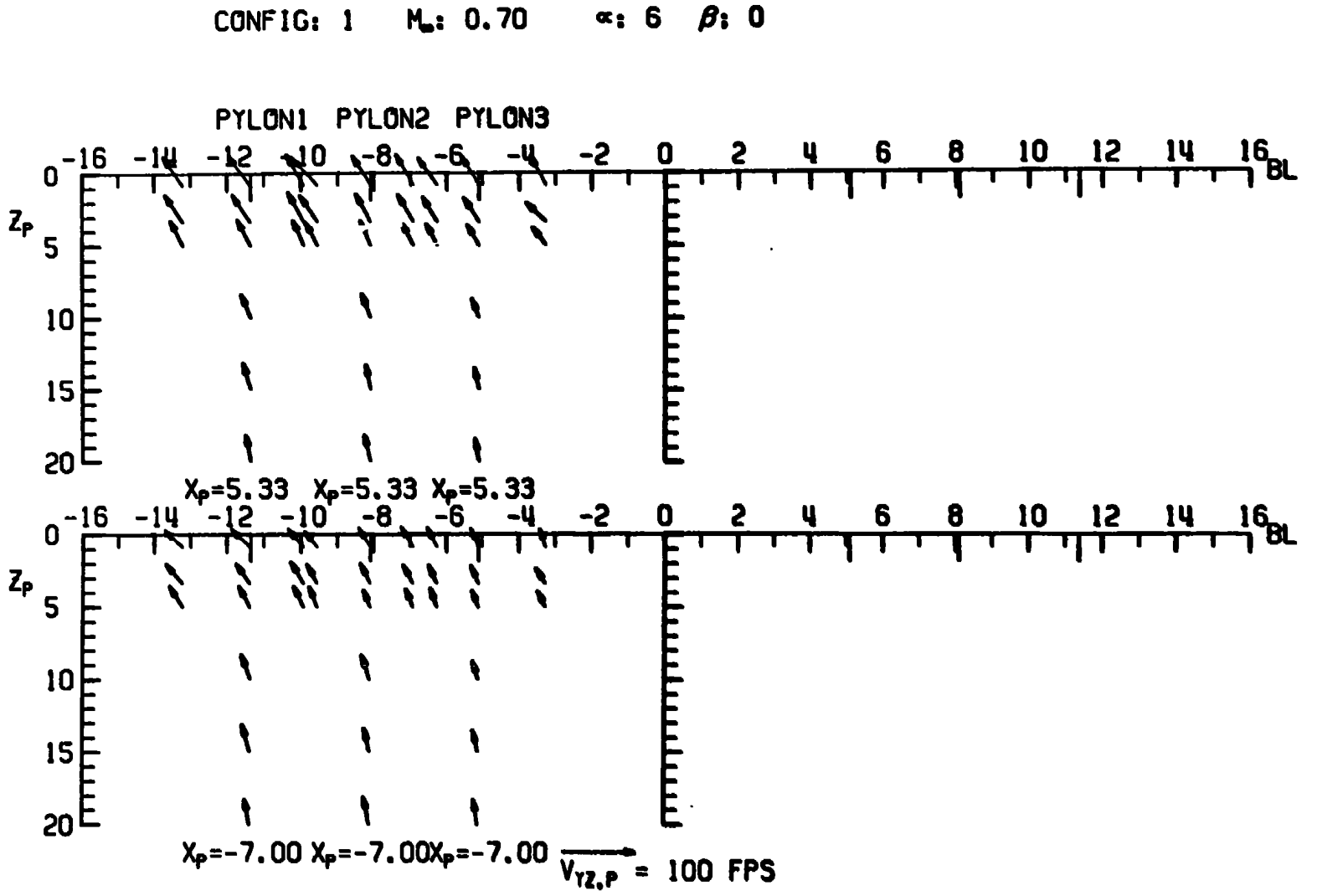

b. M_∞ = 0.70, α = 6 deg

Figure 18. Continued.

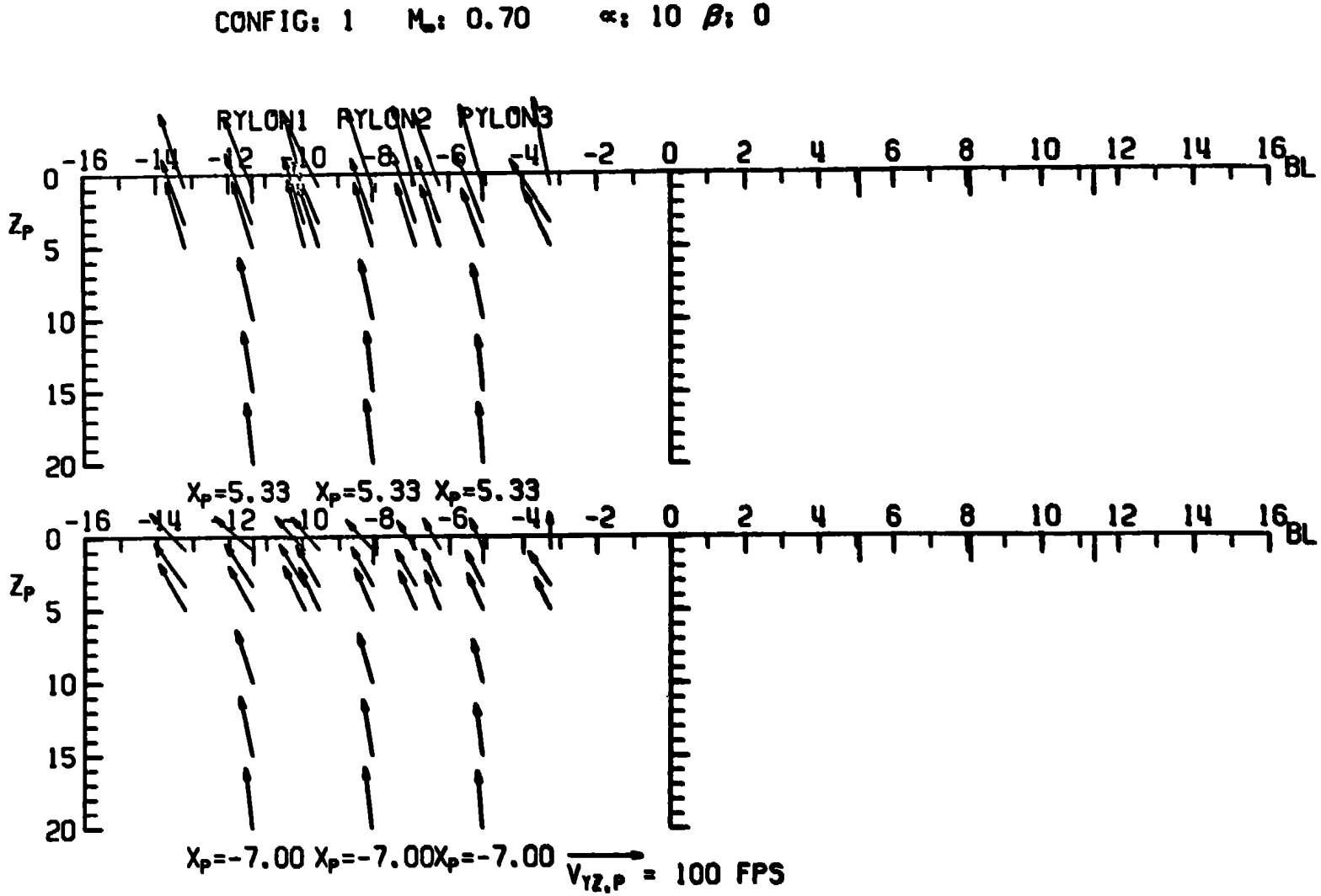

c. $M_\infty = 0.70$, $\alpha = 10$ deg

Figure 18. Continued.

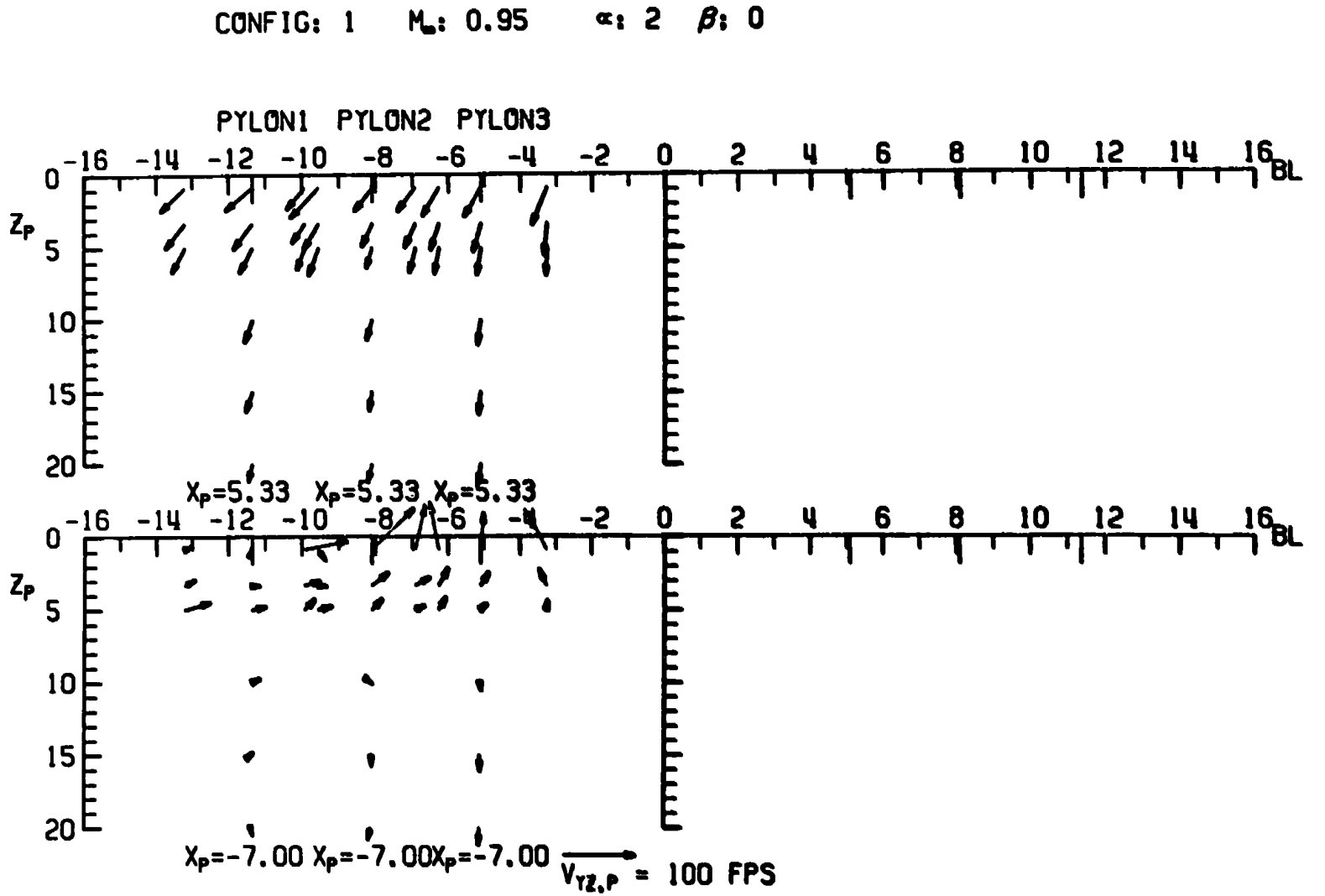

d. M_∞ = 0.95, α = 2 deg

Figure 18. Continued.

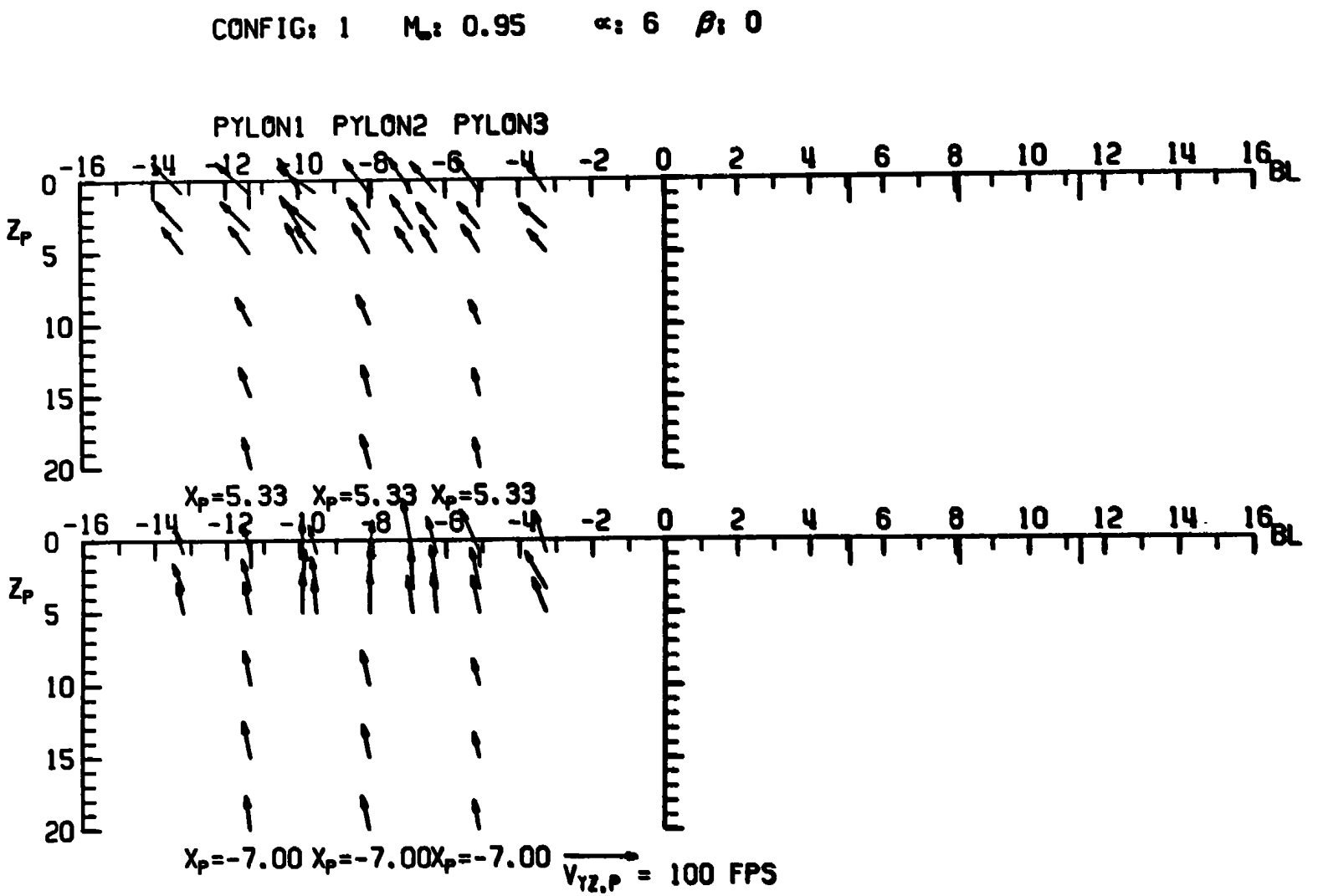

e. $M_\infty = 0.95$, $\alpha = 6$ deg

Figure 18. Concluded.

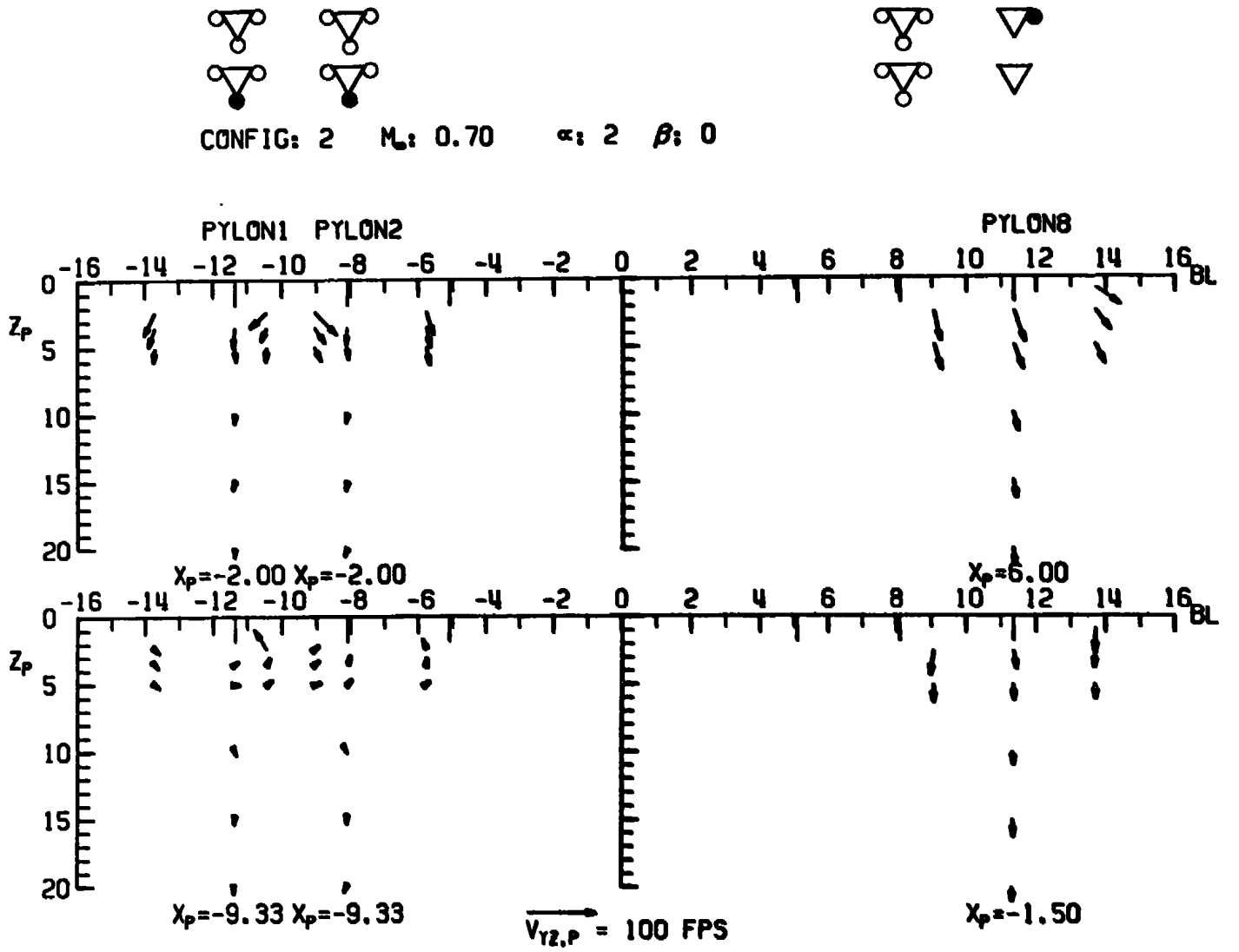

a. $M_\infty = 0.70$, $\alpha = 2$ deg

Figure 19. Flow-field measurements under the left and right wings of the A-7D with external stores, configuration 2.

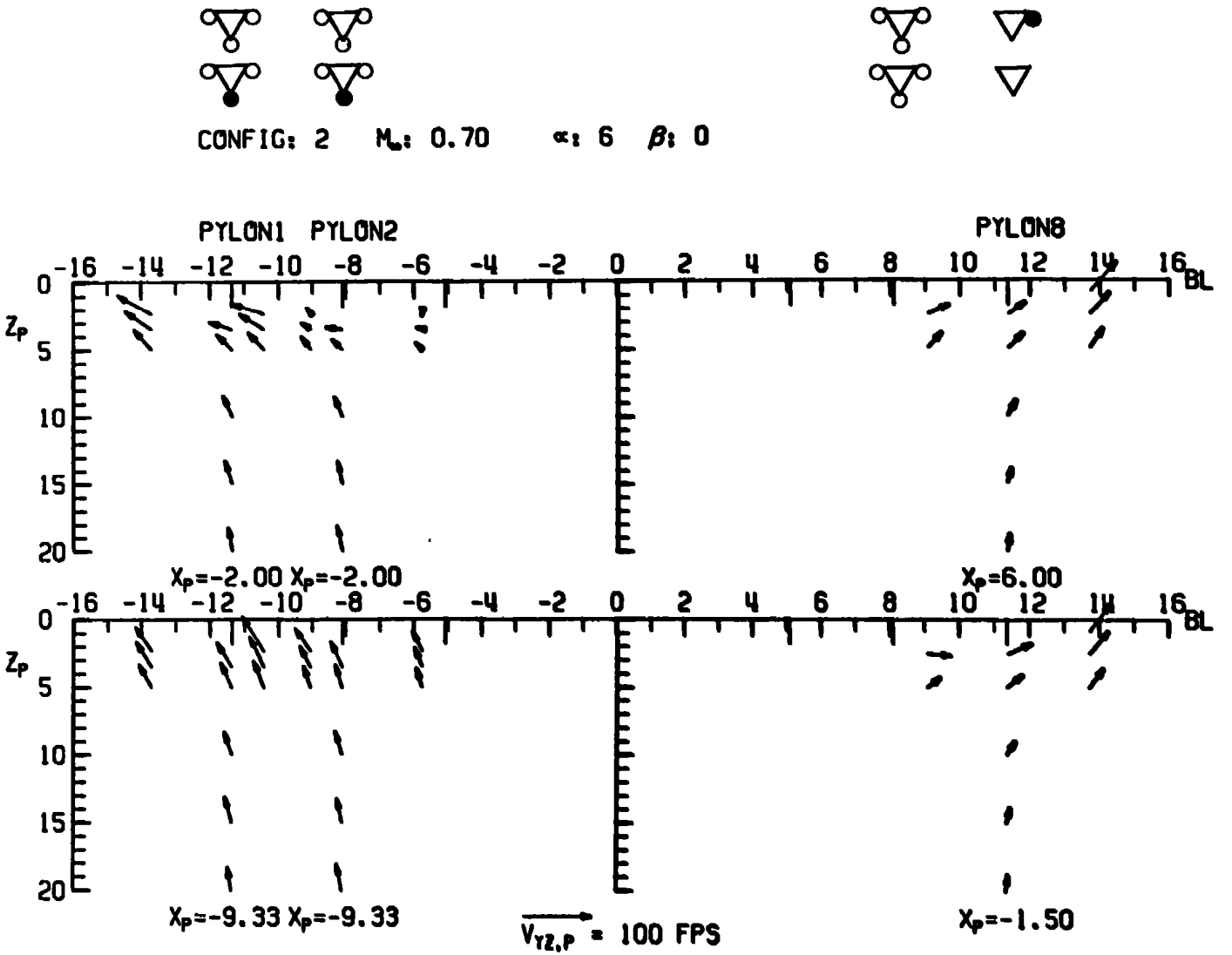

b. $M_\infty = 0.70$, $\alpha = 6$ deg

Figure 19. Continued.

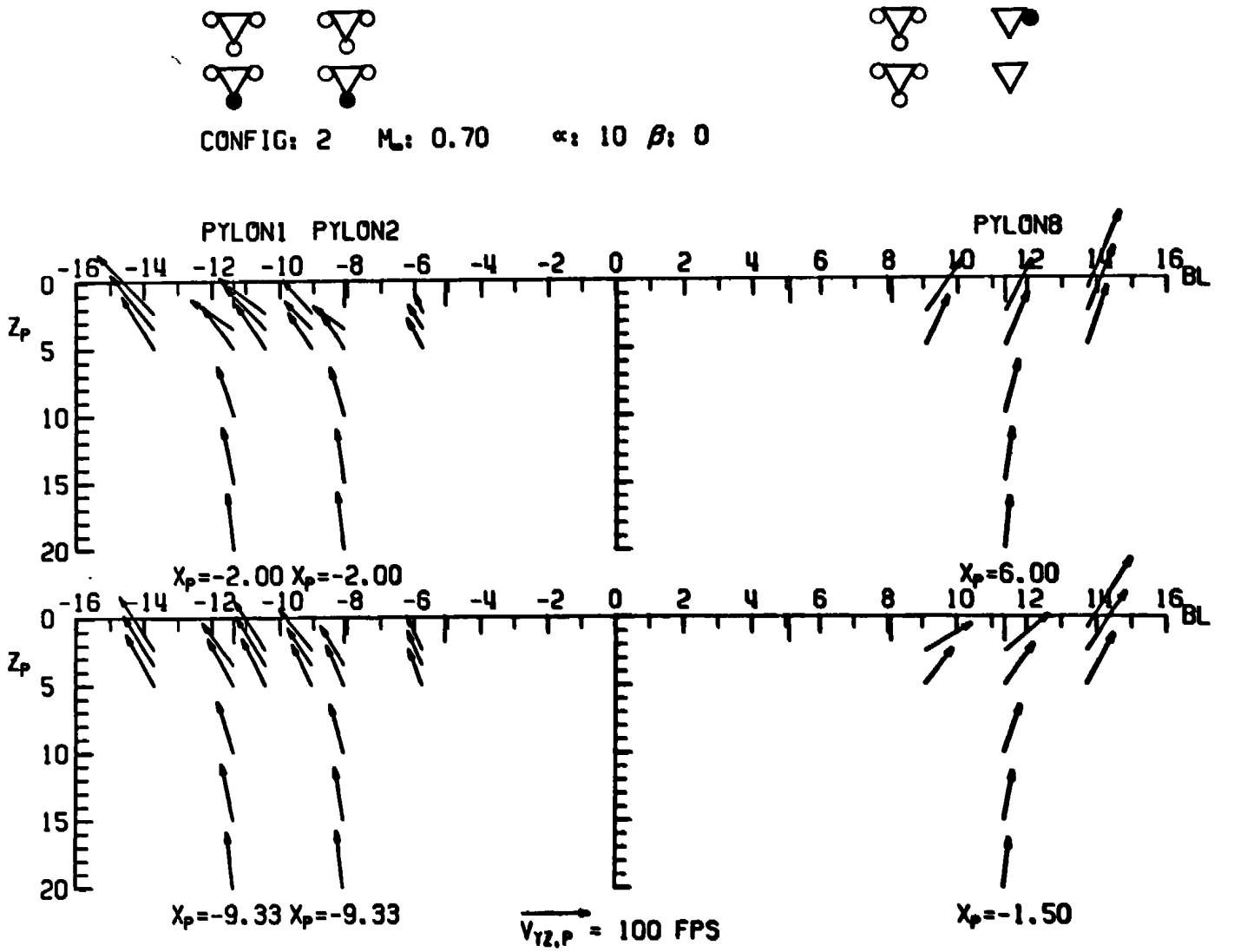

c. M_∞ = 0.70, α = 10 deg

Figure 19. Continued.

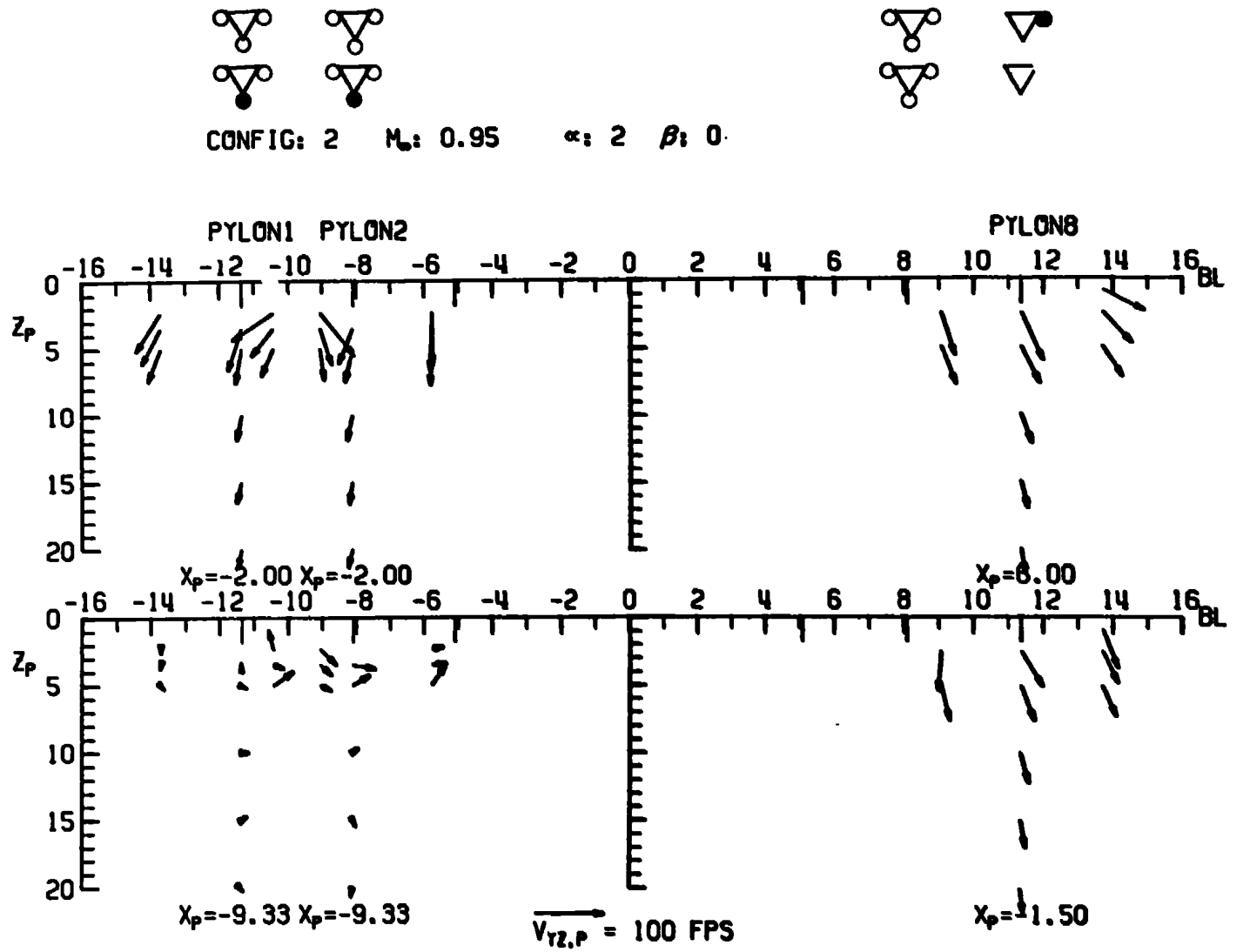

d. $M_\infty = 0.95$, $\alpha = 2$ deg
Figure 19. Continued.

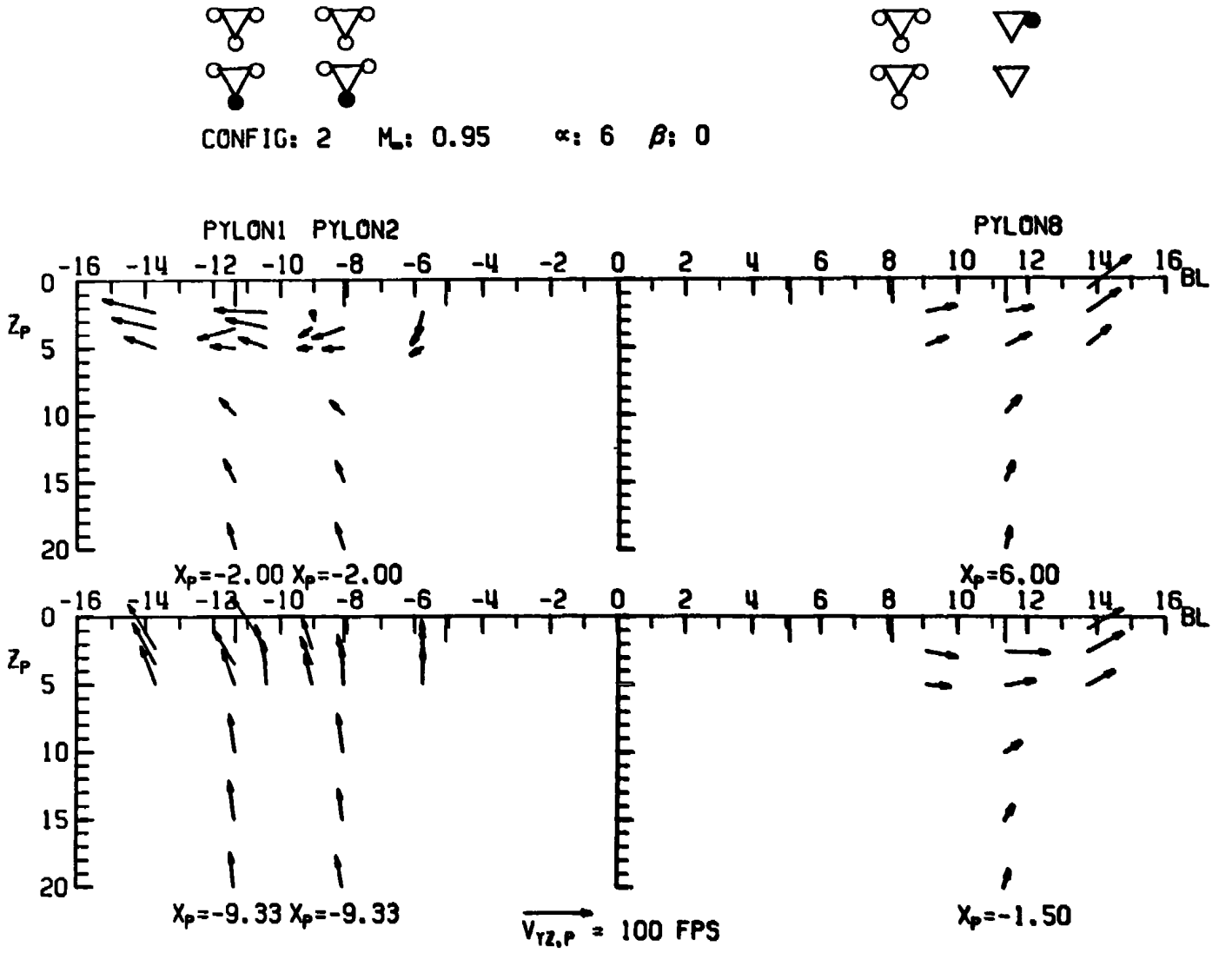

e. $M_\infty = 0.95$, $\alpha = 6$ deg

Figure 19. Concluded.

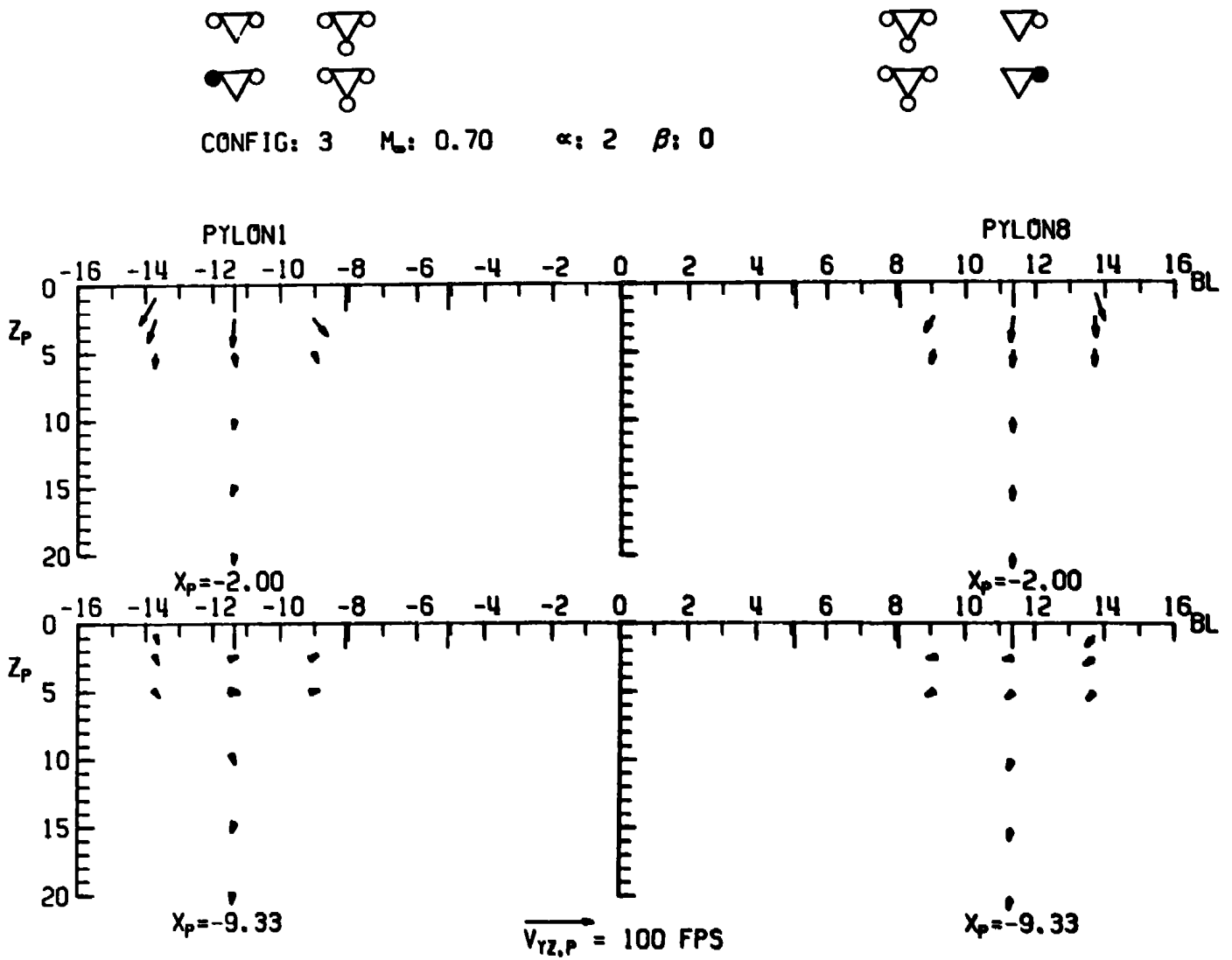

a. $M_\infty = 0.70$, $\alpha = 2$ deg

Figure 20. Flow-field measurements under the left and right wings of the A-7D with external stores, configuration 3.

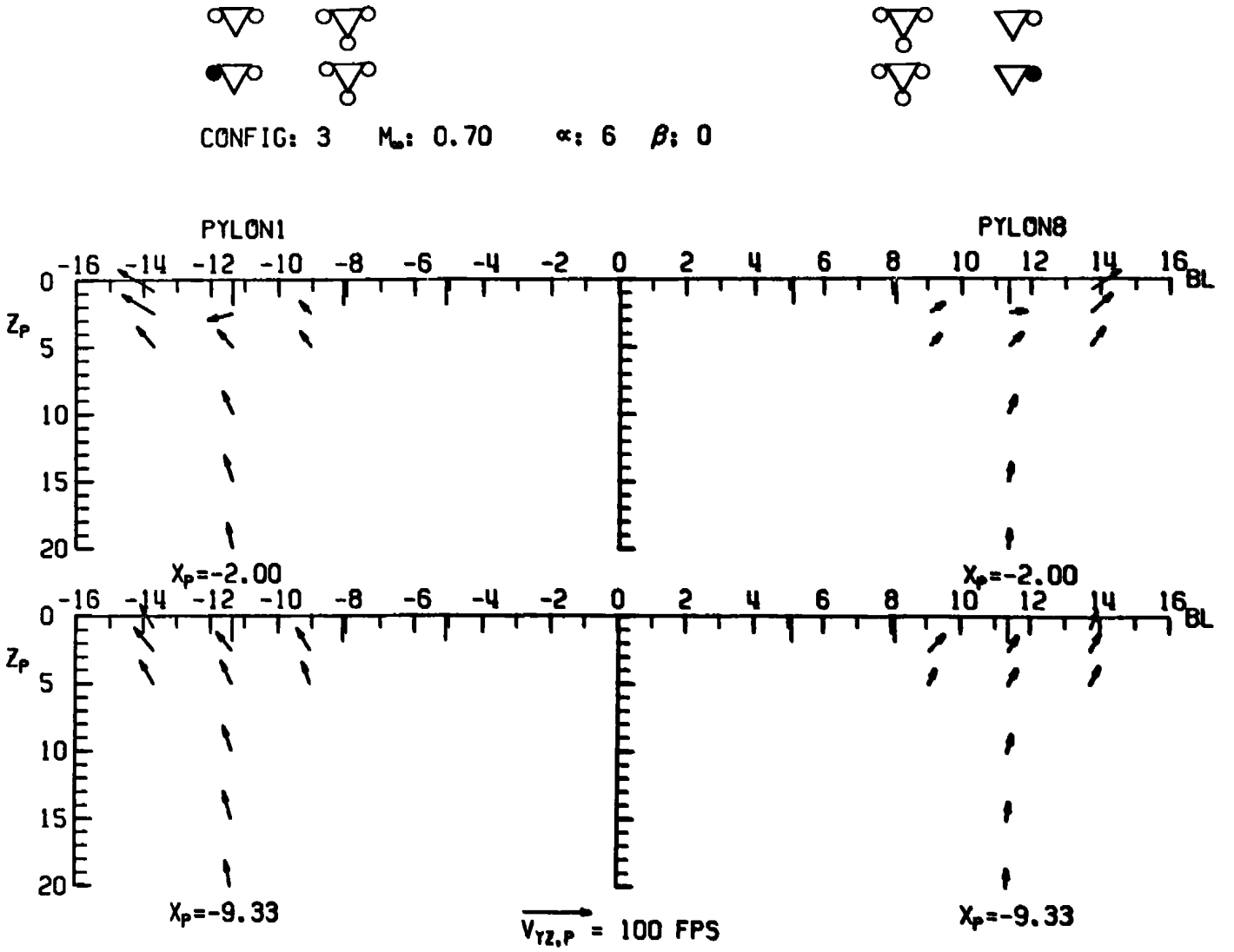

b. $M_\infty = 0.70$, $\alpha = 6$ deg

Figure 20. Continued.

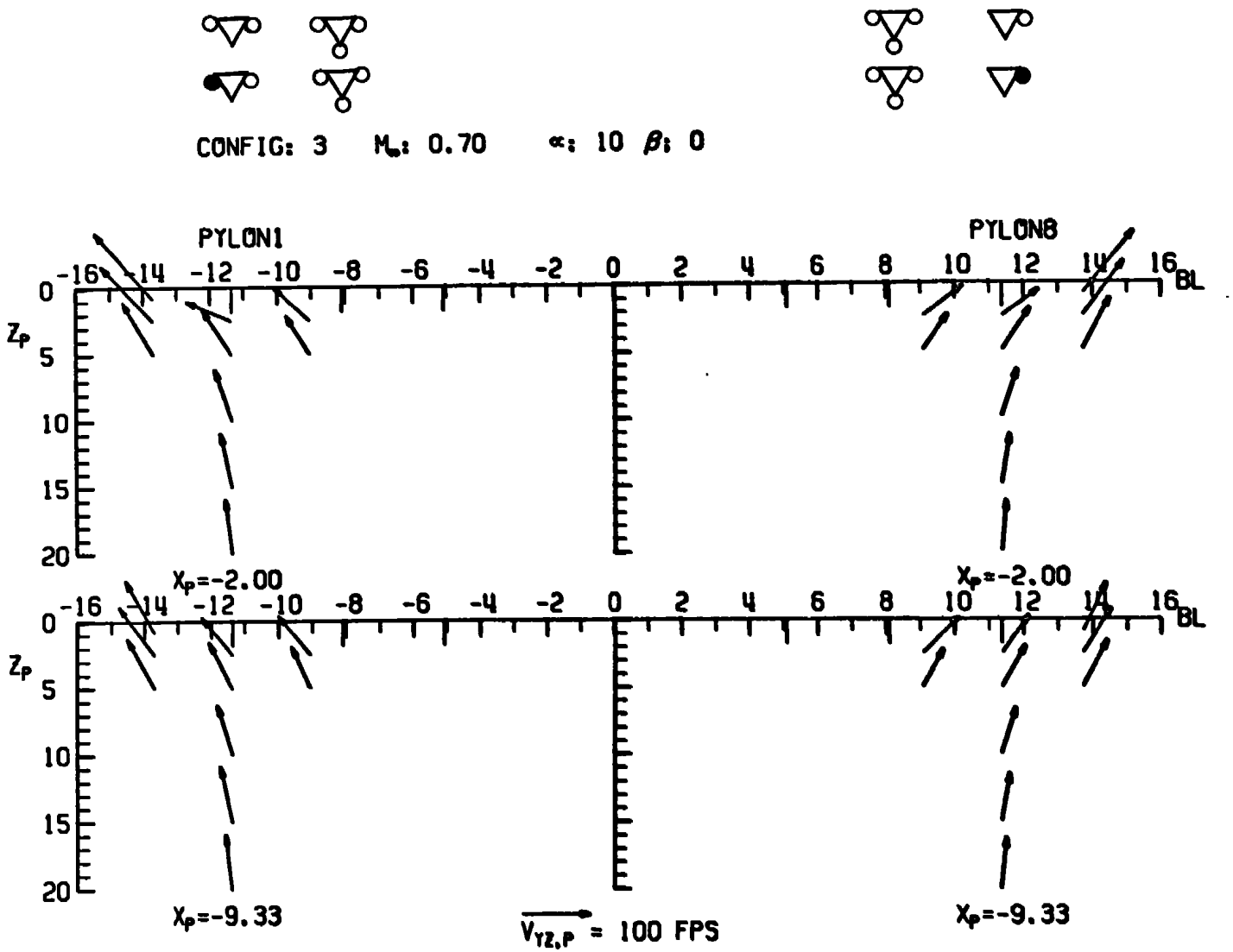

c. $M_\infty = 0.70$, $\alpha = 10$ deg
Figure 20. Continued.

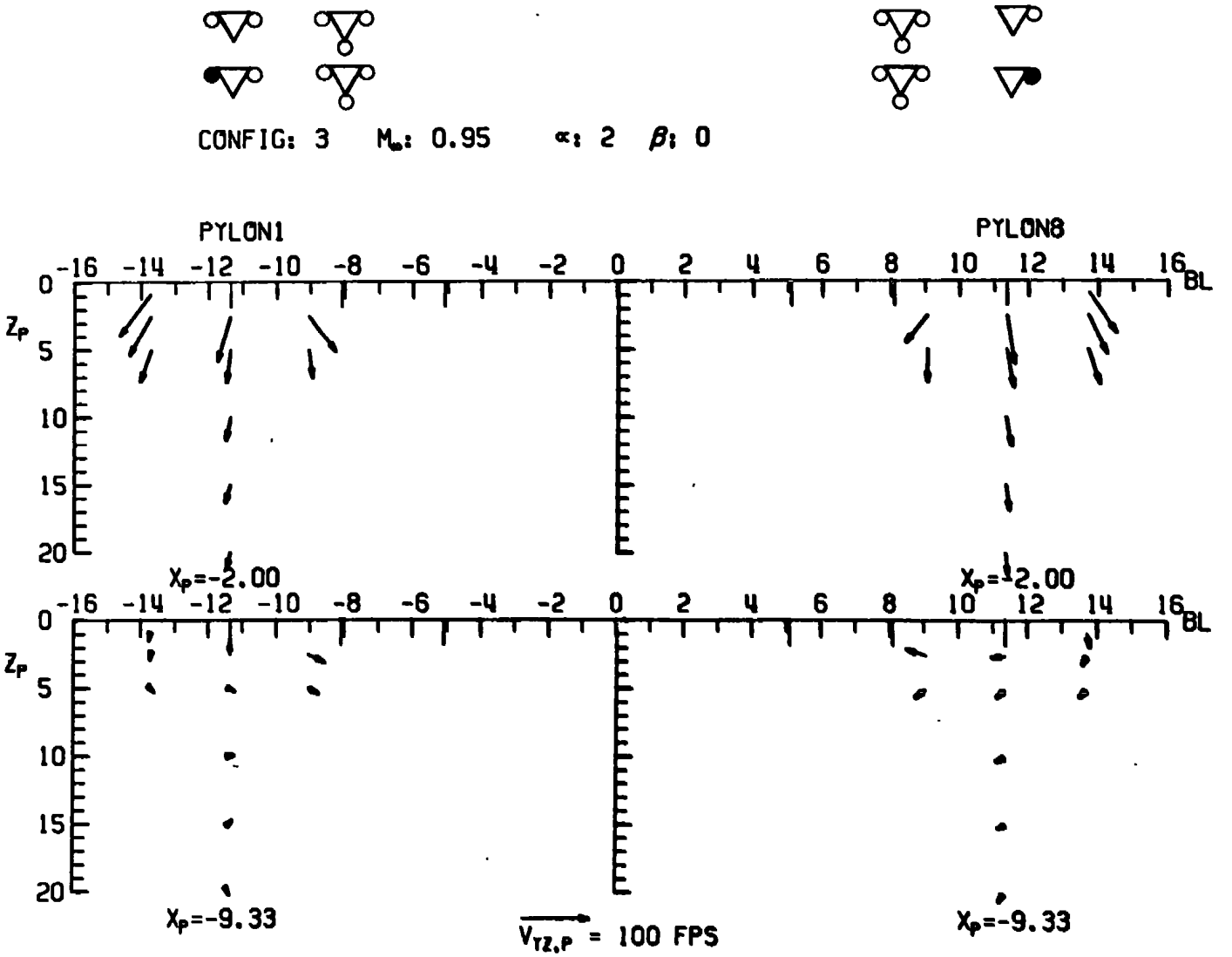

d. $M_\infty = 0.95$, $\alpha = 2$ deg

Figure 20. Continued.

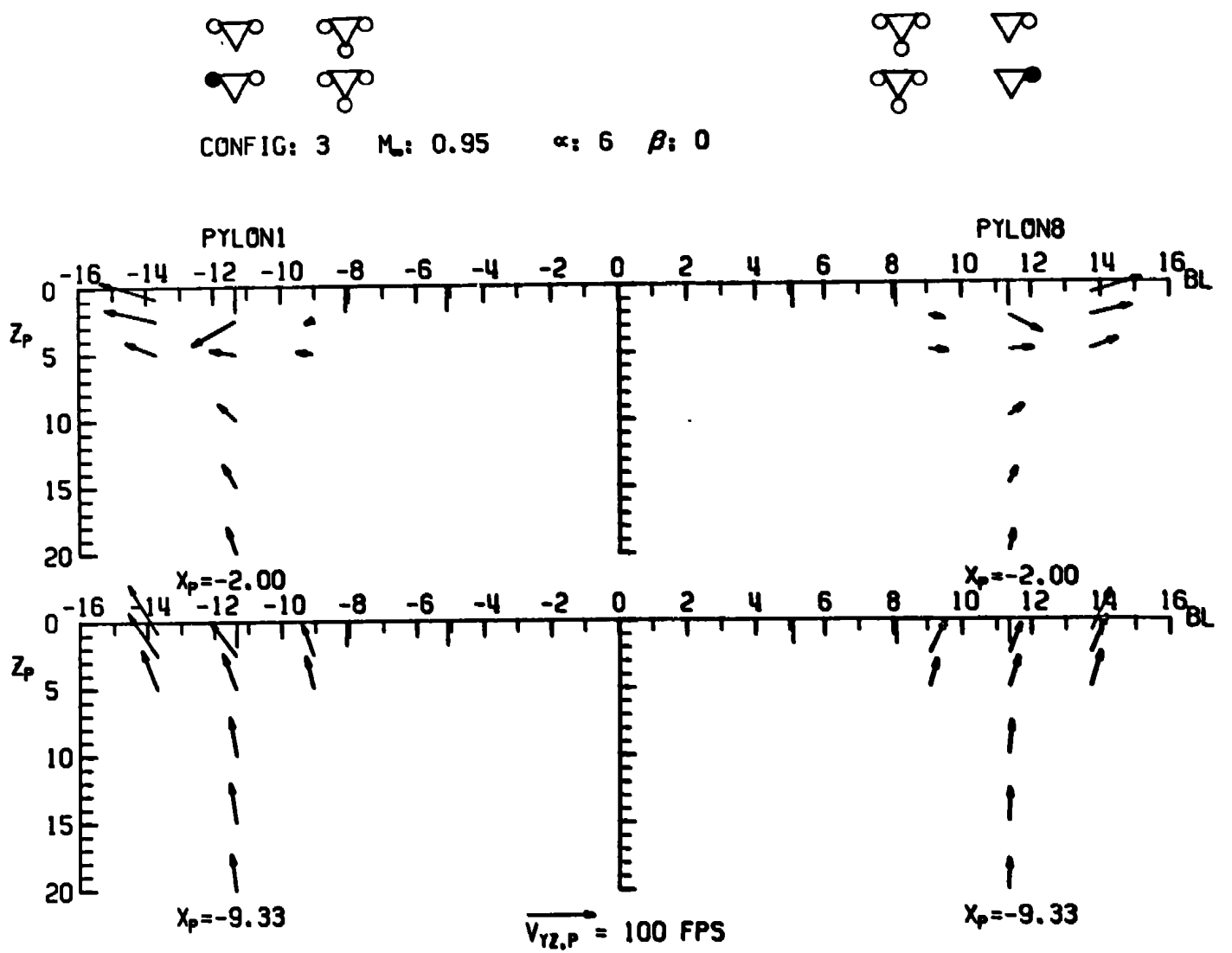

e. $M_\infty = 0.95$, $\alpha = 6$ deg

Figure 20. Concluded.

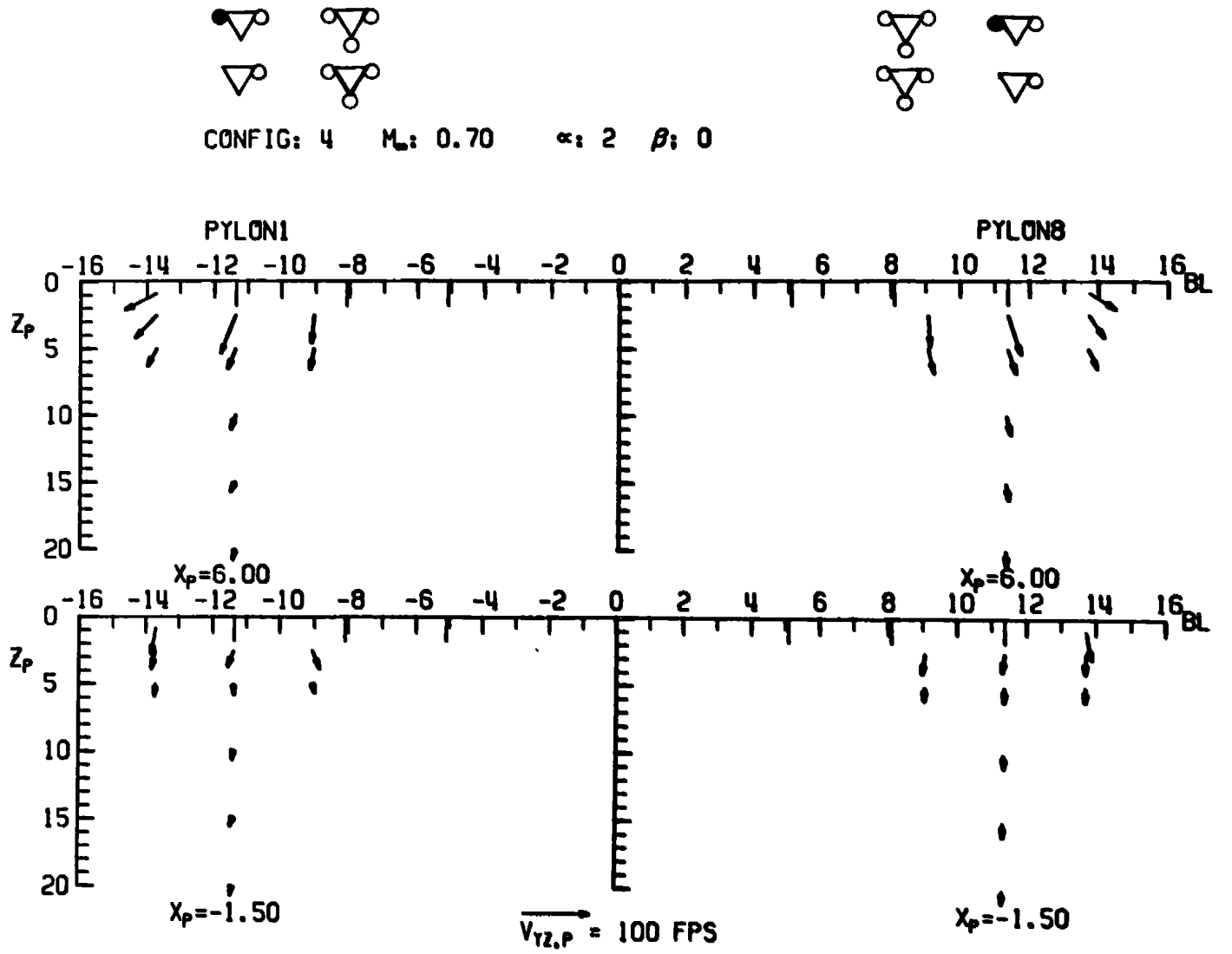

a. $M_\infty = 0.70$, $\alpha = 2$ deg

Figure 21. Flow-field measurements under the left and right wings of the A-7D with external stores, configuration 4.

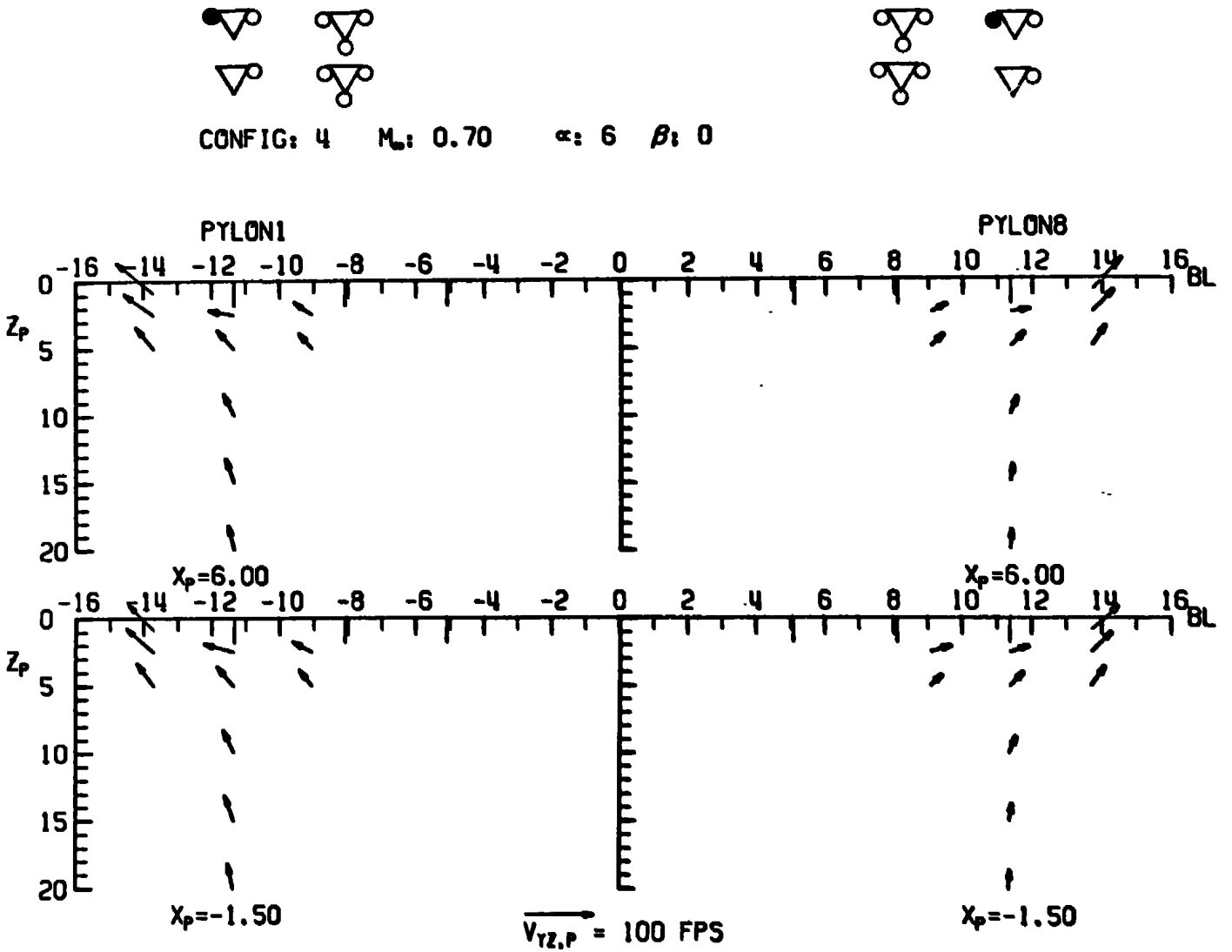

b. $M_\infty = 0.70$, $\alpha = 6$ deg

Figure 21. Continued.

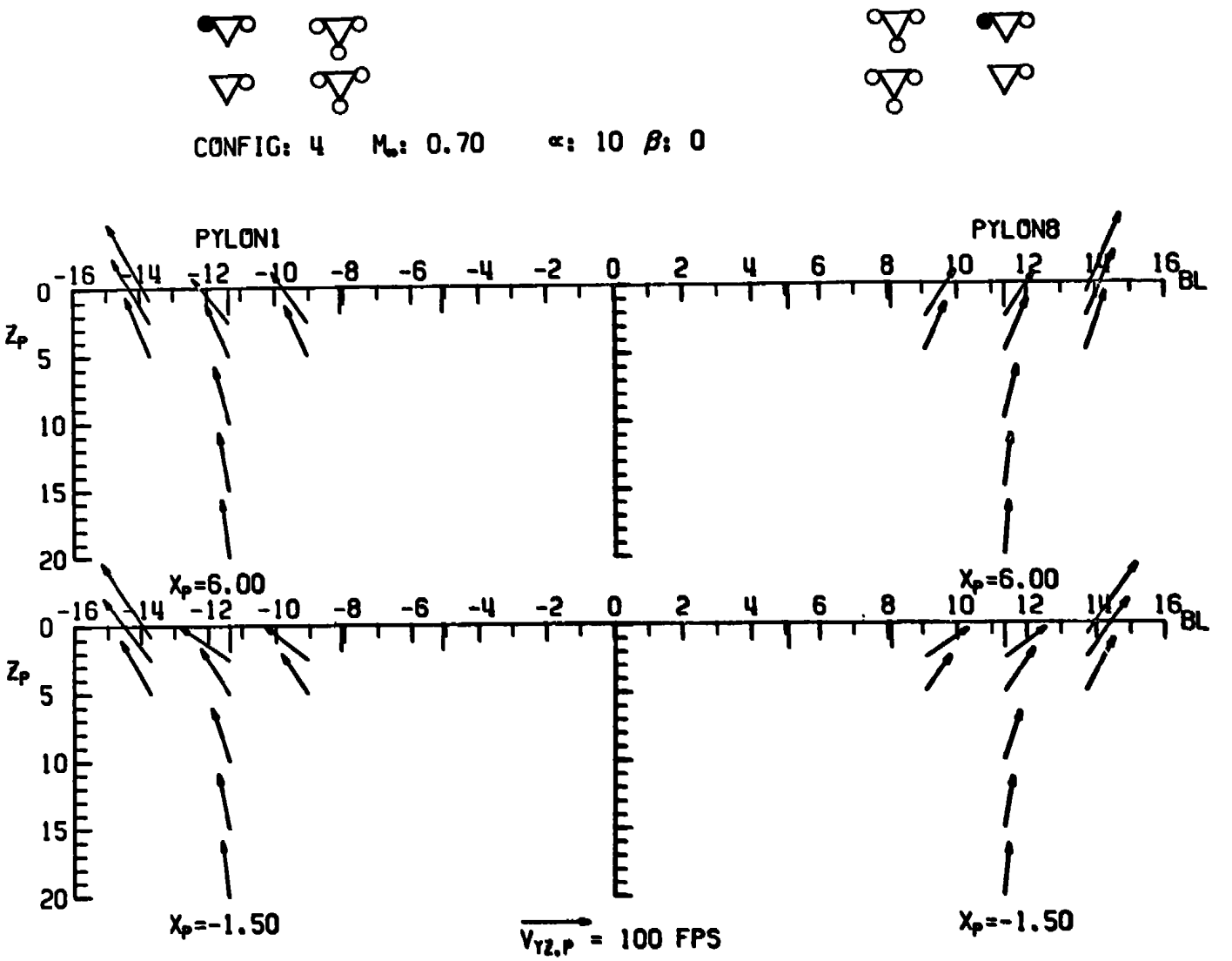

c. M_∞ = 0.70, α = 10 deg

Figure 21. Continued.

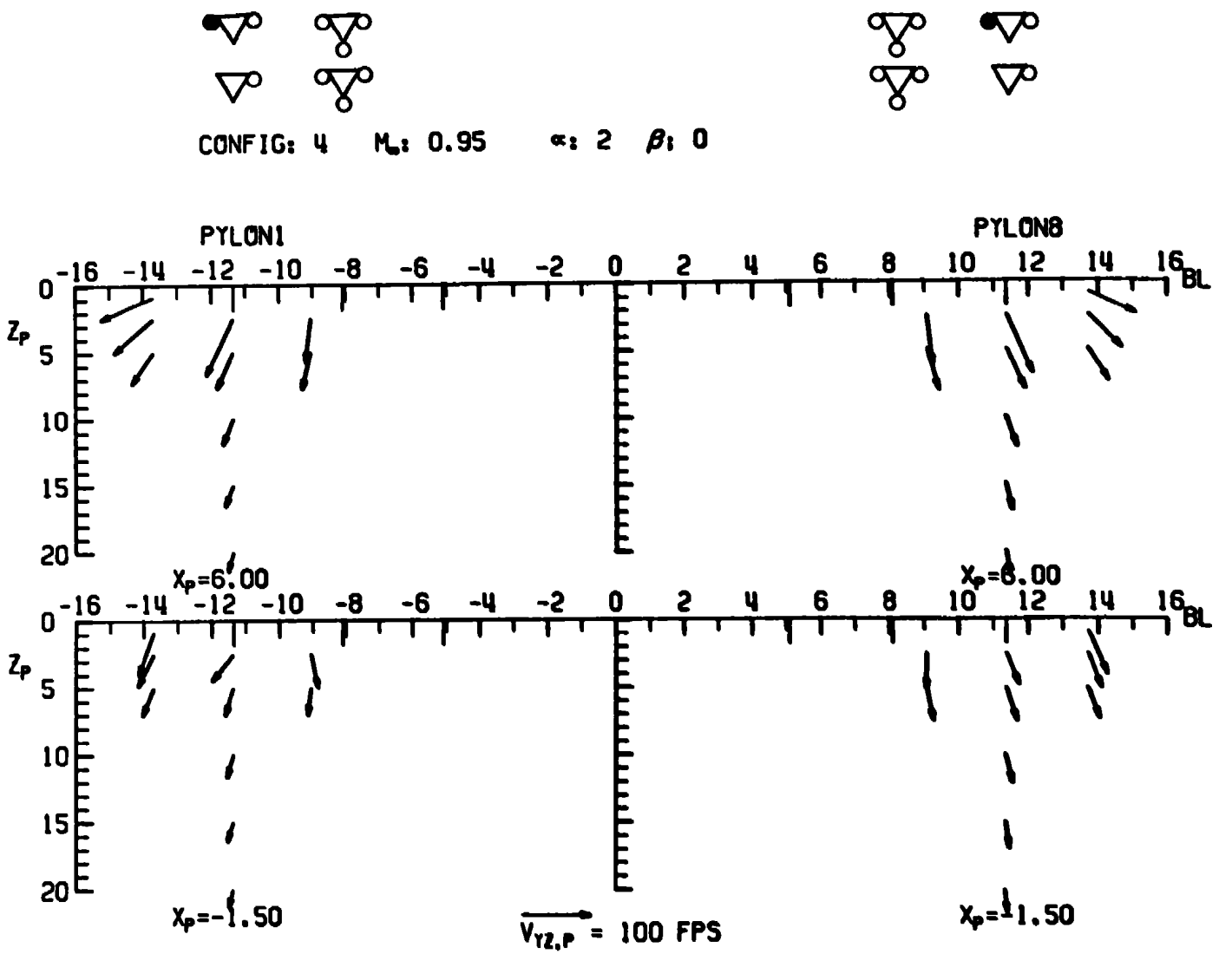

d. $M_\infty = 0.95$, $\alpha = 2$ deg

Figure 21. Continued.

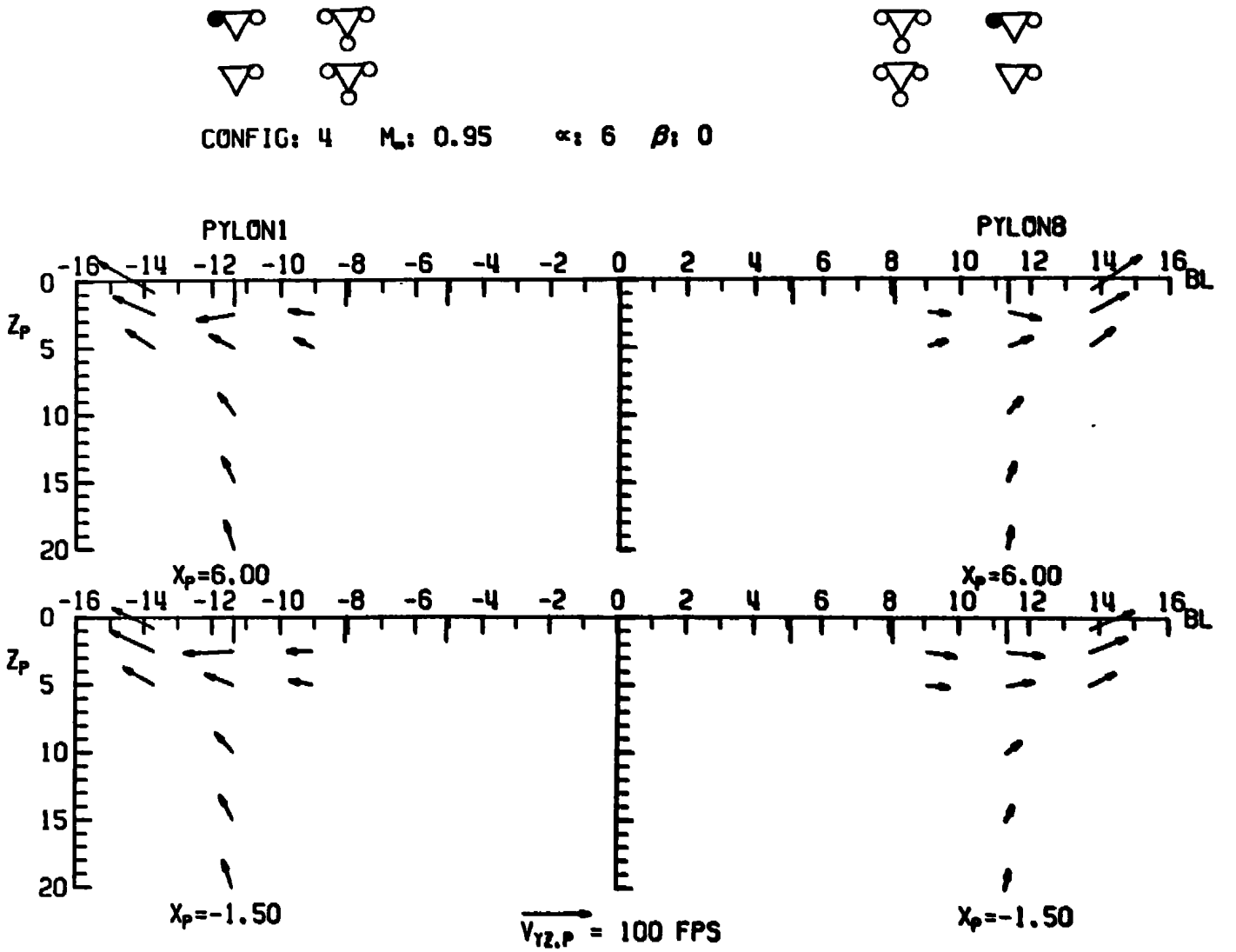

e. M_∞ = 0.95, α = 6 deg

Figure 21. Concluded.

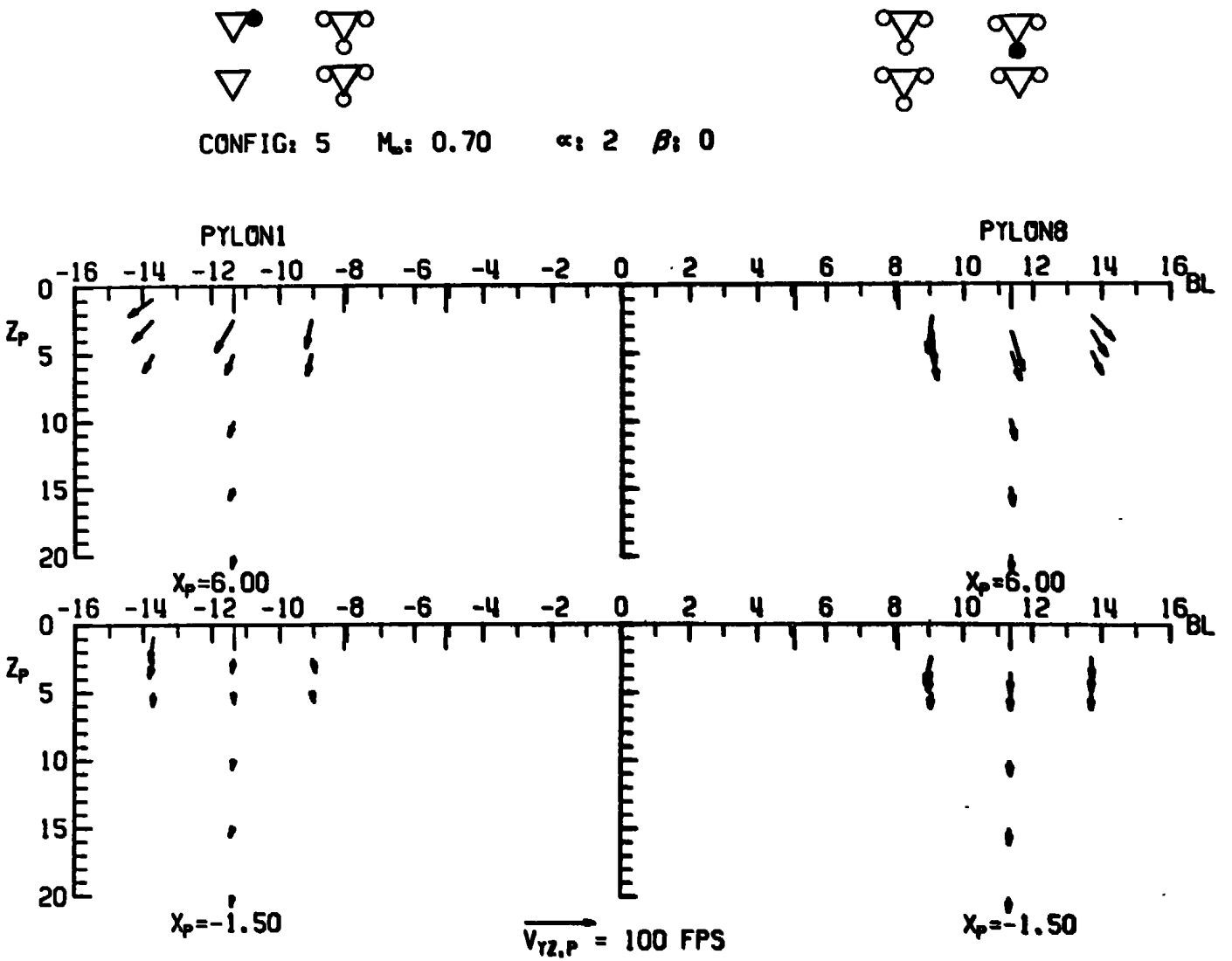

a. $M_\infty = 0.70$, $\alpha = 2$ deg

Figure 22. Flow-field measurements under the left and right wings of the A-7D with external stores, configuration 5.

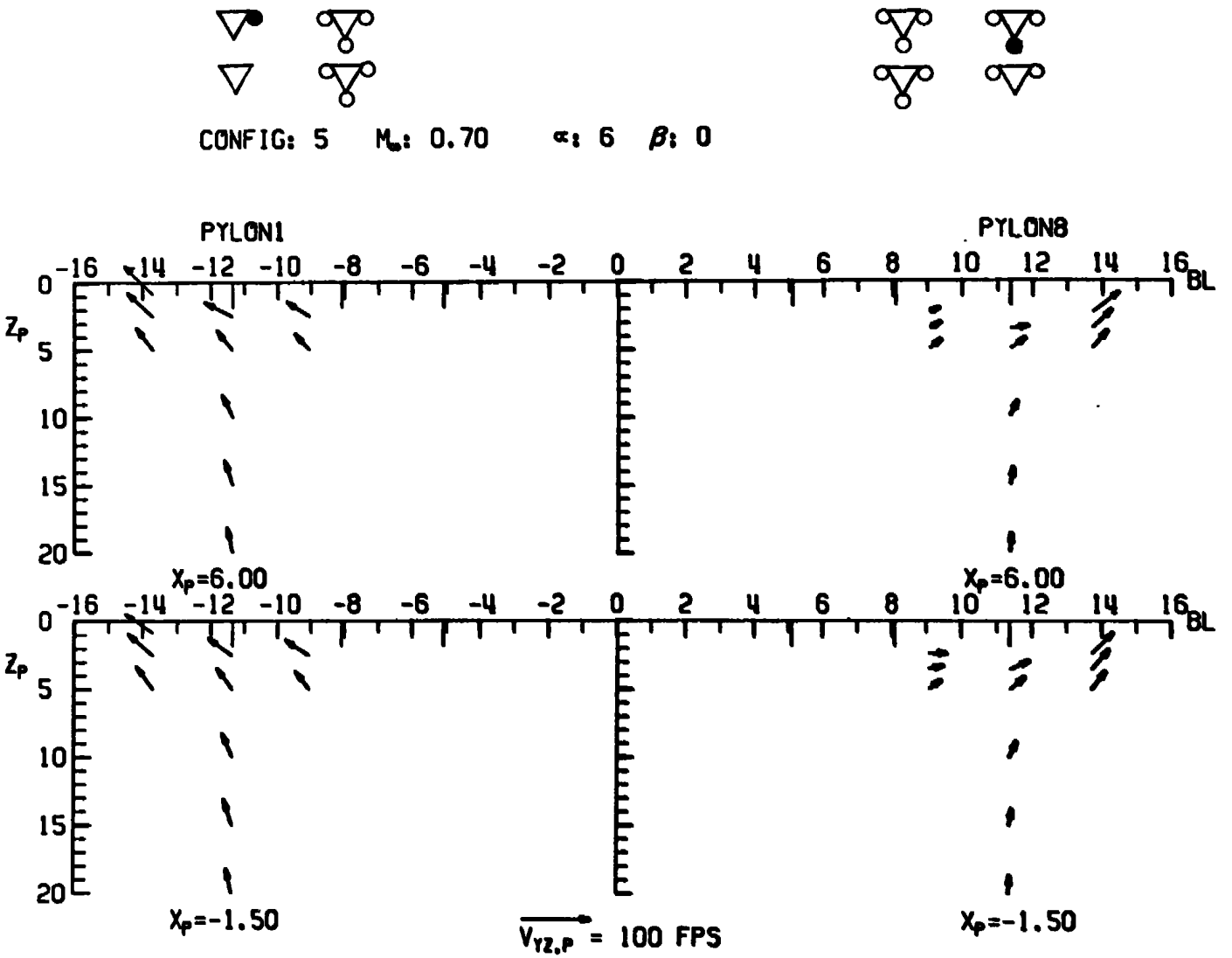

b. $M_\infty = 0.70$, $\alpha = 6$ deg
Figure 22. Continued.

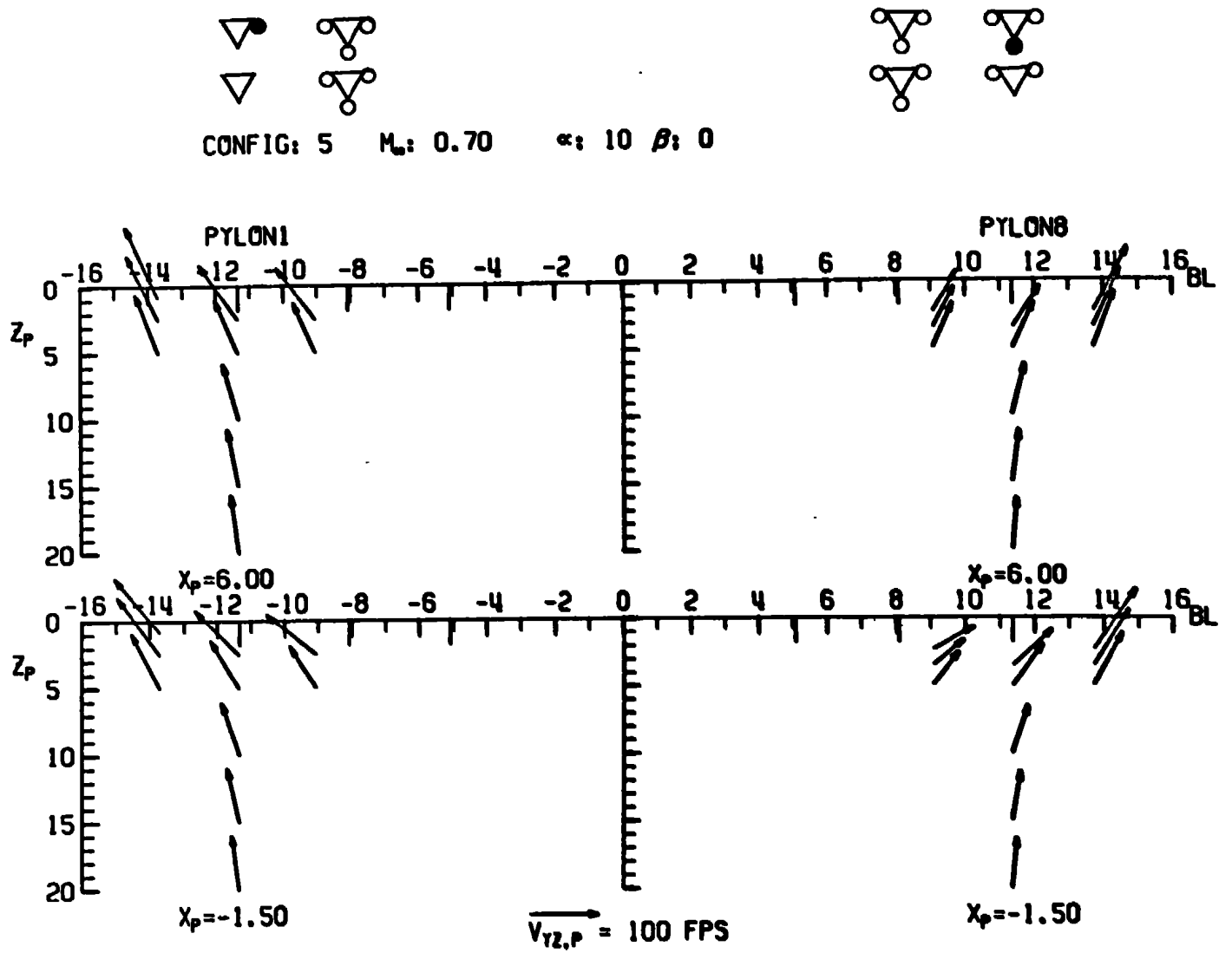

c. $M_\infty = 0.70$, $\alpha = 10$ deg

Figure 22. Continued.

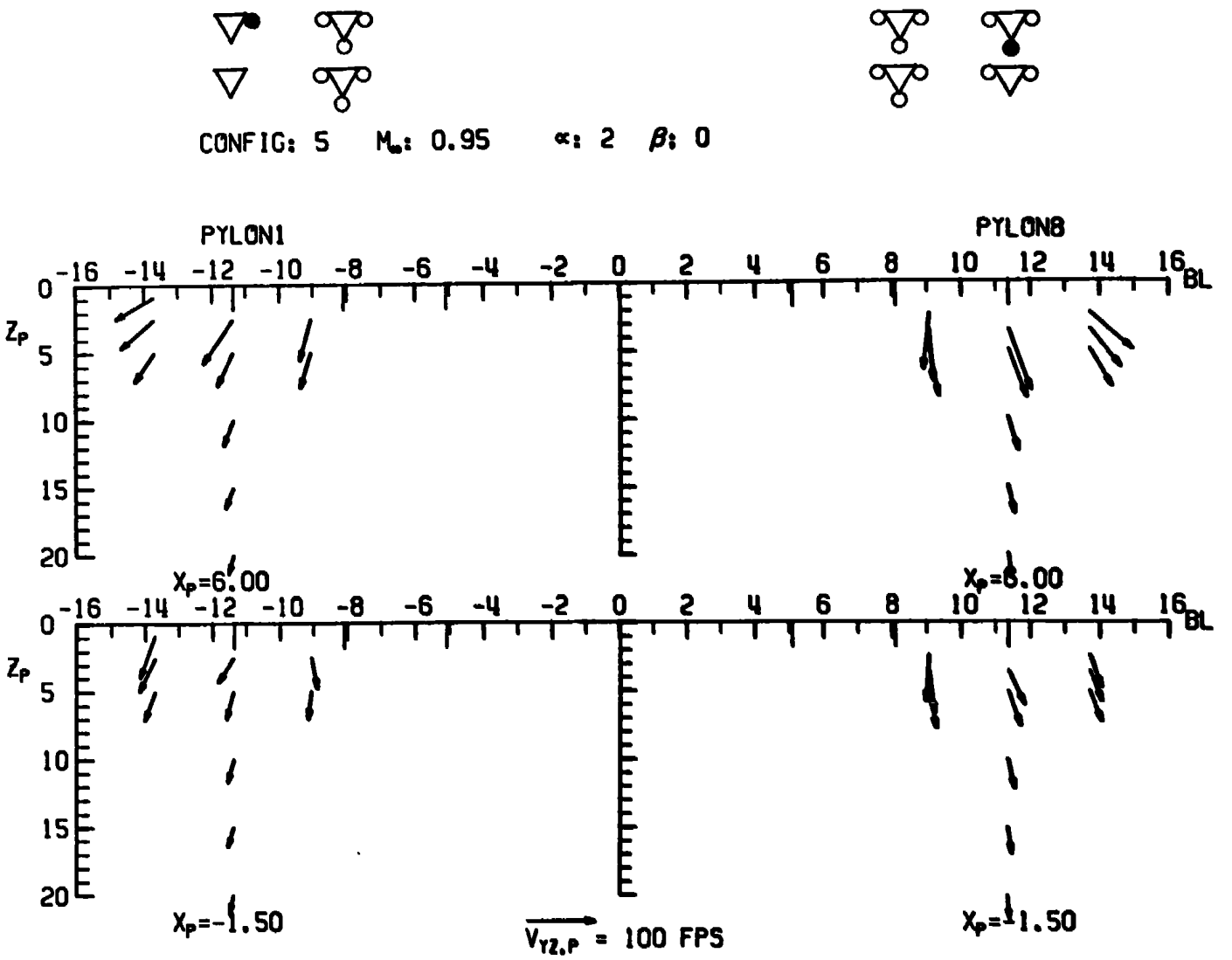

d. $M_\infty = 0.95$, $\alpha = 2$ deg

Figure 22. Continued.

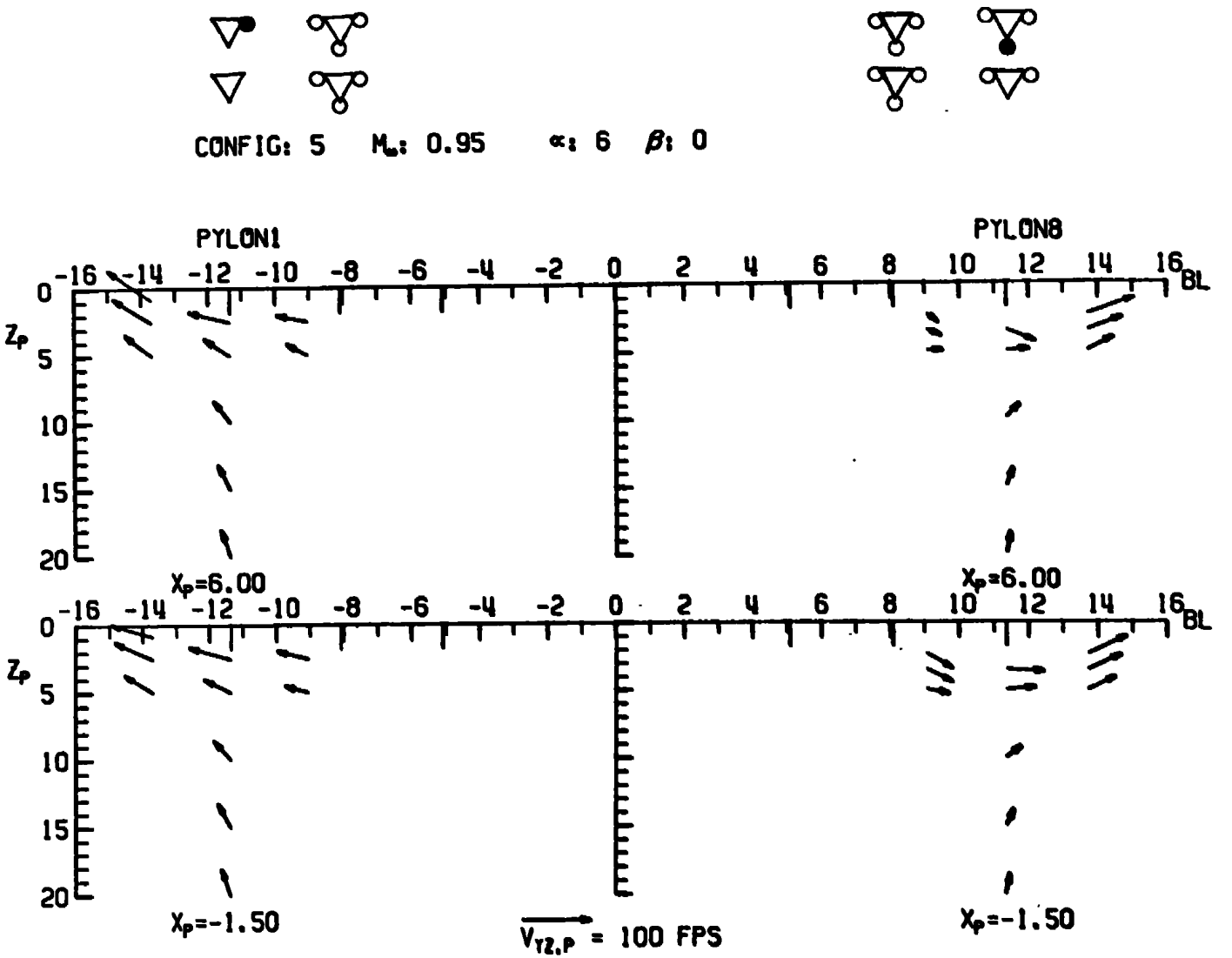

e. $M_\infty = 0.95$, $\alpha = 6$ deg

Figure 22. Concluded.

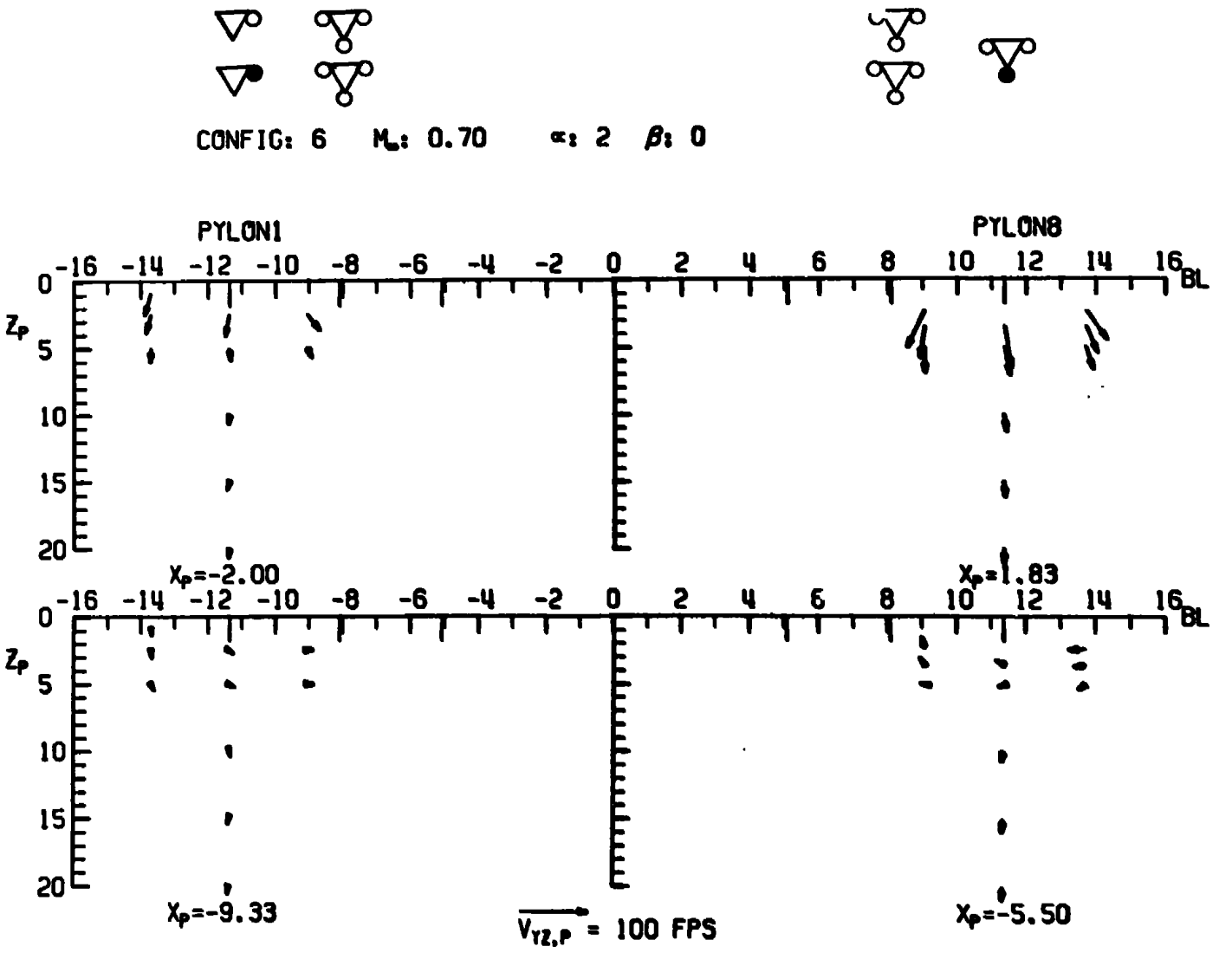

a. $M_\infty = 0.70$, $\alpha = 2$ deg

Figure 23. Flow-field measurements under the left and right wings of the A-7D with external stores, configuration 6.

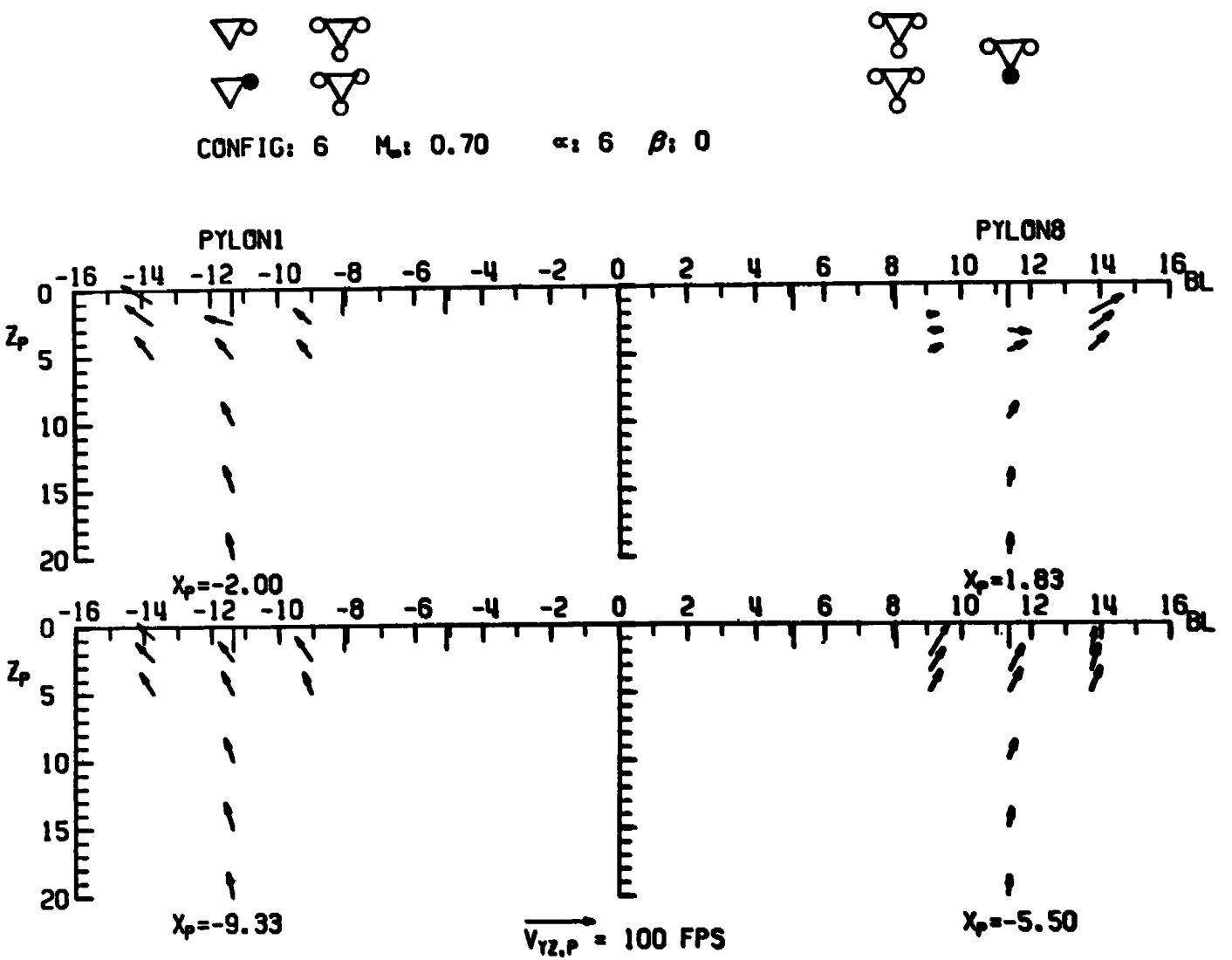

b. $M_\infty = 0.70$, $\alpha = 6$ deg

Figure 23. Continued.

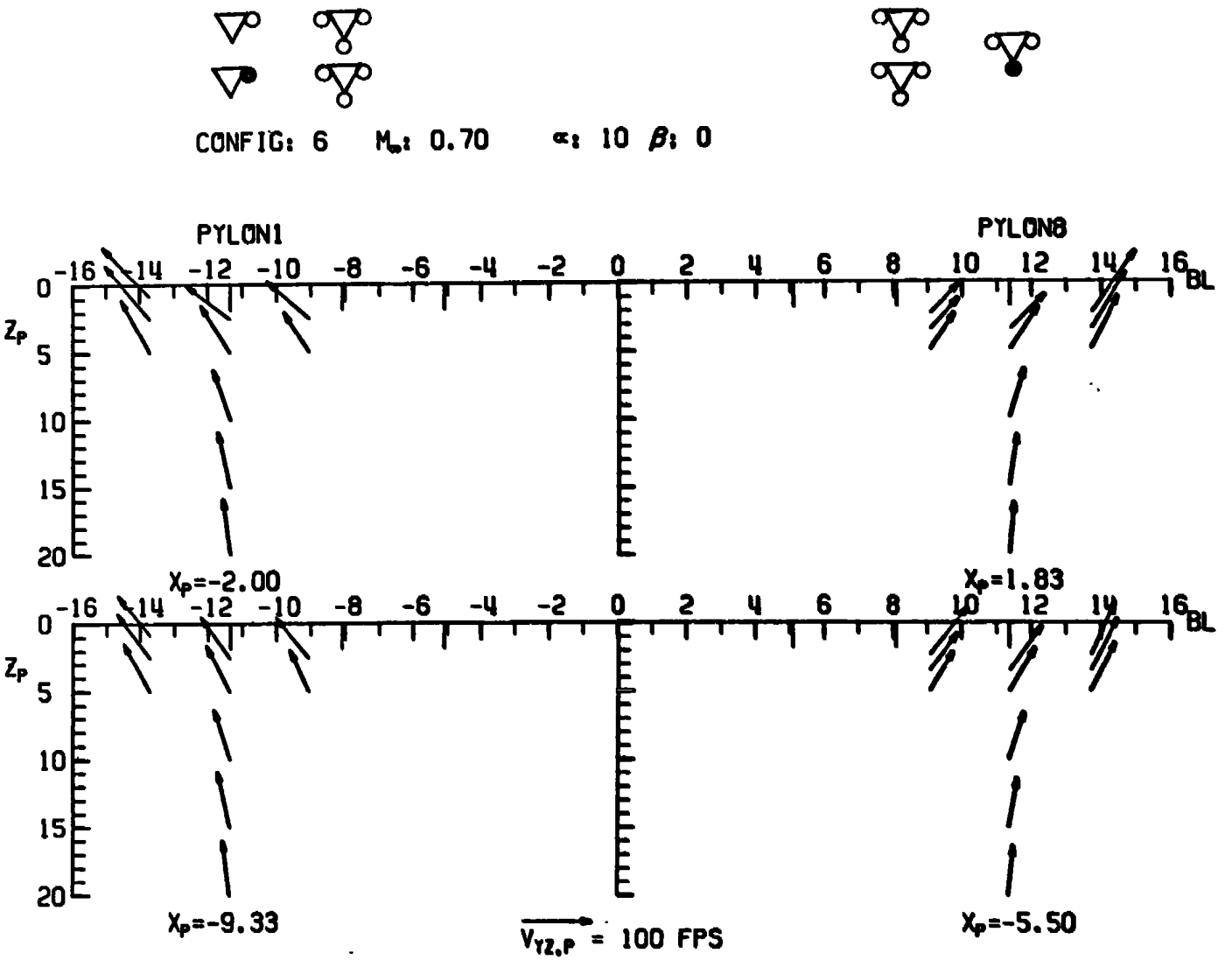

c. $M_\infty = 0.70$, $\alpha = 10$ deg

Figure 23. Continued.

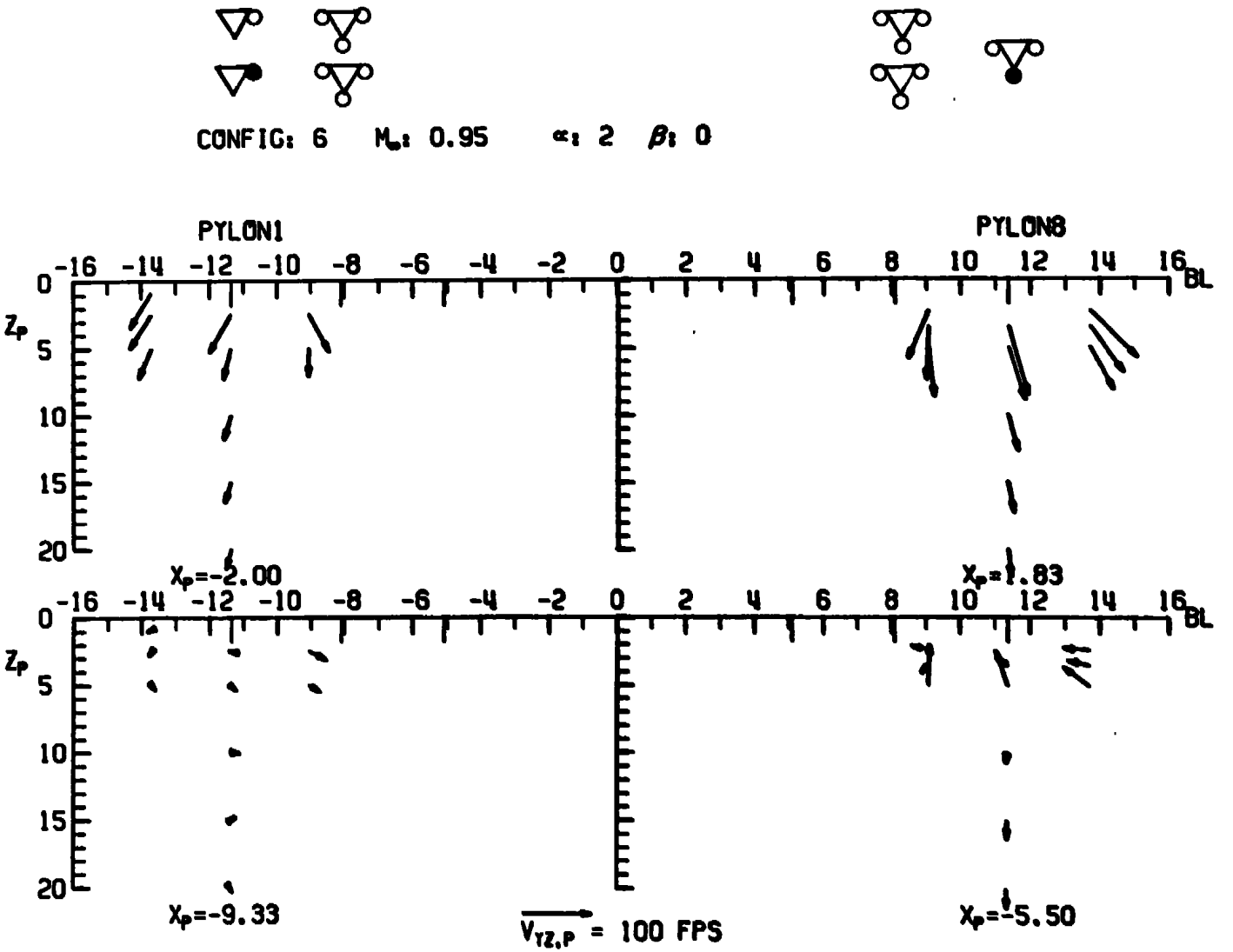

d. $M_\infty = 0.95$, $\alpha = 2$ deg

Figure 23. Continued.

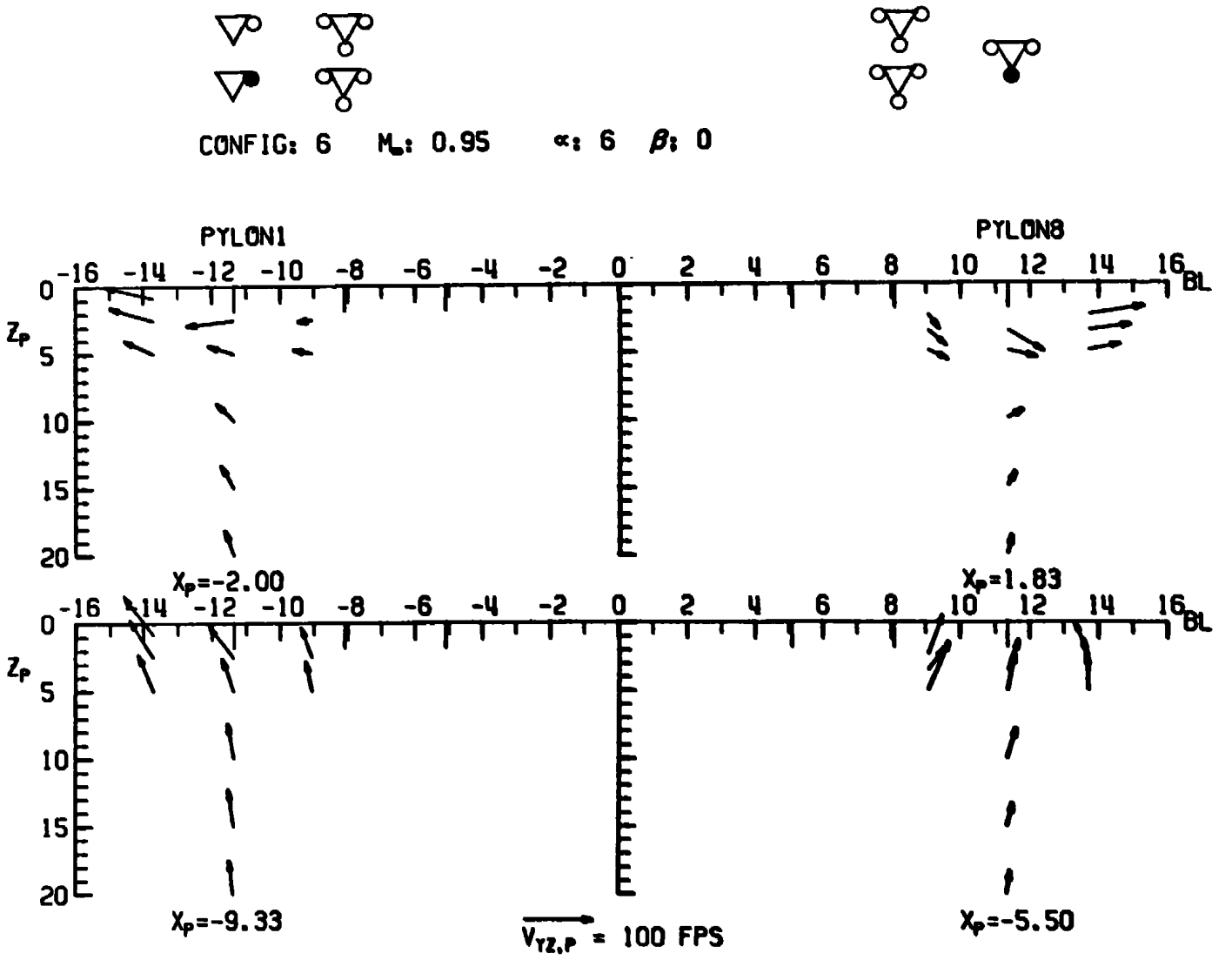

e. $M_\infty = 0.95$, $\alpha = 6$ deg

Figure 23. Concluded.

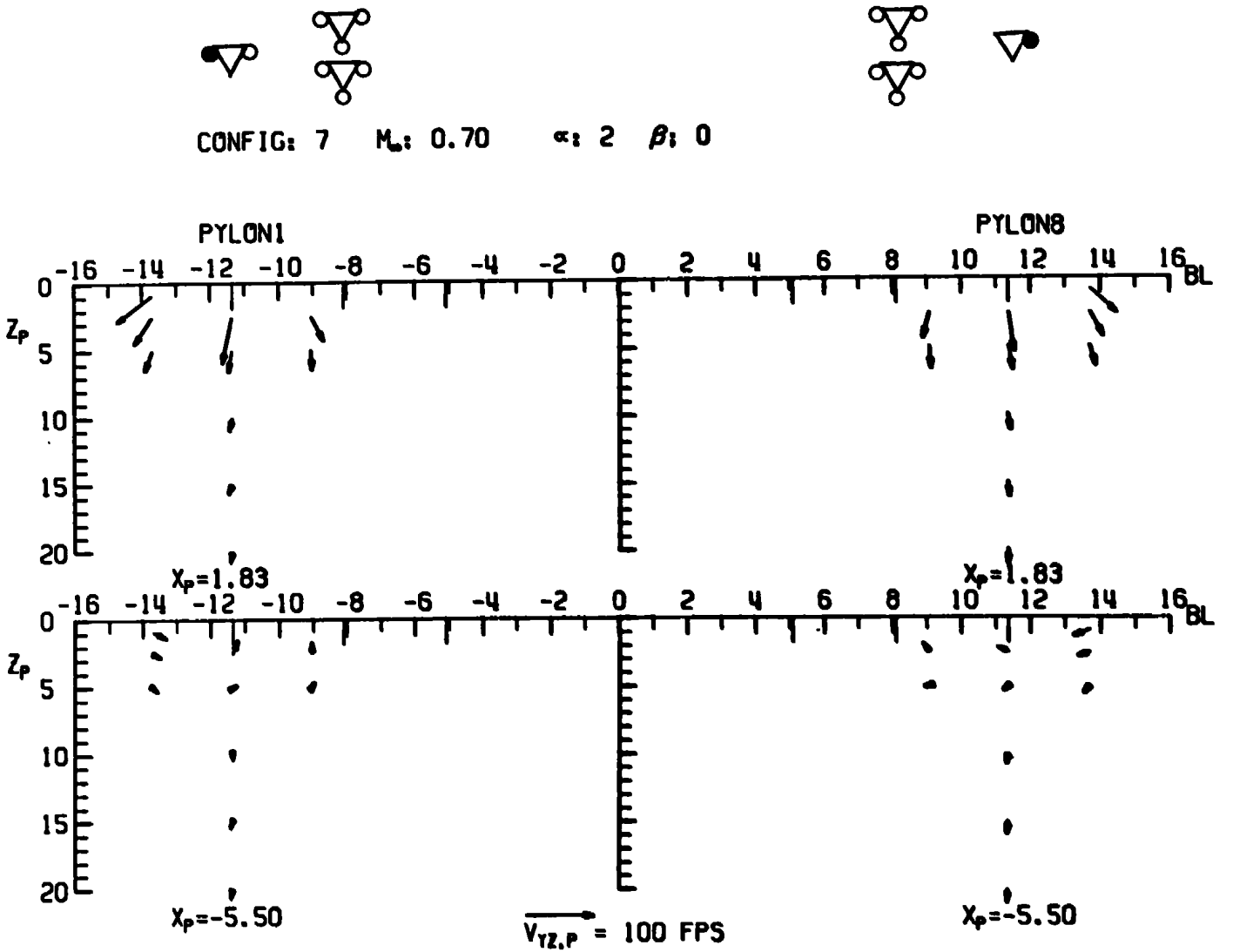

a. $M_\infty = 0.70$, $\alpha = 2$ deg

Figure 24. Flow-field measurements under the left and right wings of the A-7D with external stores, configuration 7.

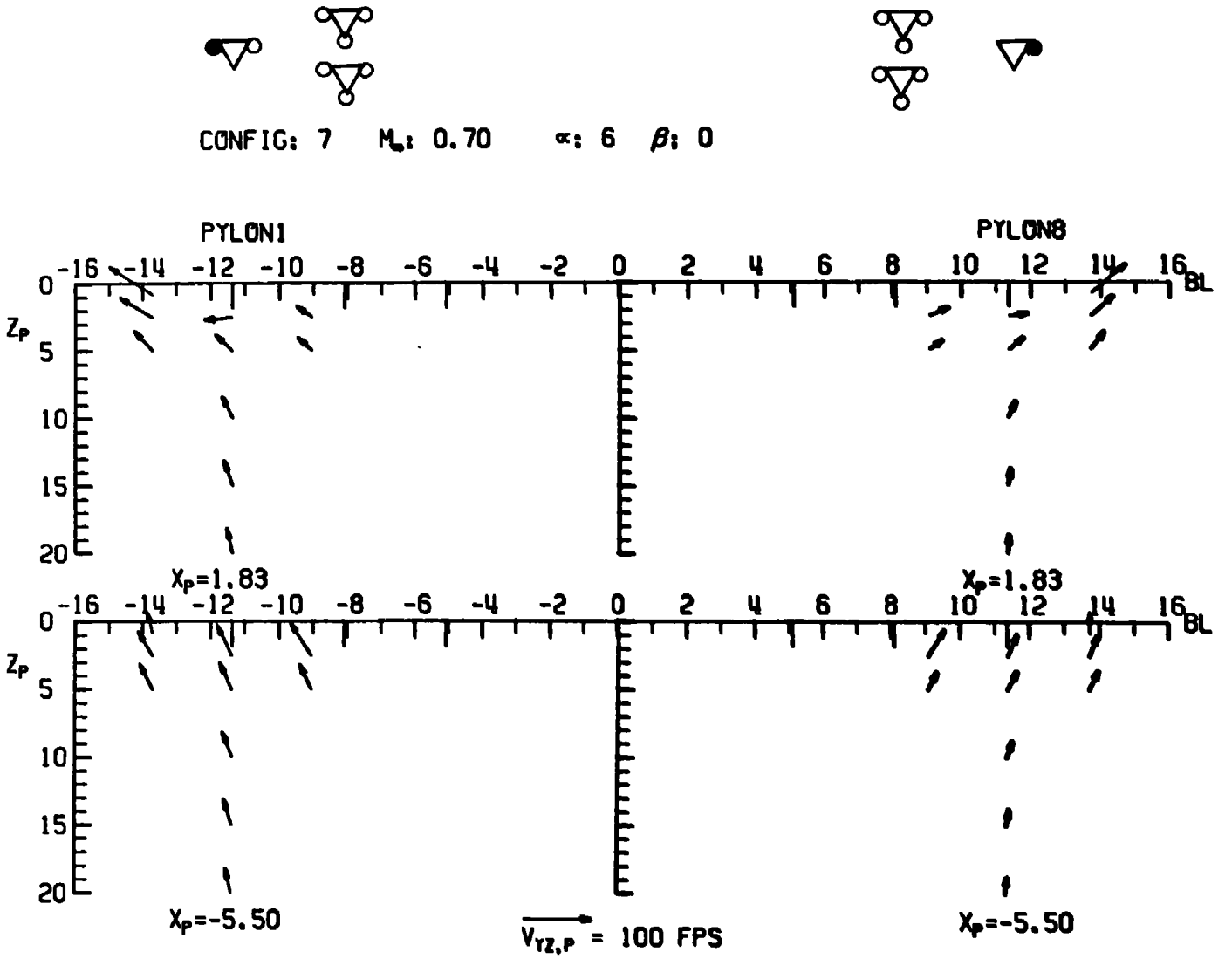

b. M_∞ = 0.70, α = 6 deg
Figure 24. Continued.

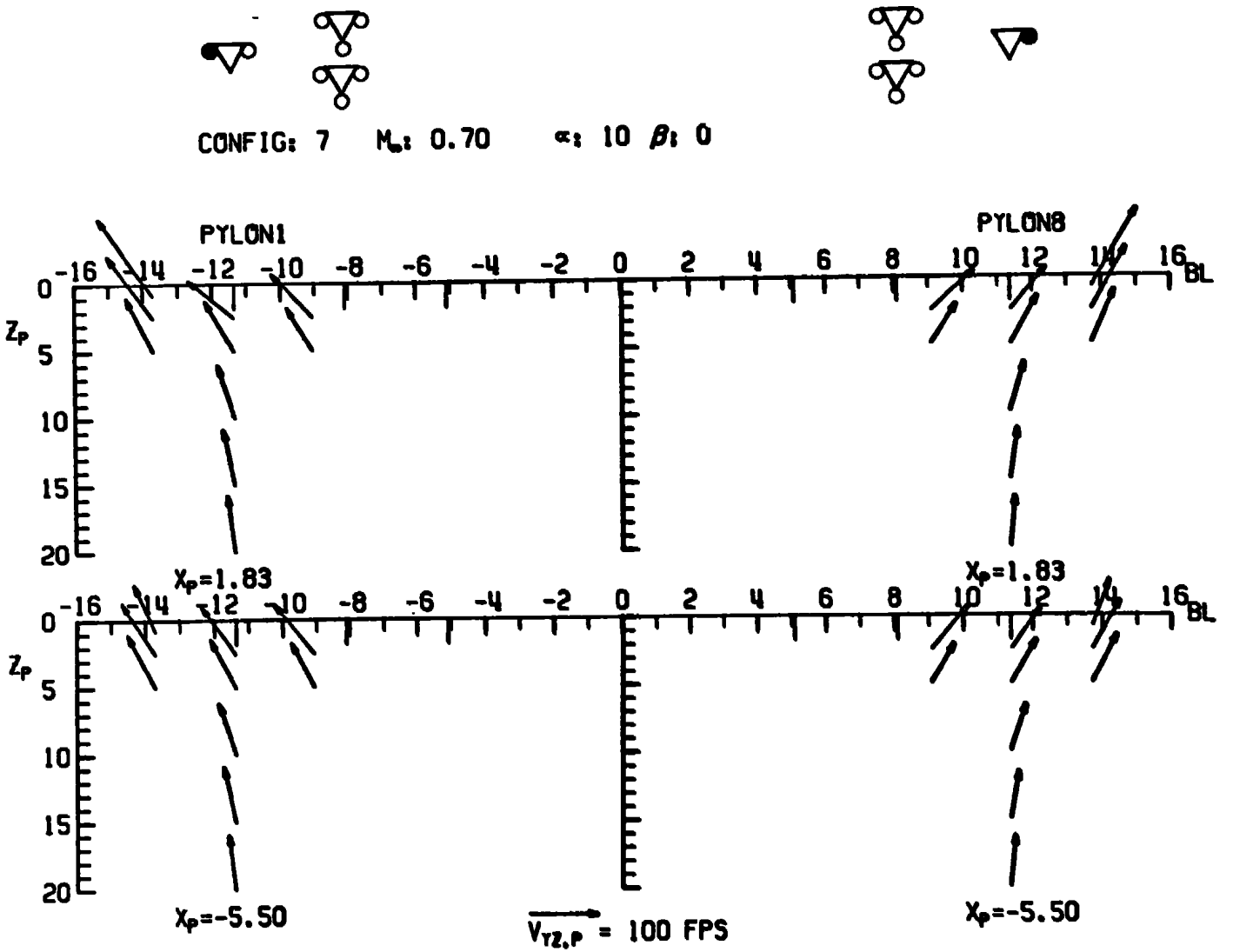

c. $M_\infty = 0.70$, $\alpha = 10$ deg

Figure 24. Continued.

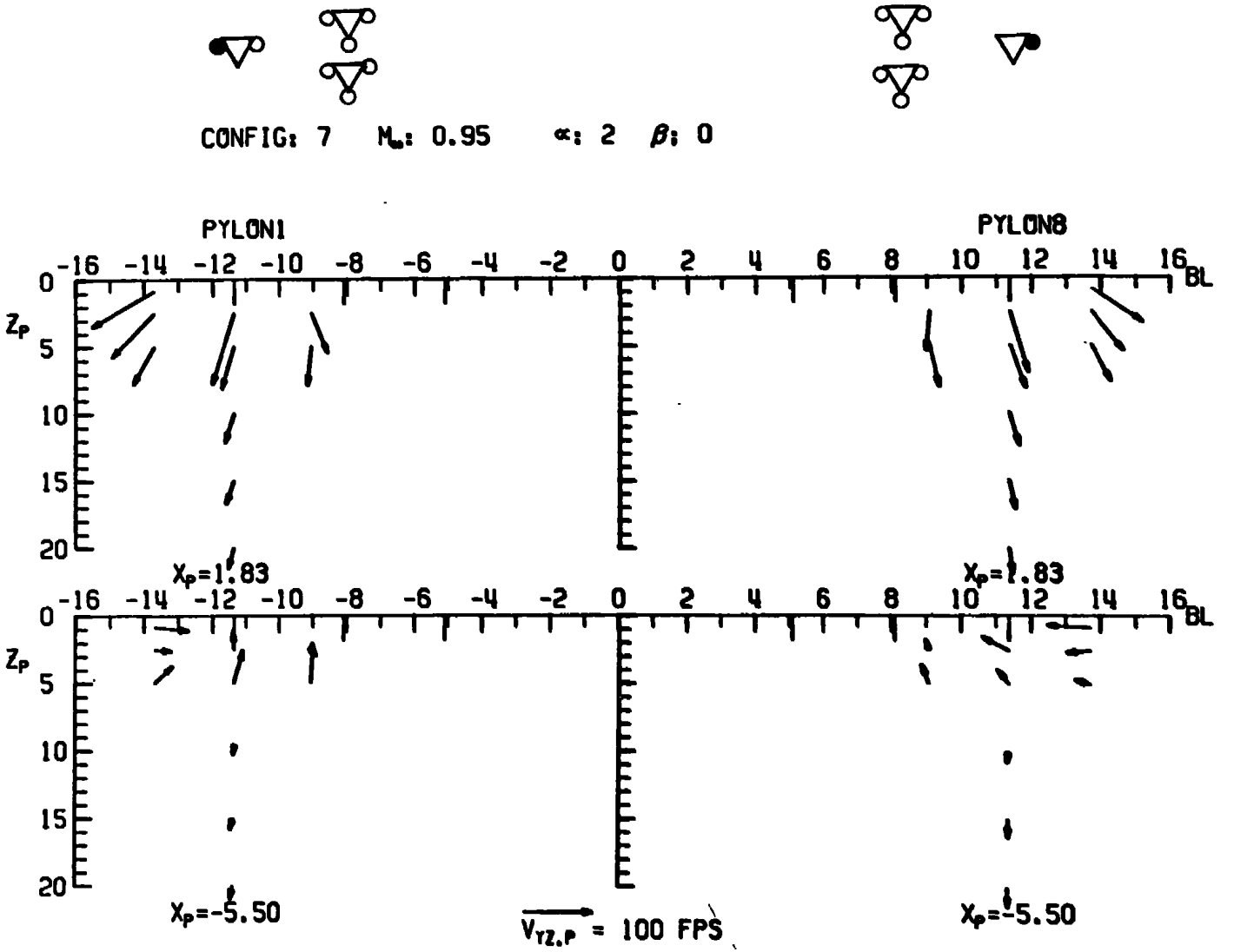

d. $M_\infty = 0.95$, $\alpha = 2$ deg

Figure 24. Continued.

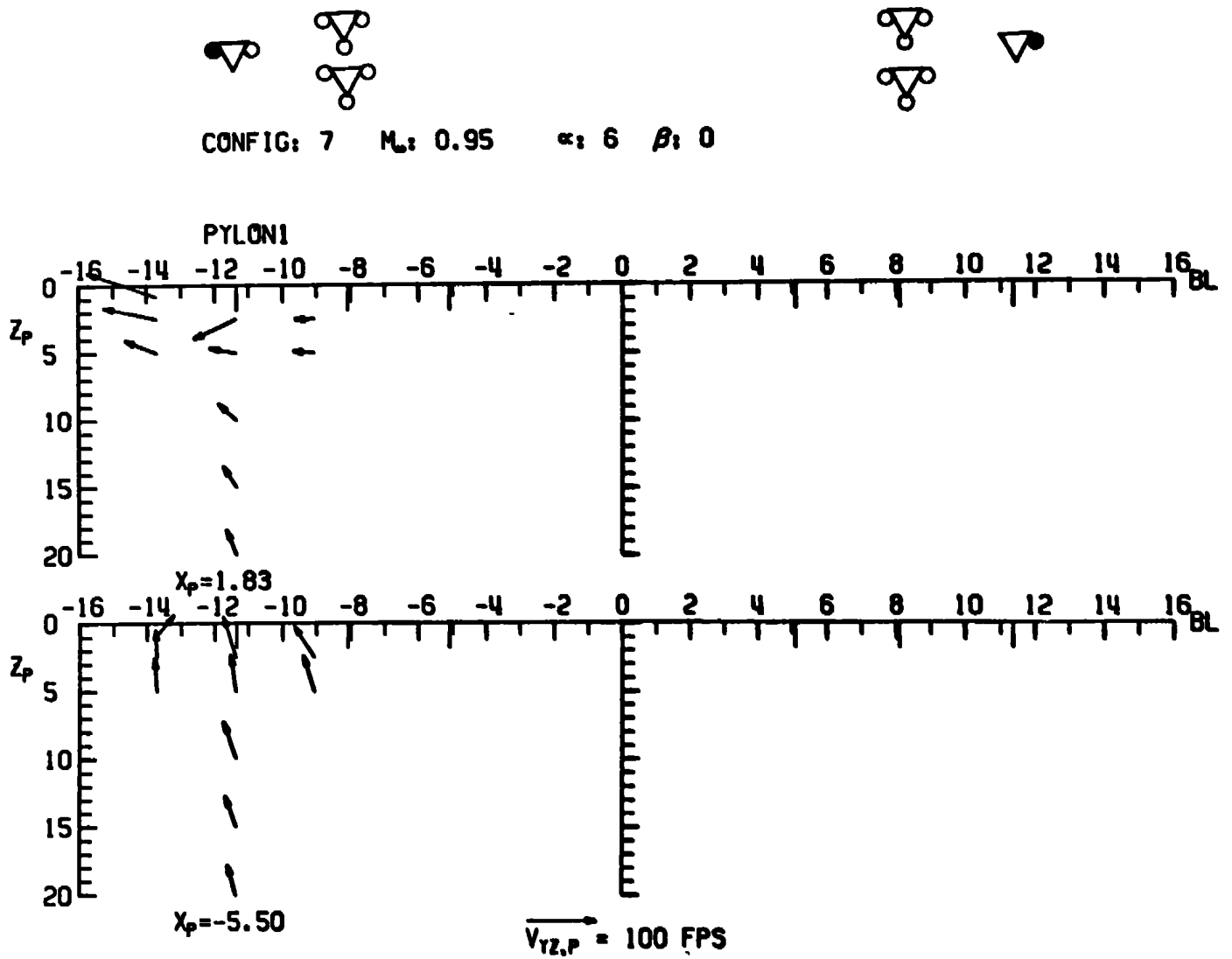

e. $M_\infty = 0.95$, $\alpha = 6$ deg

Figure 24. Concluded.

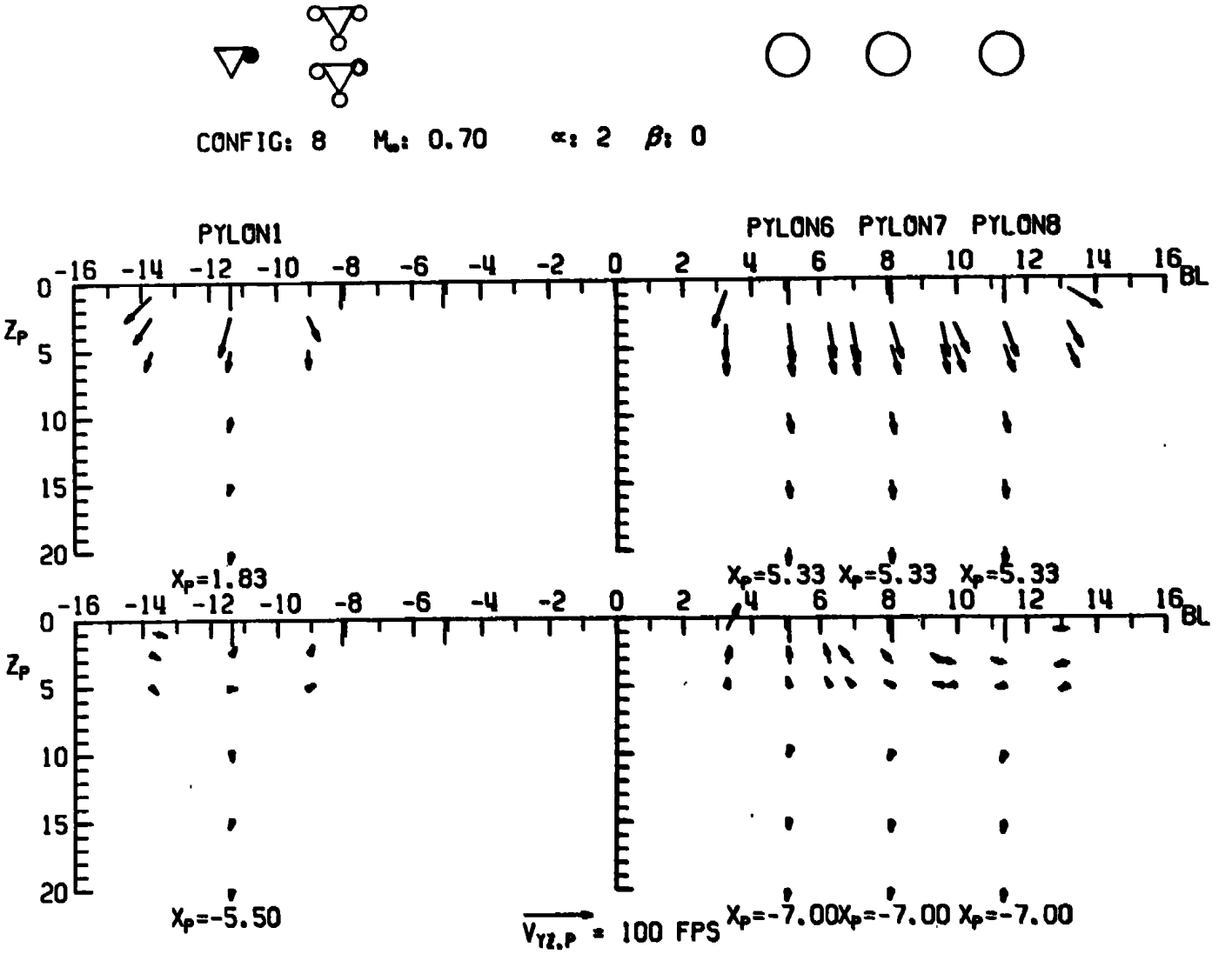

a. $M_\infty = 0.70$, $\alpha = 2$ deg

Figure 25. Flow-field measurements under the left and right wings of the A-7D with external stores, configuration 8.

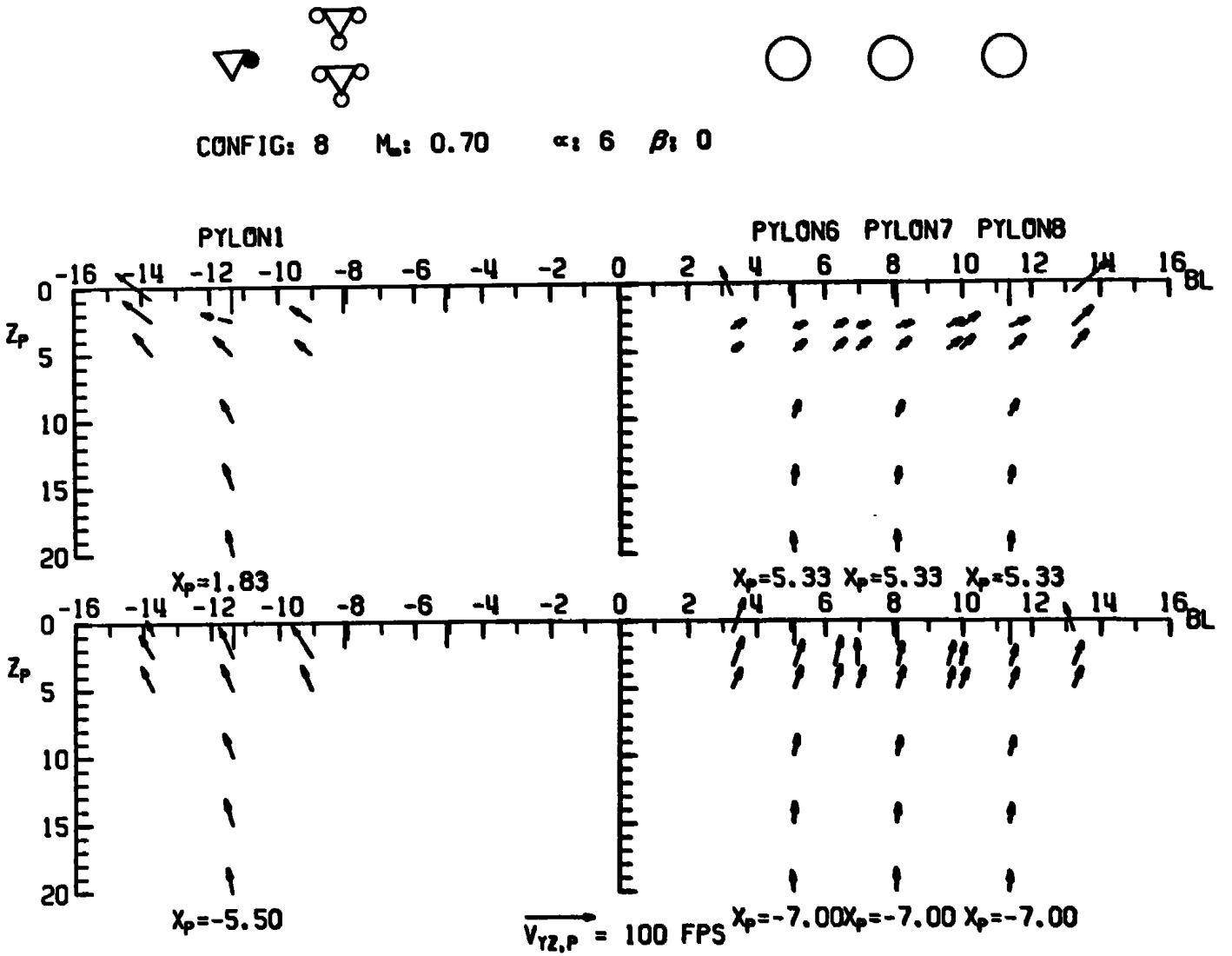

b. $M_\infty = 0.70$, $\alpha = 6$ deg

Figure 25. Continued.

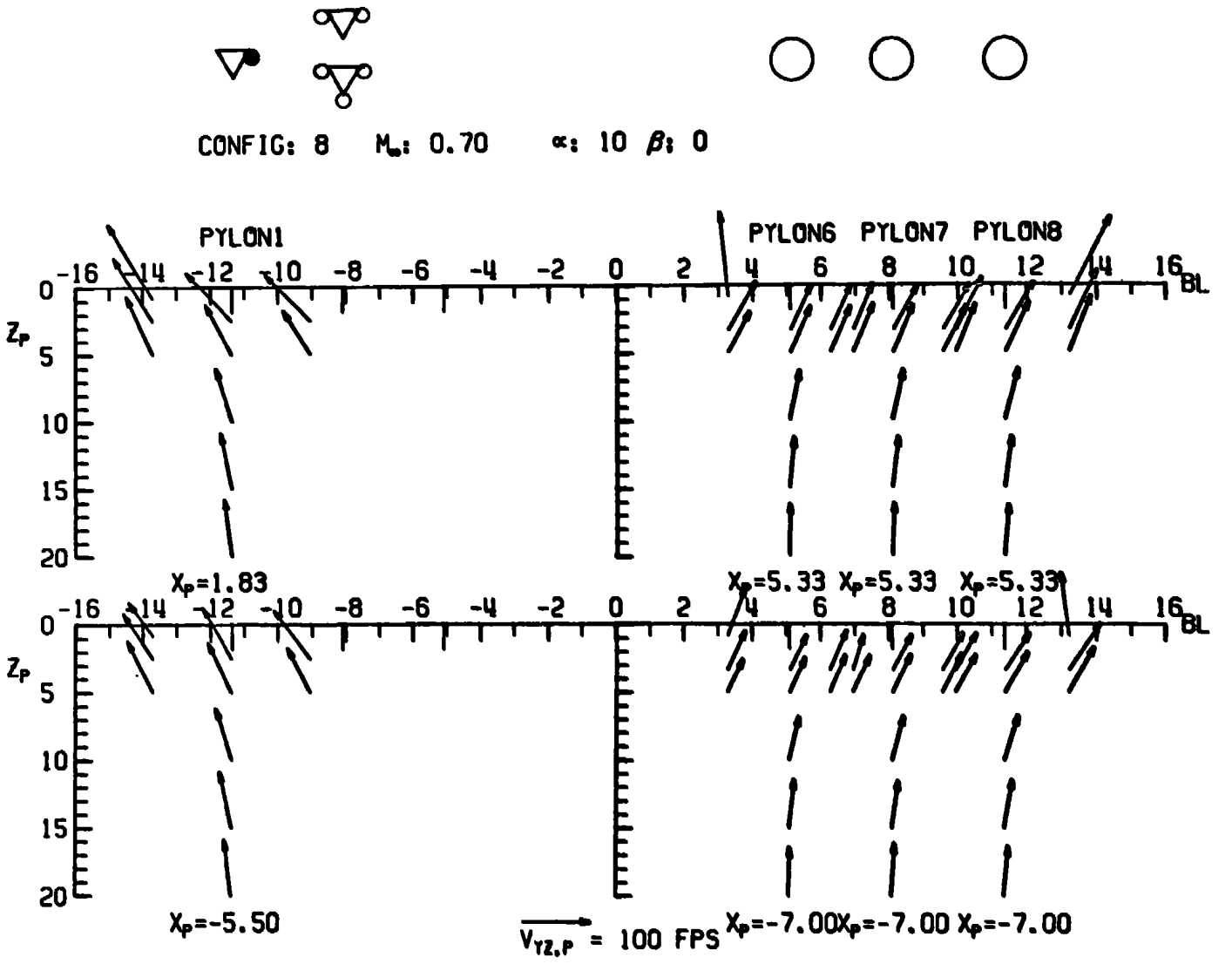

c. M_∞ = 0.70, α = 10 deg
Figure 25. Continued.

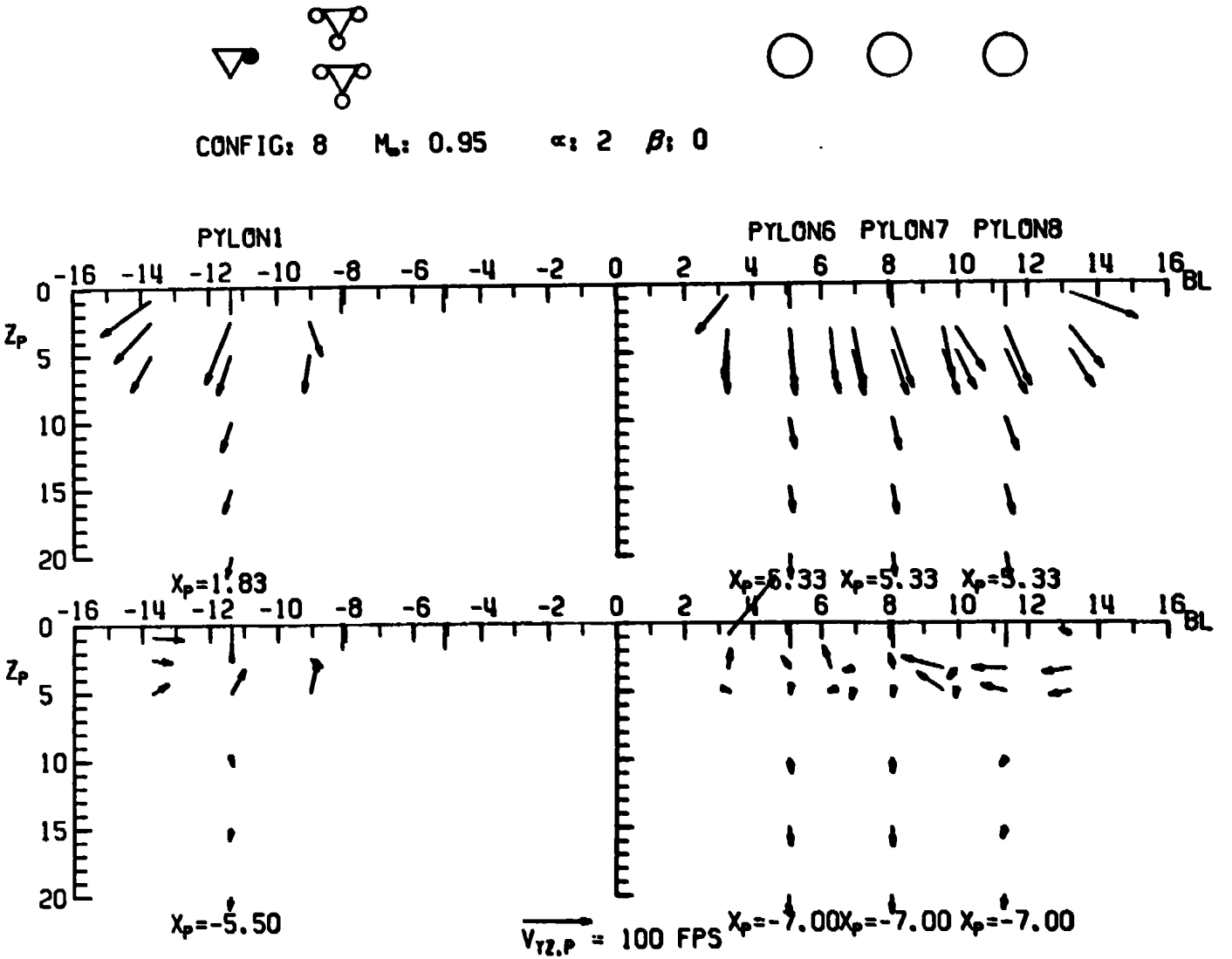

d. $M_\infty = 0.95$, $\alpha = 2$ deg

Figure 25. Continued.

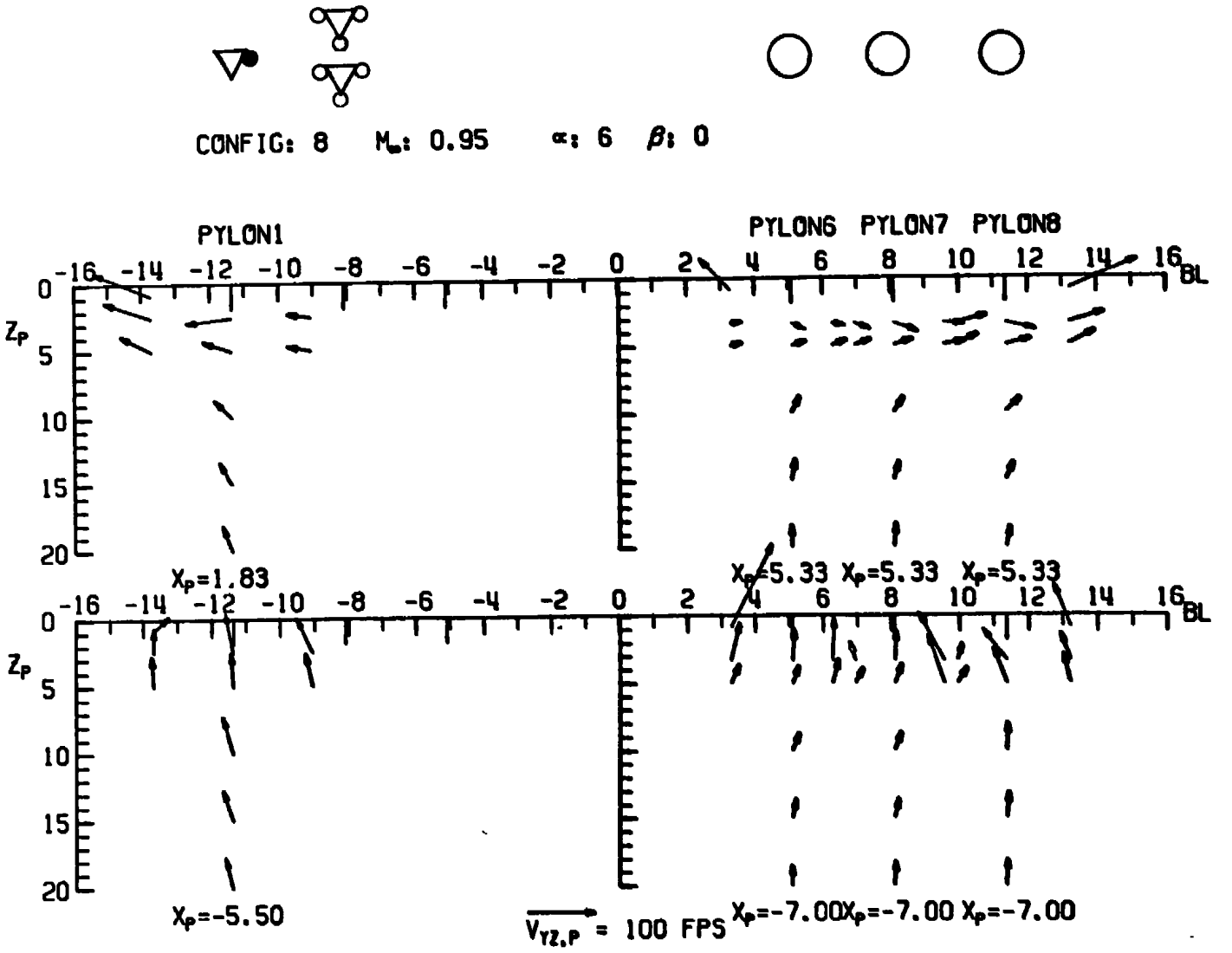

e. $M_\infty = 0.95$, $\alpha = 6$ deg

Figure 25. Concluded.

Table 1. Test Summary

Config.	M_∞	Pylon																	
		8			7			6			3			2			1		
		α			α			α			α			α			α		
		2	6	10	2	6	10	2	6	10	2	6	10	2	6	10	2	6	10
1	0.70										A*	A	A	A	A	A	A	A	A
	0.95										A	A		A	A		A	A	
2	0.70	E	E	E										B	B	B	B	B	B
	0.95	E	E											B	B		B	B	
3	0.70	D	D	D													D	D	D
	0.95	D	D														D	D	
4	0.70	E	E	E													E	E	E
	0.95	E	E														E	E	
5	0.70	C	C	C													E	E	E
	0.95	C	C														E	E	
6	0.70	F	F	F													D	D	D
	0.95	F	F														D	D	
7	0.70	G	G	G													G	G	G
	0.95	G	G														G	G	
8	0.70	H	H	H	H	H	H	H	H	H							G	G	G
	0.95	H	H		H	H		H	H								G	G	
9	0.70					E	E							D	D	D			
	0.95				E	E								D	D				
10	0.70				D	D	D							E	E	E			
	0.95				D	D								E	E				

*See Table 2 for X_p, Y_p, Z_p locations.

Table 1. Continued

Config.	M_∞	Pylon																		
		8			7			6			3			2			1		
		α			α			α			α			α			α		
		2	6	10	2	6	10	2	6	10	2	6	10	2	6	10	2	6	10
11	0.70				E*	E	E							D	D	D			
	0.95				E	E								D	D				
12	0.70				C	C	C							E	E	E			
	0.95				C	C								E	E				
13	0.70				F	F	F							G	G	G			
	0.95				F	F								G	G				
14	0.70				G	G	G							G	G	G			
	0.95				G	G								G	G				
15	0.70				C	C	C				I	I	I	B	B	B			
	0.95				C	C								B	B				
16	0.70				E	E	E				I	I	I	D	D	D			
	0.95				E	E					I	I		D	D				
17	0.70							K	K	K							F	F	F
	0.95							K	K								F	F	
18	0.70							J	J	J							G	G	G
	0.95							J	J								G	G	
19	0.70				C	C	C								B	B			
	0.95				C	C								B	B				
20	0.70				E	E	E							D	D	D			
	0.95				E	E								D	D				

*See Table 2 for X_P, Y_P, Z_P locations.

Table 1. Concluded

Config.	M_∞	Pylon																	
		8			7			6			3			2			1		
		α			α			α			α			α			α		
		2	6	10	2	6	10	2	6	10	2	6	10	2	6	10	2	6	10
21	0.70				C*	C	C				I	I	I	B	B	B			
	0.95				C	C					I	I		B	B				
22	0.70				E	E	E							D	D	D			
	0.95				E	E								D	D				
	0.70																		
	0.95																		
	0.70																		
	0.95																		
	0.70																		
	0.95																		
	0.70																		
	0.95																		
	0.70																		
	0.95																		
	0.70																		
	0.95																		
	0.70																		
	0.95																		
	0.70																		
	0.95																		

*See Table 2 for X_p, Y_p, Z_p locations.

Table 2. Survey Positions

Set	X_P	Y_P	Z_P
A	5.33, -7.00	±1.83	0.83, 3.33, 5
		0	0.83, 3.33, 5, 10, 15, 20
B	-2.00, -9.33	±2.33	2.33, 3.50, 5
		0	3.50, 5, 10, 15, 20
C	6.00, -1.50	±2.33	2.33, 3.50, 5
		0	3.50, 5, 10, 15, 20
D	-2.00, -9.33	±2.33	0.83*, 2.50, 5
		0	2.50, 5, 10, 15, 20
E	6.00, -1.50	±2.33	0.83*, 2.50, 5
		0	2.50, 5, 10, 15, 20
F	1.83, -5.50	±2.33	2.33, 3.50, 5
		0	3.50, 5, 10, 15, 20
G	1.83, -5.50	±2.33	0.83*, 2.50, 5
		0	2.50, 5, 10, 15, 20
H	5.33, -7.00	±1.83	0.83*, 3.33, 5
		0	3.33, 5, 10, 15, 20
I	6.67, -12.00	±2.00	0.83*, 3.00, 5
		0	3.00, 5, 10, 15, 20
J	1.83, -5.50	±2.00	2.33, 3.50, 5
		0	3.50, 5, 10, 15, 20
K	1.83, -5.50	±2.00	0.83*, 2.50, 5
		0	2.50, 5, 10, 15, 20

*This point sometimes not obtained because of adjacent store interference.

Table 3. A-7D Load Configurations

Config.	Pylon					
	Left Wing Outboard (1)	Left Wing Center (2)	Left Wing Inboard (3)	Right Wing Inboard (6)	Right Wing Center (7)	Right Wing Outboard (8)
1	Empty*	Empty	Empty	Empty	Empty	Empty
2	MK-82GP	MK-82SE			MK-82GP,SE	MK-82GP
3	MK-82GP					MK-82GP
4	MK-82GP					MK-82GP
5	MK-82GP					MK-82GP
6	MK-82GP					MK-82GP
7	MK-82GP					MK-82GP

Denotes MER

Denotes TER

*Denotes no store on pylon.

Table 3. Continued

Config.	Pylon					
	Left Wing Outboard (1)	Left Wing Center (2)	Left Wing Inboard (3)	Right Wing Inboard (6)	Right Wing Center (7)	Right Wing Outboard (8)
8	MK-82GP	MK-82SE	Empty	MK-84 EOGB	MK-84 EOGB	MK-84 EOGB
9	QRC-335A ECM	MK-82GP		Empty	MK-82GP	QRC-335A ECM
10		MK-82GP			MK-82GP	
11		MK-82GP			MK-82GP	
12		MK-82GP			MK-82GP	
13		MK-82GP			MK-82GP	
14		MK-82GP			MK-82GP	

Denotes MER

Denotes TER

*Denotes no store on pylon.

Table 3. Continued

Config.	Pylon					
	Left Wing Outboard (1)	Left Wing Center (2)	Left Wing Inboard (3)	Right Wing Inboard (6)	Right Wing Center (7)	Right Wing Outboard (8)
15	Empty	MK-20	300-gal Fuel Tank	300-gal Fuel Tank	MK-20	Empty
16		MK-20			MK-20	
17	MK-20	MK-20		MK-20	Empty	
18	MK-20			MK-20		
19	QRC-335A ECM	SUU-30H/B		300-gal Fuel Tank	SUU-30H/B	QRC-335A ECM
20		SUU-30H/B			SUU-30H/B	
21	Empty	MK-82GP			MK-82GP	Empty

Denotes MER

Denotes TER

*Denotes no store on pylon.

Table 3. Concluded

Config.	Pylon					
	Left Wing Outboard (1)	Left Wing Center (2)	Left Wing Inboard (3)	Right Wing Inboard (4)	Right Wing Center (5)	Right Wing Outboard (6)
22	Empty	MK-82GP	300-gal Fuel Tank	300-gal Fuel Tank	MK-82GP	Empty

Denotes MER

Denotes TER

*Denotes no store on pylon.

NOMENCLATURE

BL	Aircraft buttock line from plane of symmetry, in., model scale
FS	Aircraft fuselage station, in., model scale
M_∞	Free-stream Mach number
p_t	Free-stream total pressure, psfa
p_∞	Free-stream static pressure, psfa
q_∞	Free-stream dynamic pressure, psf
Re_∞	Free-stream unit Reynolds number, per ft
T_t	Free-stream total temperature, °R
V_L	Local velocity vector, ft/sec (see Fig. 17)
$V_{X,P}$	Component of local velocity along probe X_P axis, ft/sec (see Fig. 17)
$V_{Y,P}$	Component of local velocity along probe Y_P axis, ft/sec (see Fig. 17)
$V_{YZ,P}$	Component of local velocity in probe Y_P-Z_P plane, ft/sec (see Fig. 17)
$V_{Z,P}$	Component of local velocity along probe Z_P axis, ft/sec (see Fig. 17)
V_∞	Free-stream velocity, ft/sec
WL	Aircraft waterline from reference horizontal plane, in., model scale
X_P	Location of the probe in the pylon-axis system X_P direction, ft, full scale measured from the reference position
Y_P	Location of the probe in the pylon-axis system Y_P direction, ft, full scale measured from the reference position
Z_P	Location of the probe in the pylon-axis system Z_P direction, ft, full scale measured from the reference position
α	Parent-aircraft model angle of attack relative to the free-stream velocity vector, deg
β	Parent-aircraft model sideslip angle relative to the free-stream velocity vector, deg

FLIGHT-AXIS SYSTEM COORDINATES

Directions

X_F Parallel to the free-stream wind vector, positive direction is forward as seen by the pilot

Y_F Perpendicular to the X_F and Z_F directions, positive direction is to the right as seen by the pilot

Z_F In the aircraft plane of symmetry, perpendicular to the free-stream wind vector, positive direction is downward

The flight-axis system origin is coincident with the aircraft cg and remains fixed with respect to the parent aircraft during a survey. The X_F, Y_F, and Z_F coordinate axes do not rotate with respect to the initial flight direction and attitude.

PYLON-AXIS SYSTEM COORDINATES

Directions

X_P Parallel to the probe longitudinal axis and the lower surface of the pylon, positive direction is forward as seen by the pilot

Y_P Perpendicular to the X_P axis and parallel to the flight-axis system X_F-Y_F plane, positive direction is to the right as seen by the pilot

Z_P Perpendicular to both the X_P and Y_P axes, positive direction is downward

The pylon-axis system origin is defined as the forward 30-in. suspension point on the lower surface of each respective pylon. The axes are rotated with respect to the flight-axis system by the initial yaw and pitch angles of the probe. Both the origin and the direction of the coordinate axes remain fixed with respect to the flight-axis system throughout the survey.